AWARD NUMBER: W81XWH-16-1-0059

TITLE: Therapeutic Targeting of Spliceosomal-Mutant Acquired Bone Marrow Failure Disorders

PRINCIPAL INVESTIGATOR: Omar Abdel-Wahab MD

RECIPIENT: Sloan Kettering Institute for Cancer Research
New York, NY 10065

REPORT DATE: May 2017

TYPE OF REPORT: Annual

PREPARED FOR: U.S. Army Medical Research and Materiel Command
Fort Detrick, Maryland 21702-5012

REPORT DOCUMENTATION PAGE

Form Approved
OMB No. 0704-0188

1. REPORT DATE	**2. REPORT TYPE**	**3. DATES COVERED**
May 2017	Annual	1 May 2016 - 30 Apr 2017

4. TITLE AND SUBTITLE

Therapeutic Targeting of Spliceosomal-Mutant Acquired Bone Marrow Failure Disorders

5a. CONTRACT NUMBER

5b. GRANT NUMBER
W81XWH-16-1-0059

5c. PROGRAM ELEMENT NUMBER

6. AUTHOR(S)

Omar Abdel-Wahab M.D.

E-Mail: abdelwao@mskcc.org

5d. PROJECT NUMBER

5e. TASK NUMBER

5f. WORK UNIT NUMBER

7. PERFORMING ORGANIZATION NAME(S) AND ADDRESS(ES)

Sloan Kettering Institute for Cancer Research
1275 York Avenue
New York, NY 10065-6007

8. PERFORMING ORGANIZATION REPORT NUMBER

9. SPONSORING / MONITORING AGENCY NAME(S) AND ADDRESS(ES)
U.S. Army Medical Research and Materiel Command
Fort Detrick, Maryland 21702-5012

10. SPONSOR/MONITOR'S ACRONYM(S)

11. SPONSOR/MONITOR'S REPORT NUMBER(S)

12. DISTRIBUTION / AVAILABILITY STATEMENT
Approved for Public Release; Distribution Unlimited

13. SUPPLEMENTARY NOTES

14. ABSTRACT

Genes encoding core components of the RNA splicing machinery are the most common mutational targets in acquired bone marrow failure (BMF) due to myelodysplastic syndromes (MDS). The goals of this proposal were to identify (1) the subset of biologically and therapeutically relevant targets that link spliceosomal mutations to MDS and (2) therapeutic strategies that interfere with the altered function of mutant spliceosomal proteins. Since award of this grant we have found that different spliceosomal mutations, despite imparting distinct effects on splicing and gene expression, are negatively selected for when co-expressed in the same cell or in a homozygous state. At the same time, aberrant splicing of distinct targets/events by mutant SF3B1 and SRSF2 results in hyperactivated NF-κ □□ si convergent biological consequences of splicing factor mutations and the basis for their mutual exclusivity and heterozygous nature. In addition, we have completed both a negative selection shRNA screen and a genome-wide CRISPR dropout screen to identify genes selectively required in spliceosomal mutant cells. This effort has also highlighted a requirement for innate immune signaling in SF3B1-mutant MDS and has implicated a few specific proteins as potential novel therapeutic targets for spliceosomal mutant MDS.

15. SUBJECT TERMS
MDS, SF3B1, Splicing, SRSF2, U2AF1, ZRSR2.

16. SECURITY CLASSIFICATION OF:			**17. LIMITATION OF ABSTRACT**	**18. NUMBER OF PAGES**	**19a. NAME OF RESPONSIBLE PERSON**
a. REPORT	**b. ABSTRACT**	**c. THIS PAGE**			USAMRMC
U	U	U	UU	68	**19b. TELEPHONE NUMBER** *(include area code)*

TABLE OF CONTENTS

1. INTRODUCTION:

Genes encoding core components of the RNA splicing machinery are the most common mutational targets in acquired bone marrow failure (BMF) due to myelodysplastic syndromes (MDS). MDS-associated "spliceosomal mutations" most frequently affect *SF3B1*, *SRSF2*, and *U2AF1*. Mutations in each of these genes conspicuously occur as heterozygous point mutations at highly restricted residues and are mutually exclusive, suggesting that they are oncogenic gain-of-function alterations. While these data suggest that each RNA splicing factor mutation may share downstream targets, currently few mis-spliced genes have been conclusively identified as downstream targets of any mutant splicing protein, and no shared targets downstream of all three spliceosomal gene mutations have been identified. Thus, the goals of this proposal were to identify (1) the subset of biologically and therapeutically relevant targets that link spliceosomal mutations to MDS and (2) therapeutic strategies that interfere with the altered function of mutant spliceosomal proteins.

2. KEYWORDS:

MDS, SF3B1, Splicing, SRSF2, U2AF1, ZRSR2

3. ACCOMPLISHMENTS:

What were the major goals of the project?

The major goals of this project were as follows:

Specific Aim 1. Identify unifying molecular abnormalities across spliceosomal mutations using combined genomic and proteomic approaches.

Specific Aim 2. Identify additional genes that are required for the survival of cells carrying different spliceosomal mutations with synthetic lethality screens.

Specific Aim 3. Identify novel therapeutic strategies specifically targeting mutant spliceosomal protein function.

What was accomplished under these goals?

Aim 1 accomplishments: We have recently identified that different spliceosomal mutations, despite imparting distinct effects on splicing and gene expression, are negatively selected for when co-expressed in the same cell or in a homozygous state. At the same time, aberrant splicing of distinct targets/events by mutant SF3B1 and SRSF2 results in hyperactivated NF-κB signaling. Specifically, mutations in SF3B1 result in aberrant splicing and consequent downregulation of MAP3K7 while mutations in SRSF2 generate a stable truncated form of Caspase 8. Each of these alterations result in activation of NFk-B signaling. These data identify convergent biological consequences of splicing factor mutations and the basis for their mutual exclusivity and heterozygous nature. We have a shared manuscript currently under review at *Cancer Cell* describing these data as follows:

Stanley Chun-Wei Lee (co-first), Khrystyna Dilai (co-first), Eunhee Kim, Esther Obeng, Sydney X. Lu, Bo Liu, Daichi Inoue, Akihide Yoshimi, Michelle Ki, Xiao Jing Zhang, Min Kyung Kim, Young Rock Chung, Justin Taylor, Benjamin H. Durham, James Palacino, Michael Seiler, Silvia Buonamici, Peter G. Smith, Benjamin L. Ebert, Robert K. Bradley (co-corresponding), Omar Abdel-Wahab (co-corresponding). Synthetic lethal and convergent biological effects of cancer-associated spliceosomal gene mutations.

Aim 2 accomplishments: We utilized our K562 cells with the SF3B1 K700E and K666N mutations knocked into their endogenous loci to complete a negative-selection shRNA screen targeting the "Druggable Genome" (~2200 genes, 5 shRNAs per gene where the shRNA library was cloned into the T3G-eGFP-mirE-puromycin-IRES-rtTA3 (LT3GEPIR) lentiviral vector). Genes with ≥3 shRNAs depleted specifically in *SF3B1* mutant cells ($\log_2$ fold-change ≥ -2; D_{21} vs D_0) while remaining relatively unchanged in *SF3B1* wildtype parental cells were considered a positive hit. The primary screen yielded 101 candidate genes whose suppression were synthetic lethal in *SF3B1* K700E or K666N cells while having no effect on *SF3B1* wildtype cells. One "positive hit" that has validated successfully using 4 independent shRNAs is *STAT1*, an essential component of interferon (IFN) signaling. Of note, the essential nature of *STAT1* for the growth and survival of *SF3B1* mutant leukemias has been confirmed in K562 as well as NALM6 cells containing *SF3B1* K700K, K700E, and K666N mutations.

In addition, we recently identified that spliceosomal mutant cells are preferentially sensitive to genetic or pharmacologic perturbations to the splicing process. This work was published in the following paper which acknowledged this grant: Lee SC, Dvinge H, Kim E, Cho H, Micol JB, Chung YR, Durham BH, Yoshimi A, Kim YJ, Thomas M, Lobry C, Chen CW, Pastore A, Taylor J, Wang X, Krivtsov A, Armstrong SA, Palacino J, Buonamici S, Smith PG, Bradley RK, Abdel-Wahab O. Modulation of splicing catalysis for therapeutic targeting of leukemia with mutations in genes encoding spliceosomal proteins. Nat Med. 2016 Jun;22(6):672-8. doi: 10.1038/nm.4097. Epub 2016 May 2. PubMed PMID: 27135740; PubMed Central PMCID: PMC4899191.

Aim 3 accomplishments: We have now generated 2 minigenes mimicking an aberrant splicing event mediated by mutant SF3B1. One of them is an aberrant splicing event in MAP3K7 (described above) and the other is in BRD9. We have generated these in fluorescent and non-fluorescent reporters.

What opportunities for training and professional development has the project provided?

Nothing to Report

How were the results disseminated to communities of interest?

Nothing to Report

What do you plan to do during the next reporting period to accomplish the goals?

Aim 1: We plan to perform label-free mass spectrometric analysis of hematopoietic cells with and without SRSF2, SF3B1, and U2AF1 mutations to determine the effect of these mutations on the proteome. Gene expression and splicing data from RNA-seq analyses will be integrated with proteomic data to identify the effects of splicing events at the level of protein.

Aim 2: We have recently completed a genome-wide CRISPR dropout screen in the same cells in which the shRNA screen was performed. Once the sequencing data from this has returned we will validate these data in additional cell lines and in patient materials (and possibly in vivo).

Aim 3: Now that we have generated SF3B1-mutant selective reporters, we plan to carry out a small molecule screen to identify drugs that block the aberrant splicing of these events.

4. IMPACT:

What was the impact on the development of the principal discipline(s) of the project?

One of the main findings from our work thus far is that cells which contains mutations in RNA splicing factors have enhanced sensitivity to drugs that further alter the RNA splicing process. This has led to a clinical trial of a novel RNA splicing inhibitor in patients with MDS and other forms of myeloid leukemia (clinicaltrials.gov identifier NCT02841540). This is a phase I clinical trial sponsored by the company H3 Biomedicine Inc. and is designed to test the safety of this approach and ability to block splicing in patients.

What was the impact on other disciplines?

Nothing to Report

What was the impact on technology transfer?

Nothing to Report

What was the impact on society beyond science and technology?

Nothing to Report

5. CHANGES/PROBLEMS:
Changes in approach and reasons for change

Nothing to Report

Actual or anticipated problems or delays and actions or plans to resolve them

The only delays we have had thus far are in completing the DoD animal use and human subjects approvals. We are hopefully in the final stages of those approvals.

Changes that had a significant impact on expenditures

None.

Significant changes in use or care of human subjects, vertebrate animals, biohazards, and/or select agents

Significant changes in use or care of human subjects

None.

Significant changes in use or care of vertebrate animals.

None.

Significant changes in use of biohazards and/or select agents

None.

6. PRODUCTS:

- **Publications, conference papers, and presentations**

Journal publications.

Lee SC, Dvinge H, Kim E, Cho H, Micol JB, Chung YR, Durham BH, Yoshimi A, Kim YJ, Thomas M, Lobry C, Chen CW, Pastore A, Taylor J, Wang X, Krivtsov A, Armstrong SA, Palacino J, Buonamici S, Smith PG, Bradley RK, Abdel-Wahab O. Modulation of splicing catalysis for therapeutic targeting of leukemia with mutations in genes encoding spliceosomal proteins. Nat Med. 2016 Jun;22(6):672-8. doi: 10.1038/nm.4097. Epub 2016 May 2. PubMed PMID: 27135740; PubMed Central PMCID: PMC4899191.

Stanley Chun-Wei Lee (co-first), Khrystyna Dilai (co-first), Eunhee Kim, Esther Obeng, Sydney X. Lu, Bo Liu, Daichi Inoue, Akihide Yoshimi, Michelle Ki, Xiao Jing Zhang, Min Kyung Kim, Young Rock Chung, Justin Taylor, Benjamin H. Durham, James Palacino, Michael Seiler, Silvia Buonamici, Peter G. Smith, Benjamin L. Ebert, Robert K. Bradley (co-corresponding), Omar Abdel-Wahab (co-corresponding). Synthetic lethal and convergent biological effects of cancer-associated spliceosomal gene mutations. Under Review at *Cancer Cell.*

Yoshimi A, Abdel-Wahab O. Splicing factor mutations in MDS RARS and MDS/MPN-RS-T. Int J Hematol. 2017 Jun;105(6):720-731. doi: 10.1007/s12185-017-2242-0. Epub 2017 May 2. Review. PubMed PMID: 28466384.

Joshi P, Halene S, Abdel-Wahab O. How do messenger RNA splicing alterations drive myelodysplasia? Blood. 2017 May 4;129(18):2465-2470. doi: 10.1182/blood-2017-02-692715. Epub 2017 Mar 27. Review. PubMed PMID: 28348147; PubMed Central PMCID: PMC5418633.

Lee SC, Abdel-Wahab O. Therapeutic targeting of splicing in cancer. Nat Med. 2016 Sep 7;22(9):976-86. doi: 10.1038/nm.4165. Review. PubMed PMID: 27603132.

Dvinge H, Kim E, Abdel-Wahab O, Bradley RK. RNA splicing factors as oncoproteins and tumour suppressors. Nat Rev Cancer. 2016 Jul;16(7):413-30. doi: 10.1038/nrc.2016.51. Epub 2016 Jun 10. Review. PubMed PMID: 27282250; PubMed Central PMCID: PMC5094465.

Books or other non-periodical, one-time publications.

None.

Other publications, conference papers, and presentations.

Presentations by Drs. Bradley and Abdel-Wahab together:

2016 AACR Recent Advances in Diagnosis and Therapy Session, AACR Annual Meeting, New Orleans, LA

2016 Plenary Speakers, 2nd Spliceosomal Gene Mutations in Cancer Workshop, Broad Institute of Harvard & MIT, Cambridge, MA

Presentations by Dr. Omar Abdel-Wahab alone:

2016 Plenary Speaker, Japanese Society of Hematology, 78th Annual Meeting, Yokohama, Japan

2017 Keystone Symposium RNA Processing in Human Disease, Taos, New Mexico

2017 Curie Institute, Future of Oncology Symposium, Paris, France

2017 AACR Annual Meeting, Scientific Session on Molecular Pathogenesis of MDS, Washington D.C.

2017 Gordon Research Conference, Cancer Epigenetics, Lucca Italy

2017 Hallmarks of Cancer Symposium (RNA Society Satellite Symposium): Focus on RNA, Prague, Czech Republic

- **Website(s) or other Internet site(s)**

None.

- **Technologies or techniques**

None.

- **Inventions, patent applications, and/or licenses**

None.

- **Other Products**

We have deposited our RNA-seq datasets at the Gene Expression Omnibus database under accession numbers GSE74064 and GSE97452.

7. PARTICIPANTS & OTHER COLLABORATING ORGANIZATIONS

What individuals have worked on the project?

Name:	*Omar Abdel-Wahab*
Project Role:	*PI*
Researcher Identifier (e.g. ORCID ID):	*None*
Nearest person month worked:	*12*
Contribution to Project:	*Overseeing all experiments in conjunction with Dr. Bradley.*
Funding Support:	*US National Institutes of Health (NIH)-NHLBI grant R01 HL128239*
Name:	*Robert Bradley*
Project Role:	*co-PI*
Researcher Identifier (e.g. ORCID ID):	*None*
Nearest person month worked:	*12*
Contribution to Project:	*Overseeing all experiments in conjunction with Dr. Abdel-Wahab.*
Funding Support:	*US National Institutes of Health (NIH)-NHLBI grant R01 HL128239*
Name:	*Stanley Chun-Wei Lee*
Project Role:	*Postdoctoral fellow*
Researcher Identifier (e.g. ORCID ID):	*None*
Nearest person month worked:	*12*
Contribution to Project:	*Stanley has performed all in vivo experiments related to Specific Aim 1 and the shRNA screen in Aim 2.*
Funding Support:	*Leukemia and Lymphoma Society Special Fellow Award.*
Name:	*Bo Liu*
Project Role:	*Postdoctoral fellow*
Researcher Identifier (e.g. ORCID ID):	*None*
Nearest person month worked:	*5*
Contribution to Project:	*Bo generated the splicing reporters described in Aim 3.*
Funding Support:	*Josie Robertson Award (MSKCC)*
Name:	*Heidi Dvinge*
Project Role:	*Postdoctoral fellow*
Researcher Identifier (e.g. ORCID ID):	*None*
Nearest person month worked:	*12*
Contribution to Project:	*Heidi performed the informatics analyses to understand the effects of modulating splicing genetically and pharmacologically in cells bearing a spliceosomal gene mutation.*
Funding Support:	*US Department of Defense Breast Cancer Research Program grant W81XWH-14-1-0044*
Name:	*Khrystyna Dilai*
Project Role:	*Graduate Student*
Researcher Identifier (e.g. ORCID ID):	*None*
Nearest person month worked:	*6*
Contribution to Project:	*Khrystyna performed the informatics analyses to identify convergent effects of spliceosomal gene mutations in Aim 1.*
Funding Support:	*US National Institutes of Health (NIH)-NHLBI grant R01 HL128239*
Name:	*Janine Ilagan*
Project Role:	*Postdoctoral fellow*
Researcher Identifier (e.g. ORCID ID):	*None*
Nearest person month worked:	*12*
Contribution to Project:	*Janine performed the CRISPR screen in Aim 2.*
Funding Support:	*US National Institutes of Health (NIH)-NHLBI grant R01 HL128239*

Has there been a change in the active other support of the PD/PI(s) or senior/key personnel since the last reporting period?

SEE APPENDIX FOR CHANGES IN ACTIVE SUPPORT

What other organizations were involved as partners?

Organization Name: Fred Hutchinson Cancer Research Center
Location of Organization: (if foreign location list country): Seattle, WA
Partner's contribution to the project (identify one or more)
- *Collaboration (e.g., partner's staff work with project staff on the project);*

8. SPECIAL REPORTING REQUIREMENTS

COLLABORATIVE AWARDS: For collaborative awards, independent reports are required from BOTH the Initiating PI and the Collaborating/Partnering PI. A duplicative report is acceptable; however, tasks shall be clearly marked with the responsible PI and research site. A report shall be submitted to **https://ers.amedd.army.mil** for each unique award.

QUAD CHARTS: If applicable, the Quad Chart (available on https://www.usamraa.army.mil) should be updated and submitted with attachments.

9. APPENDICES:

Attach all appendices that contain information that supplements, clarifies or supports the text. Examples include original copies of journal articles, reprints of manuscripts and abstracts, a curriculum vitae, patent applications, study questionnaires, and surveys, etc.

The appendix includes the following two publications (one published, the other submitted):

- Lee SC, Dvinge H, Kim E, Cho H, Micol JB, Chung YR, Durham BH, Yoshimi A, Kim YJ, Thomas M, Lobry C, Chen CW, Pastore A, Taylor J, Wang X, Krivtsov A, Armstrong SA, Palacino J, Buonamici S, Smith PG, Bradley RK, Abdel-Wahab O. Modulation of splicing catalysis for therapeutic targeting of leukemia with mutations in genes encoding spliceosomal proteins. Nat Med. 2016 Jun;22(6):672-8. doi: 10.1038/nm.4097. Epub 2016 May 2. PubMed PMID: 27135740; PubMed Central PMCID: PMC4899191.

- Stanley Chun-Wei Lee (co-first), Khrystyna Dilai (co-first), Eunhee Kim, Esther Obeng, Sydney X. Lu, Bo Liu, Daichi Inoue, Akihide Yoshimi, Michelle Ki, Xiao Jing Zhang, Min Kyung Kim, Young Rock Chung, Justin Taylor, Benjamin H. Durham, James Palacino, Michael Seiler, Silvia Buonamici, Peter G. Smith, Benjamin L. Ebert, Robert K. Bradley (co-corresponding), Omar Abdel-Wahab (co-corresponding). Synthetic lethal and convergent biological effects of cancer-associated spliceosomal gene mutations. Under Review at *Cancer Cell*

nature medicine

Modulation of splicing catalysis for therapeutic targeting of leukemia with mutations in genes encoding spliceosomal proteins

Stanley Chun-Wei Lee[1,9], Heidi Dvinge[2,3,9], Eunhee Kim[1], Hana Cho[1], Jean-Baptiste Micol[1], Young Rock Chung[1], Benjamin H Durham[1], Akihide Yoshimi[1], Young Joon Kim[1], Michael Thomas[4], Camille Lobry[5], Chun-Wei Chen[6], Alessandro Pastore[1], Justin Taylor[1], Xujun Wang[6], Andrei Krivtsov[6], Scott A Armstrong[6,7], James Palacino[4], Silvia Buonamici[4], Peter G Smith[4], Robert K Bradley[2,3,10] & Omar Abdel-Wahab[1,8,10]

Mutations in genes encoding splicing factors (which we refer to as spliceosomal genes) are commonly found in patients with myelodysplastic syndromes (MDS) and acute myeloid leukemia (AML)[1–3]. These mutations recurrently affect specific amino acid residues, leading to perturbed normal splice site and exon recognition[4–6]. Spliceosomal gene mutations are always heterozygous and rarely occur together with one another, suggesting that cells may tolerate only a partial deviation from normal splicing activity. To test this hypothesis, we engineered mice to express a mutated allele of serine/arginine-rich splicing factor 2 (*Srsf2*^{P95H})—which commonly occurs in individuals with MDS and AML—in an inducible, hemizygous manner in hematopoietic cells. These mice rapidly succumbed to fatal bone marrow failure, demonstrating that *Srsf2*-mutated cells depend on the wild-type *Srsf2* allele for survival. In the context of leukemia, treatment with the spliceosome inhibitor E7107 (refs. 7,8) resulted in substantial reductions in leukemic burden, specifically in isogenic mouse leukemias and patient-derived xenograft AMLs carrying spliceosomal mutations. Whereas E7107 treatment of mice resulted in widespread intron retention and cassette exon skipping in leukemic cells regardless of *Srsf2* genotype, the magnitude of splicing inhibition following E7107 treatment was greater in *Srsf2*-mutated than in *Srsf2*-wild-type leukemia, consistent with the differential effect of E7107 on survival. Collectively, these data provide genetic and pharmacologic evidence that leukemias with spliceosomal gene mutations are preferentially susceptible to additional splicing perturbations *in vivo* as compared to leukemias without such mutations. Modulation of spliceosome function may thus provide a new therapeutic avenue in genetically defined subsets of individuals with MDS or AML.

Mutations in the spliceosomal genes *SRSF2*, *U2AF1*, and *SF3B1* are the most common class of mutations in patients with MDS[1–3] and occur across the entire spectrum of myeloid malignancies, including in 10–25% of patients with AML and in a higher proportion of patients with AML transformed from an antecedent MDS[9]. Recent studies revealed that heterozygous mutations in *SRSF2* (ref. 5), as well as *U2AF1* (ref. 4), drive hematopoietic stem–progenitor cell (HSPC) expansion in mice *in vivo* and that these mutations alter mRNA recognition in a sequence-specific manner[6]. However, it is still unclear why spliceosomal gene mutations occur in an exclusively heterozygous state in myeloid malignancies and why these mutations are mutually exclusive with one another. Moreover, given the frequency of these mutations and their early occurrence in myeloid malignancies[10–12], strategies to therapeutically target spliceosome-mutant malignancies are urgently needed.

We first took a genetic approach to test the hypothesis that cells carrying mutations in spliceosomal genes are sensitive to further perturbation of normal splicing. We engineered mice that conditionally expressed the *Srsf2*^{P95H} mutation in a hemizygous manner in the hematopoietic system (under the control of the *Mx1* promoter to drive the expression of Cre recombinase); conditional expression of the *Srsf2*^{P95H} allele could then be induced by administration of polyinosinic:polycytidylic acid (polyI:C). These mice enabled us to study the effects of deleting wild-type (WT) *Srsf2* and concomitantly activating expression of the *Srsf2*^{P95H} allele. *Mx1-Cre*$^{+}$*Srsf2*$^{+/fl}$ mice were crossed to *Srsf2*$^{P95H/+}$ mice to generate progeny that were WT for *Srsf2* (*Mx1-Cre*$^{+}$*Srsf2*$^{+/+}$), heterozygous knockout for *Srsf2* (*Mx1-Cre*$^{+}$*Srsf2*$^{+/fl}$), heterozygous for the *Srsf2*^{P95H} mutation (*Mx1-Cre*$^{+}$*Srsf2*$^{P95H/+}$), or hemizygous for the *Srsf2*^{P95H} mutation (*Mx1-Cre*$^{+}$*Srsf2*$^{P95H/fl}$) (**Supplementary Fig. 1a**). In noncompetitive

[1]Human Oncology and Pathogenesis Program, Memorial Sloan Kettering Cancer Center, New York, New York, USA. [2]Computational Biology Program, Public Health Sciences Division, Fred Hutchinson Cancer Research Center, Seattle, Washington, USA. [3]Basic Sciences Division, Fred Hutchinson Cancer Research Center, Seattle, Washington, USA. [4]H3 Biomedicine, Inc., Cambridge, Massachusetts, USA. [5]Institut National de la Santé et de la Recherche Medicale (INSERM) U1170, Institut Gustave Roussy, Villejuif, France. [6]Cancer Biology and Genetics Program, Memorial Sloan Kettering Cancer Center, New York, New York, USA. [7]Department of Pediatrics, Memorial Sloan Kettering Cancer Center, New York, New York, USA. [8]Leukemia Service, Department of Medicine, Memorial Sloan Kettering Cancer Center, New York, New York, USA. [9]These authors contributed equally to this work. [10]These authors jointly directed this work. Correspondence should be addressed to R.K.B. (rbradley@fredhutch.org) or O.A.-W. (abdelwao@mskcc.org).

Received 2 March; accepted 6 April; published online 2 May 2016; corrected online 11 May 2016 (details online); doi:10.1038/nm.4097

bone marrow (BM) transplantation assays, shortly after polyI:C administration, recipient mice reconstituted with BM mononuclear cells (MNCs) from hemizygous *Mx1-Cre*$^{+}$*Srsf2*$^{P95H/-}$ mice showed significantly shorter survival ($P = 0.004$) and severe BM aplasia (**Fig. 1a–c**) due to loss of HSPCs in the BM (**Supplementary Fig. 1b–f**), which was not observed in mice transplanted with BM MNCs from *Mx1-Cre*$^{+}$*Srsf2*$^{P95H/+}$, *Mx1-Cre*$^{+}$*Srsf2*$^{+/fl}$, or *Mx1-Cre*$^{+}$*Srsf2*$^{+/+}$ mice.

To determine the effect of hemizygous expression of the *Srsf2*^{P95H} allele on the transcriptome, we performed RNA-seq analysis on HSPCs (CD45.2^{+} lineage^{-} Sca1^{+}c-Kit^{+} (LSK) cells) isolated 2 weeks after polyI:C injection from mice that had been reconstituted with *Mx1-Cre*$^{+}$*Srsf2*$^{+/+}$, *Mx1-Cre*$^{+}$*Srsf2*$^{+/fl}$, *Mx1-Cre*$^{+}$*Srsf2*$^{P95H/+}$, or *Mx1-Cre*$^{+}$*Srsf2*$^{P95H/-}$ BM cells. We observed >3,000 dysregulated genes in *Srsf2*$^{P95H/-}$ HSPCs relative to all other groups, including >1.5-fold repression of many genes involved in hematopoietic stem cell self-renewal, including *Runx1*, *Erg*, and the entire *HoxA* cluster (**Fig. 1d** and **Supplementary Table 1**). Gene Ontology (GO) analysis of the differentially expressed genes in HSPCs from all four groups revealed that pathways related to cell migration, chemotaxis, cytokine production, and inflammatory responses were significantly overexpressed in *Mx1-Cre*$^{+}$*Srsf2*$^{P95H/-}$ relative to *Mx1-Cre*$^{+}$*Srsf2*$^{P95H/+}$ HSPCs (**Supplementary Fig. 1g**). We next tested whether hemizygous expression of *Srsf2*^{P95H} was associated with substantive alterations in splicing. We used Bayesian statistical methods (the MISO algorithm[13] and Wagenmakers's framework[14]) to quantify differential splicing of ~44,000 annotated alternative splicing events and ~170,000 constitutive splice junctions. We observed differential splicing of all classes of alternative splicing events, including competing 5′ and 3′ splice sites, cassette exons, and retained introns in *Mx1-Cre*$^{+}$*Srsf2*$^{P95H/-}$ cells, as well as alternative splicing and intron retention affecting normally constitutively spliced junctions. Although most splicing events remained unchanged, *Mx1-Cre*$^{+}$*Srsf2*$^{P95H/-}$ cells showed approximately two-fold more mis-splicing across all types of splicing events than did *Mx1-Cre*$^{+}$*Srsf2*$^{P95H/+}$ cells (**Supplementary Tables 1–3**).

We next tested whether increased mis-splicing in *Mx1-Cre*$^{+}$ *Srsf2*$^{P95H/-}$ cells was due to altered exon recognition. Heterozygous expression of the *SRSF2*^{P95H}, *SRSF2*^{P95L}, or *SRSF2*^{P95R} mutation alters SRSF2's recognition of specific exonic splicing enhancer (ESE) motifs and drives recurrent mis-splicing of transcripts for key hematopoietic regulators[5,15]. Quantification of the occurrence of ESE motifs within cassette exons that were differentially spliced in each genotype of LSK cells revealed a statistically significant preference for CCNG over GGNG ESE motifs in *Mx1-Cre*$^{+}$*Srsf2*$^{P95H/+}$ and *Mx1-Cre*$^{+}$*Srsf2*$^{P95H/-}$ cells (**Fig. 1e**), consistent with previous reports. CCNG motifs were enriched, and GGNG motifs were depleted, within differentially spliced cassette exons but not within flanking introns or exons (**Fig. 1f**).

To determine whether the cell lethality seen with *Srsf2*$^{P95H/-}$ hemizygosity was also present in the setting of leukemogenesis, we transduced *Srsf2*$^{P95H/fl}$ (control) or *Mx1-Cre*$^{+}$*Srsf2*$^{P95H/fl}$ (hemizygous) fetal liver cells with a green fluorescent protein (GFP)-expressing retroviral construct encoding the *KMT2A–MLLT3* fusion oncogene (also known as *MLL–AF9*) and then transplanted these cells into lethally irradiated recipient mice (**Supplementary Fig. 2a**). Although *Srsf2*$^{P95H/fl}$ control mice rapidly developed leukocytosis, anemia, thrombocytopenia, and elevated levels of donor-derived GFP^{+} cells, these features were substantially diminished in the hemizygous *Srsf2*$^{P95H/-}$ background (**Supplementary Fig. 2b–g**). Consistent with this observation, all of the mice from the control group eventually developed leukemia, whereas only five of ten *Srsf2*$^{P95H/-}$ mice succumbed to disease (**Supplementary Fig. 2h**). Moreover, leukemic cells in *Srsf2*$^{P95H/-}$ recipients uniformly escaped polyI:C-mediated recombination of the WT *loxP*-flanked (floxed) *Srsf2* allele, as compared to the cells in the blood samples taken from the same animals in the pre-leukemic state (**Supplementary Fig. 2i**). Overall, these observations revealed that *Srsf2*$^{P95H/+}$ cells specifically depend on the presence of the WT *Srsf2* allele for survival, even in the presence of a potent oncogene. These findings are consistent with the observation that mutations in genes encoding SRSF2 and other spliceosomal proteins are always heterozygous in individuals with MDS or AML, and they provide a potential explanation for the consistent heterozygous nature of spliceosomal gene mutations in cancer.

Having established, using mouse genetic models, that cells with spliceosomal gene mutations depend on WT splicing function, we hypothesized that spliceosome-mutant hematopoietic cells might display an altered response to pharmacologic inhibition of pre-mRNA splicing relative to their WT counterparts. To test this, we treated recipient mice with the splicing inhibitor E7107 (refs. 7,8). We first generated BM chimeras by transplanting *Srsf2*$^{+/+}$ or *Srsf2*$^{P95H/+}$ BM MNCs into lethally irradiated recipient mice. We then treated these mice with E7107 or vehicle starting at 6 months after transplantation (a time point at which stable engraftment of long-term hematopoiesis is expected) (**Supplementary Fig. 2j**). After five daily treatments of vehicle or E7107, we purified HSPCs (CD45.2^{+} lineage^{-} Sca1^{-} c-Kit^{+} cells) by flow cytometry and analyzed splicing and gene expression by RNA-seq. Ordination analysis by multidimensional scaling based on global cassette exon inclusion and global gene expression revealed that all of the vehicle-treated samples clustered together irrespective of *Srsf2* genotype, whereas the E7107-treated samples clustered on the basis of *Srsf2* genotype (**Fig. 2a**). These results indicate a differential gene expression and splicing response to E7107 treatment in *Srsf2*$^{P95H/+}$ hematopoietic cells as compared to their *Srsf2*$^{+/+}$ counterparts. We next examined whether this differential response to E7107 is due to the previously described altered ESE motif preference by mutant Srsf2. To do so, we performed a 'two-factor' analysis across two experimental parameters (vehicle versus E7107 and *Srsf2*$^{+/+}$ versus *Srsf2*$^{P95H/+}$) in which we systematically tested for preferential recognition of exons with different variants of the core SSNG (S = C or G) motif between each comparison (**Fig. 2b**). This analysis revealed that exons that are differentially spliced between the vehicle-treated *Srsf2*$^{+/+}$ and *Srsf2*$^{P95H/+}$ samples showed the expected difference in ESE motif preference (**Fig. 2b**, left), as previously published[5]. In contrast, there was no motif enrichment associated with the exons that were affected by E7107 in either *Srsf2*$^{+/+}$ or *Srsf2*$^{P95H/+}$ cells (**Fig. 2b**, top and bottom). However, we did observe that preferential recognition of exons with CCNG versus GGNG motifs in *Srsf2*$^{P95H/+}$ versus *Srsf2*$^{+/+}$ cells was weaker following E7107 treatment, and we identified a small subset of exons whose inclusion was affected in a genotype-dependent manner (**Fig. 2b**, right and **Supplementary Table 3**).

On the basis of these observations, we hypothesized that spliceosome-mutant leukemias might have greater sensitivity to pharmacologic inhibition of splicing than spliceosome-WT leukemias. Recent work[16] identified *SRSF2* mutations in ~10% of adult *MLL*-rearranged AMLs, suggesting that *MLL*-rearranged leukemias constitute a relevant system to study *SRSF2* mutations. By reanalyzing RNA-seq data[16] from human subjects with *MLL*-rearranged AML, we observed global alterations in splicing and ESE motif preference in *SRSF2*-mutated *MLL*-rearranged AML transcriptomes that are similar to those we previously reported in the *SRSF2*-mutated mouse model of MDS and in patients with myeloid leukemia[5] (**Fig. 2c,d**), suggesting that *SRSF2* mutations alter exon recognition in *MLL*-rearranged AML as

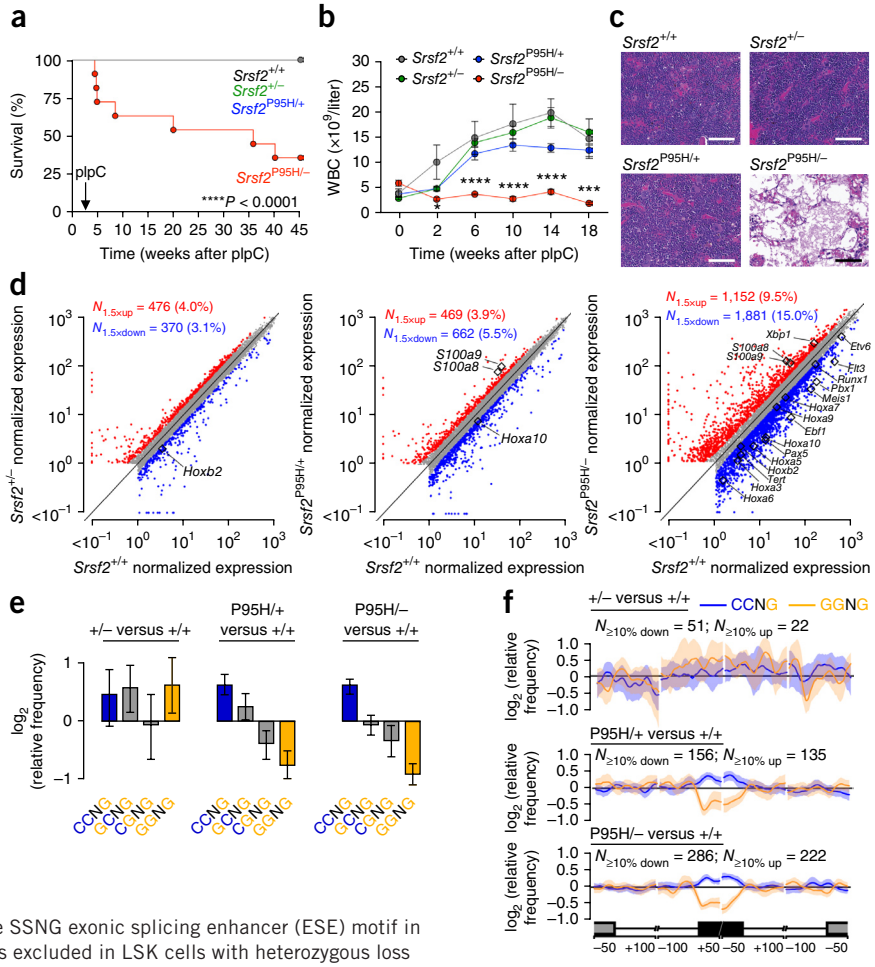

Figure 1 Spliceosome-mutant cells require the wild-type *Srsf2* allele for survival. (**a**) Kaplan–Meier survival curve of CD45.1 recipient mice transplanted with BM cells from control (*Mx1-Cre*$^{+}$*Srsf2*$^{+/+}$) mice or mice heterozygous (*Mx1-Cre*$^{+}$*Srsf2*$^{+/–}$) for the WT *Srsf2* allele, or mice heterozygous (*Mx1-Cre*$^{+}$*Srsf2*$^{P95H/+}$) or hemizygous (*Mx1-Cre*$^{+}$*Srsf2*$^{P95H/–}$) for the *Srsf2*^{P95H} (mutated) allele ($n = 10$ mice per group). Administration of polyI:C (plpC) was performed 4 weeks after transplantation. $^{****}P < 0.0001$ by Mantel–Cox log-ranked test. (**b**) White blood cell (WBC) counts in mice of each genotype over 18 weeks of noncompetitive transplantation ($n = 10$ mice per group). Error bars represent mean ± s.d. $^{***}P < 0.001$; $^{****}P < 0.0001$; by one-way analysis of variance (ANOVA). (**c**) Representative H&E-stained images of BM from CD45.1 recipient mice ($n = 10$ mice per group) that were transplanted with BM cells from the indicated mouse strains 8 weeks after transplantation. Scale bars, 200 µm. (**d**) Scatter plots comparing normalized expression of individual genes in lineage$^{–}$Sca1^{+}c-Kit^{+} (LSK) BM cells from *Mx1-Cre*$^{+}$*Srsf2*$^{+/–}$ (left), *Mx1-Cre*$^{+}$*Srsf2*$^{P95H/+}$ (middle), and *Mx1-Cre*$^{+}$*Srsf2*$^{P95H/–}$ (right) mice relative to those from WT control mice. Genes that were significantly dysregulated between comparisons (Bayes factor > 5; fold change > 1.5) are labeled in red (upregulated) and blue (downregulated), respectively. Differentially expressed genes of particular biological importance are highlighted in each plot. Units are transcripts per million. (**e**) Mean enrichment of all variants of the SSNG exonic splicing enhancer (ESE) motif in cassette exons that were differentially included versus excluded in LSK cells with heterozygous loss of (+/–), heterozygous mutation in (P95H/+), or hemizygous mutation in (P95H/–) *Srsf2* relative to the *Srsf2* control (+/+). Error bars indicate 95% confidence intervals estimated by bootstrapping. (**f**) Spatial distribution of CCNG and GGNG motifs adjacent to the sets of differentially spliced cassette exons analyzed in **e**. $N_{\geq 10\%\ down}$ and $N_{\geq 10\%\ up}$ indicate the number of exons that exhibited decreases or increases, respectively, in inclusion of absolute magnitude ≥10% in cells with the indicated genotypes relative to *Srsf2* control (+/+) cells. Shading indicates 95% confidence intervals by bootstrapping. The schematic (bottom) illustrates a portion of a metagene with the cassette exon (black box) separated from the upstream and downstream exons (gray boxes) by the beginning and end of the connecting introns. Horizontal axis indicates genomic coordinates defined with respect to the 5′ and 3′ splice sites where position 0 is the splice site itself. Vertical axis represents relative frequency of the indicated motifs over genomic loci containing cassette exons included versus those excluded in the indicated genotype comparisons (log scale).

expected. We therefore created an isogenic mouse leukemia model by retroviral overexpression of the *MLL–AF9* fusion oncogene in *Vav-Cre*$^{+}$*Srsf2*$^{+/+}$ or *Vav-Cre*$^{+}$*Srsf2*$^{P95H/+}$ BM cells (in which the *Vav* promoter drives hematopoietic-specific expression of the Cre recombinase) followed by transplantation into lethally irradiated recipient mice (**Supplementary Fig. 3a**). Overexpression of *MLL–AF9* in *Vav-Cre*$^{+}$*Srsf2*$^{+/+}$ or *Vav-Cre*$^{+}$*Srsf2*$^{P95H/+}$ BM cells resulted in fully penetrant AML with similar survival latencies and marked splenomegaly and hepatomegaly for both groups of mice (**Supplementary Fig. 3b,c**). Although *Srsf2*-mutated leukemias showed altered gene expression related to processes such as cell migration and response to external stimuli relative to their WT counterparts (**Supplementary Fig. 3d**), immunophenotype or histological and cytological analyses of BM, spleen, and liver revealed no obvious differences between the two genotypes (**Supplementary Fig. 3e–g**). We next examined the effects of pharmacological spliceosomal inhibition *in vivo*. To accomplish this, equal numbers of primary *MLL–AF9* leukemic cells from *Srsf2*$^{+/+}$ or *Srsf2*$^{P95H/+}$ mice were transplanted into secondary (2°) recipient mice to generate secondary leukemias, and the secondary recipient mice were then treated with either E7107 or vehicle (**Fig. 2e**). Ten days of intravenous (i.v.) administration of E7107 at 4 mg per kg of body weight per day (mg/kg/d) resulted in decreased disease burden—as assessed by peripheral blood leukocyte counts and the percentage of GFP^{+} cells (**Fig. 2f**), histological analyses (**Supplementary Fig. 3h**), and survival benefit in *Srsf2*$^{P95H/+}$ mice ($P = 0.001$)—whereas the same treatment regimen had no impact on overall survival of *Srsf2*$^{+/+}$ mice ($P = 0.621$) (**Fig. 2g**). E7107 treatment also improved anemia and thrombocytopenia in both *Srsf2*$^{+/+}$ or *Srsf2*$^{P95H/+}$ mice, with a slightly greater improvement observed in *Srsf2*$^{P95H/+}$ mice (**Supplementary Fig. 3i,j**).

To determine the mechanistic origins of the Srsf2-mutant-selective effects of E7107, we analyzed transcriptional changes after 5 d of E7107 treatment *in vivo* (**Fig. 3a**). Myeloid leukemic cells (marked by GFP^{+}Mac1^{+}) were purified from the BM of recipient mice exactly 3 h after the fifth dose of E7107 and subjected to RNA-seq analysis. E7107 exposure resulted in global splicing inhibition in both genotypes, typified by widespread intron retention and cassette exon skipping that is expected from inefficient splicing catalysis

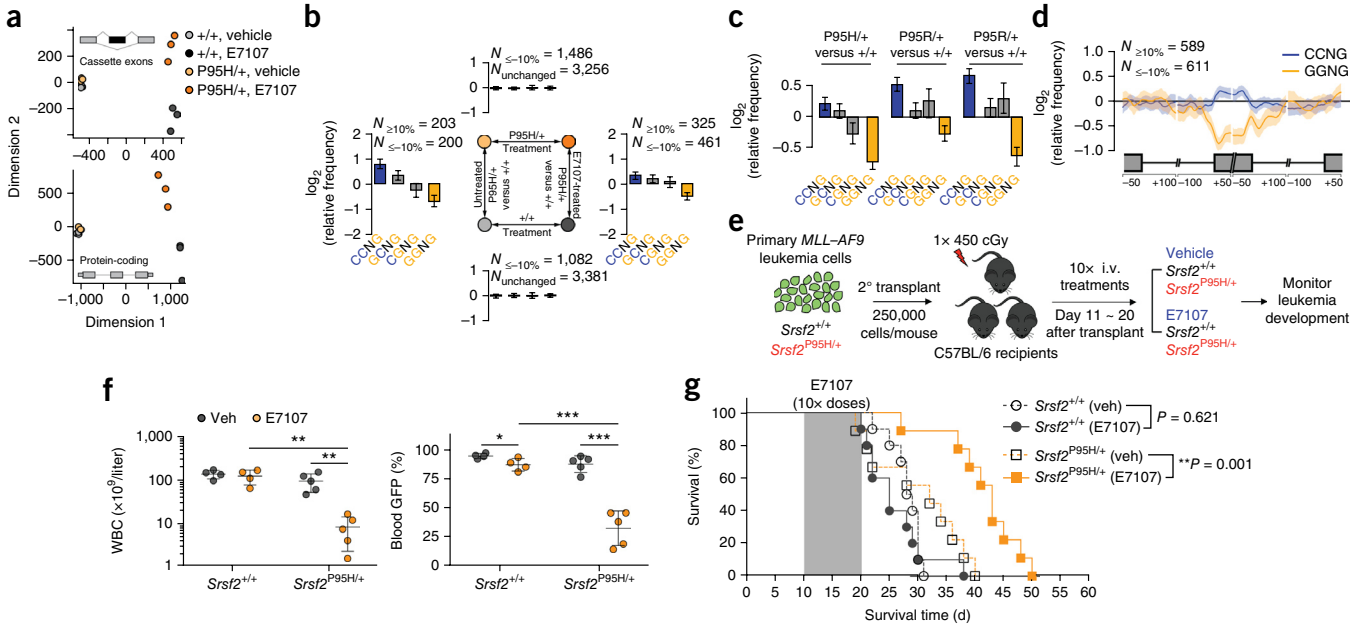

Figure 2 *SRSF2*-mutated myeloid leukemias are preferentially sensitive to pharmacologic modulation of splicing catalysis. (**a**) Multidimensional scaling using alternatively spliced cassette exons (top) and protein-coding genes (bottom) in LSK cells from the BM of *Mx1-Cre*$^{+}$*Srsf2*$^{P95H/+}$ and *Mx1-Cre*$^{+}$*Srsf2*$^{+/+}$ mice that were treated with vehicle or E7107 (4 mg/kg) for 5 d ($n = 3$ mice per group). (**b**) Mean enrichment of all variants of the SSNG ESE motif in cassette exons that were differentially included versus excluded in a two-factor comparison across all four experimental groups. $N_{\geq 10\%}$ and $N_{\leq -10\%}$ indicate the numbers of exons that exhibited increases and decreases in inclusion, respectively, of absolute magnitude ≥10% for the illustrated comparisons. For each comparison, enrichment was computed by comparing the indicated sets of exons (for example, cassette exons of each sequence from E7107-treated *Mx1-Cre*$^{+}$*Srsf2*$^{P95H/+}$ mice were compared with those from E7107-treated *Mx1-Cre*$^{+}$*Srsf2*$^{+/+}$ mice for the right-hand comparison). For sample comparisons where differentially spliced exons showing increased inclusion were not present (top and bottom), cassette exons that exhibited differential splicing of an absolute magnitude ≤10% were used as a background set to compute motif enrichment instead. The individual comparison that was used to generate each set of bar graphs is shown in the schema in the center of the figure. Error bars indicate 95% confidence intervals, as estimated by bootstrapping. (**c**) Mean enrichment of all variants of the SSNG ESE motif in individual *SRSF2*-mutant *MLL*-rearranged human AML samples relative to the median of 28 *SRSF2*-wildtype *MLL*-rearranged AML samples. Error bars indicate 95% confidence intervals estimated by bootstrapping. (**d**) Spatial distribution of CCNG and GGNG motifs along cassette exons that were included or excluded in the *SRSF2*-mutated samples relative to those in the median WT control among the *MLL*-rearranged AML samples. (**e**) Schematic of secondary transplantation experiments of mouse *MLL–AF9* leukemias in *Srsf2*$^{+/+}$ (*Vav-Cre*$^{+}$*Srsf2*$^{+/+}$) and *Srsf2*$^{P95H/+}$ (*Vav-Cre*$^{+}$*Srsf2*$^{P95H/+}$) backgrounds to test the effects of E7107 treatment *in vivo*. (**f**) WBC counts (left) and percentage of WBC cells expressing GFP (right) after 10 d of E7107 administration. (**g**) Kaplan–Meier survival curves of secondary recipient mice that were transplanted with *Srsf2*$^{+/+}$ or *Srsf2*$^{P95H/+}$ leukemic cells and treated with vehicle or E7107 (at 4 mg/kg) (*Srsf2*$^{+/+}$, $n = 10$ mice per group; *Srsf2*$^{P95H/+}$, $n = 9$ mice per group). Shaded area represents period of vehicle or E7107 dosing. Throughout, error bars represent mean ± s.d. $^{*}P < 0.05$; $^{**}P < 0.005$; $^{***}P < 0.001$; by Student's *t*-test.

(**Fig. 3b–d** (top and middle) and **Supplementary Fig. 4a**). Whereas E7107-induced splicing dysregulation was highly variable across animals in both *Srsf2*$^{P95H/+}$ and *Srsf2*$^{+/+}$ backgrounds, effects on global expression of protein coding genes was highly distinct between the genotypes (**Fig. 3b–d** (bottom) **Supplementary Fig. 4b,c**, and **Supplementary Table 1**). Moreover, the magnitude of splicing inhibition following E7107 treatment was more severe in *Srsf2*$^{P95H/+}$ versus *Srsf2*$^{+/+}$ mice, consistent with its differential effect on the survival of mice of these two genotypes (**Supplementary Fig. 4d**). GO analysis revealed that differentially expressed genes in *Srsf2*$^{P95H/+}$ relative to *Srsf2*$^{+/+}$ leukemic cells after E7107 treatment were enriched in biological pathways related to cytokine and immune signaling and to leukocyte activation and migration (**Supplementary Fig. 4e**).

Notably, genes involved in maintaining the leukemogenic programs in *MLL*-rearranged leukemias, including Dot1-like histone H3 methyltransferase (*Dot1l*) and Meis homeobox 1 (*Meis1*), were among the most differentially spliced genes in *Srsf2*$^{P95H/+}$ mice in response to E7107 treatment (**Fig. 3e** and **Supplementary Table 3**). Given the known importance of DOT1L to *MLL*-mediated leukemogenesis[17,18], we investigated the effects of E7107 treatment on *Dot1l* splicing further. Treatment with E7107 resulted in more pronounced exon skipping and intron retention within a region encoding the catalytic domain of the Dot1l protein in *MLL–AF9*;*Srsf2*$^{P95H/+}$ cells relative to their *MLL–AF9*;*Srsf2*$^{+/+}$ counterparts, which was readily detectable by RT–PCR and qRT–PCR during a time course of drug exposure (**Fig. 3f,g**). A similar increase in cassette exon skipping within *Meis1* was also observed by RT–PCR and qRT–PCR in *MLL–AF9*;*Srsf2*$^{P95H/+}$ cells as compared to that in *MLL–AF9*;*Srsf2*$^{+/+}$ cells (**Fig. 3f,g**). This increased mis-splicing in *Dot1l* and *Meis1* in the *Srsf2*-mutated background after E7107 exposure correlated with a mild decrease in Meis1 protein and Dot1l-mediated histone H3 Lys79 dimethylation (H3K79me2), indicating a reduction in Dot1l catalytic activity (**Supplementary Fig. 4f,g**). Conversely, exogenous re-expression of *DOT1L* cDNA resulted in a mild but consistent restoration in cellular proliferation in *MLL–AF9*;*Srsf2*$^{P95H/+}$ cells relative to that in *MLL–AF9*;*Srsf2*$^{+/+}$ cells after exposure to E7107 (**Supplementary Fig. 5a,b**). In contrast, *Meis1* overexpression was unable to rescue the inhibition of cell proliferation that was induced by E7107 treatment (**Supplementary Fig. 5c,d**). Of note, stable introduction of a previously identified point mutation in the gene splicing factor 3b, subunit 1 (*SF3B1*) known to cause E7107 resistance (*SF3B1*^{R1074H})[19] in *MLL–AF9*;*Srsf2*$^{P95H/+}$ cells (**Supplementary Fig. 5e–g**) rendered these cells almost completely insensitive to E7107, with a half-maximal inhibitory concentration (IC_{50}) nearly 300-fold greater than that

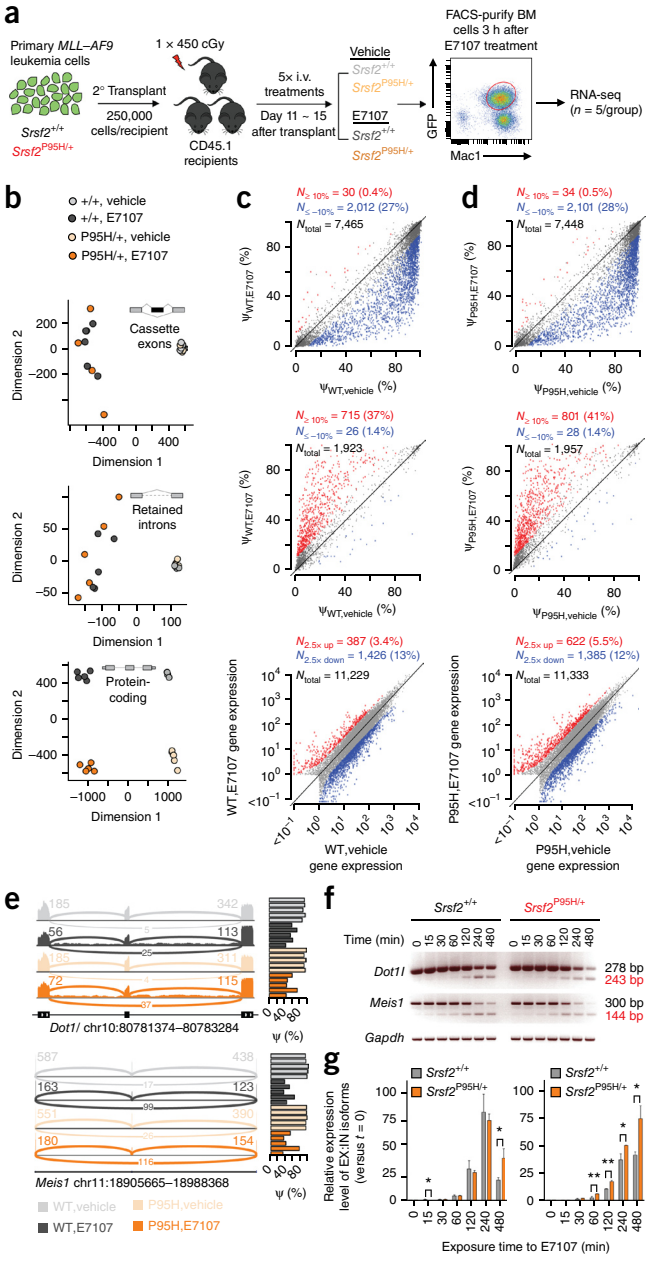

Figure 3 Splicing and gene expression changes in *Srsf2*-WT or *Srsf2*-mutated leukemia cells that were treated with E7107. (**a**) Schematic of secondary transplantation experimentation, with E7107 treatment for a defined amount of time followed by euthanization of the mice for RNA-seq analyses. Sublethally irradiated mice were transplanted with *MLL–AF9*;*Srsf2*$^{+/+}$ or *MLL–AF9*;*Srsf2*$^{P95H/+}$ primary leukemias, followed by treatment with E7107 (4 mg/kg/d) or vehicle for 5 d. GFP^{+}Mac1^{+} BM cells that were sorted 3 h after the fifth treatment were used for RNA-seq ($n = 5$ mice per group). (**b**) Multidimensional scaling analysis of all 20 mice from **a**, on the basis of alternatively spliced cassette exons ($N = 6{,}369$) (top), alternatively spliced retained introns ($N = 1{,}791$) (middle), and expressed protein-coding genes ($N = 9{,}339$) (bottom). (**c**,**d**) Scatter plots of cassette exon splicing (isoform ratios represented as percentage spliced in (PSI, Ψ) values) (top), retained introns (Ψ values) (middle), and gene expression (normalized expression values) (bottom) from *MLL–AF9*;*Srsf2*$^{+/+}$ (**c**) or *MLL–AF9*;*Srsf2*$^{P95H/+}$ (**d**) mice that were treated with vehicle or E7107. Percentages indicate the fraction of differentially spliced cassette exons or retained introns (inclusion rates increased or decreased by absolute magnitude ≥10% with $P < 0.01$) or the number of differentially expressed genes (fold change ≥ 2.5 with $P < 0.01$). Red and blue dots represent individual splicing events or coding genes whose expression is increased or decreased after treatment with E7107 versus vehicle, respectively. (**e**) Sashimi plots[28,29] across splice junctions surrounding differentially spliced cassette exons in *Dot1l* (top) and *Meis1* (bottom), with reads summarized across five replicate mice. Bar plots represent the percentage of spliced (ψ) cassette exon inclusion ratios across all samples. (**f**) Representative RT–PCR analysis of the effect of acute exposure to E7107 (10 nM) on splicing of *Dot1l* and *Meis1* in *MLL–AF9*;*Srsf2*$^{+/+}$ and *MLL–AF9*;*Srsf2*$^{P95H/+}$ leukemia cells *in vitro* ($n = 3$ biological replicates per group). (**g**) Quantification, by qRT–PCR, of the relative levels of exclusion (EX) and inclusion (IN) isoforms of *Dot1l* (left) and *Meis1* (right) following acute exposure to E7107 (10 nM) *in vitro* ($n = 3$ biological replicates per group). Error bars represent mean ± s.d. $^{*}P < 0.05$; $^{**}P < 0.01$; by Student's *t*-test.

of the parental or *SF3B1*^{WT}-overexpressing cells (**Supplementary Fig. 5h**). *SF3B1*^{R1074H}-expressing cells were also impervious to E7107-mediated inhibition of splicing (**Supplementary Fig. 5h**,**i**). Collectively, our data suggest that E7107 treatment induces phenotypic changes in *MLL–AF9* leukemia through aberrant splicing of multiple downstream targets, including *Dot1l* and *Meis1*, and provides genetic confirmation that E7107 affects cells through on-target inhibition of SF3B1.

Given that the above-mentioned data were generated in the specific context of *MLL*-rearranged mouse leukemias, we next sought to analyze the effect of splicing inhibition in the context of human AMLs in which endogenous *SRSF2* mutations also co-occur with a spectrum of mutations commonly found in myeloid leukemias. First, we tested the effect of E7107 on a previously described cassette exon inclusion event in the polycomb repressive complex (PRC) 2–subunit-encoding gene enhancer of zeste 2 (*EZH2*)[5] in human leukemia cell lines that were WT (TF-1) or mutated (K052) for *SRSF2*. RT–PCR and qRT–PCR analyses revealed that E7107 treatment inhibits SRSF2 mutant-specific *EZH2* mis-splicing in a dose-dependent manner (**Fig. 4a**,**b**). Next, to evaluate *in vivo* drug effects in primary human AMLs, we generated patient-derived xenografts (PDXs) from a cohort of patients with primary AML ($n = 2$ without a spliceosomal gene mutation, $n = 3$ with a spliceosomal gene mutation; **Supplementary Table 4**). Primary leukemia cells from each individual patient were transplanted via tail-vein injection into ten adult immunodeficient NOD–Scid *Il2rg*^{null} (NSG) mice. After the human CD45^{+} cells reached >25% of the total cells in the BM of NSG mice (median of 86 d after transplantation; range 62–148 d), mice were treated with E7107 (4 mg/kg/d) or vehicle for 10 d (**Fig. 4c**). In each PDX model, targeted genomic analysis of purified human leukemic cells from the BM confirmed faithful engraftment of the major leukemic clones that were found in the primary patient samples (**Supplementary Fig. 6a**) and revealed that spliceosomal gene mutations were present in the major leukemic clones following E7107 treatment *in vivo* (**Supplementary Fig. 6b**). All spliceosome-mutant AML PDXs showed significant reductions in human leukemic burden in response to E7107 treatment, whereas the response in AML cells that were WT for splicing was less robust (**Fig. 4d**,**e**). Further examination revealed that two of three spliceosome-mutant AMLs had a substantial decrease in hCD45^{+} hCD34^{+} HSPC subsets (**Supplementary Fig. 6c**). In contrast, AMLs that were WT for splicing showed less substantial reductions in leukemic cells, as well as in hCD45^{+} hCD34^{+} cell subsets (**Fig. 4d**,**e** and **Supplementary Fig. 6c–e**). Although E7107 treatment resulted in reduced cell proliferation 3 h after treatment *in vivo* regardless of spliceosome mutational status (**Fig. 4f**), the preferential sensitivity to E7107 in spliceosome-mutant AML was associated with substantially increased apoptosis only in spliceosome-mutant PDX samples (**Fig. 4g**,**h** and **Supplementary Fig. 6f**). These data establish

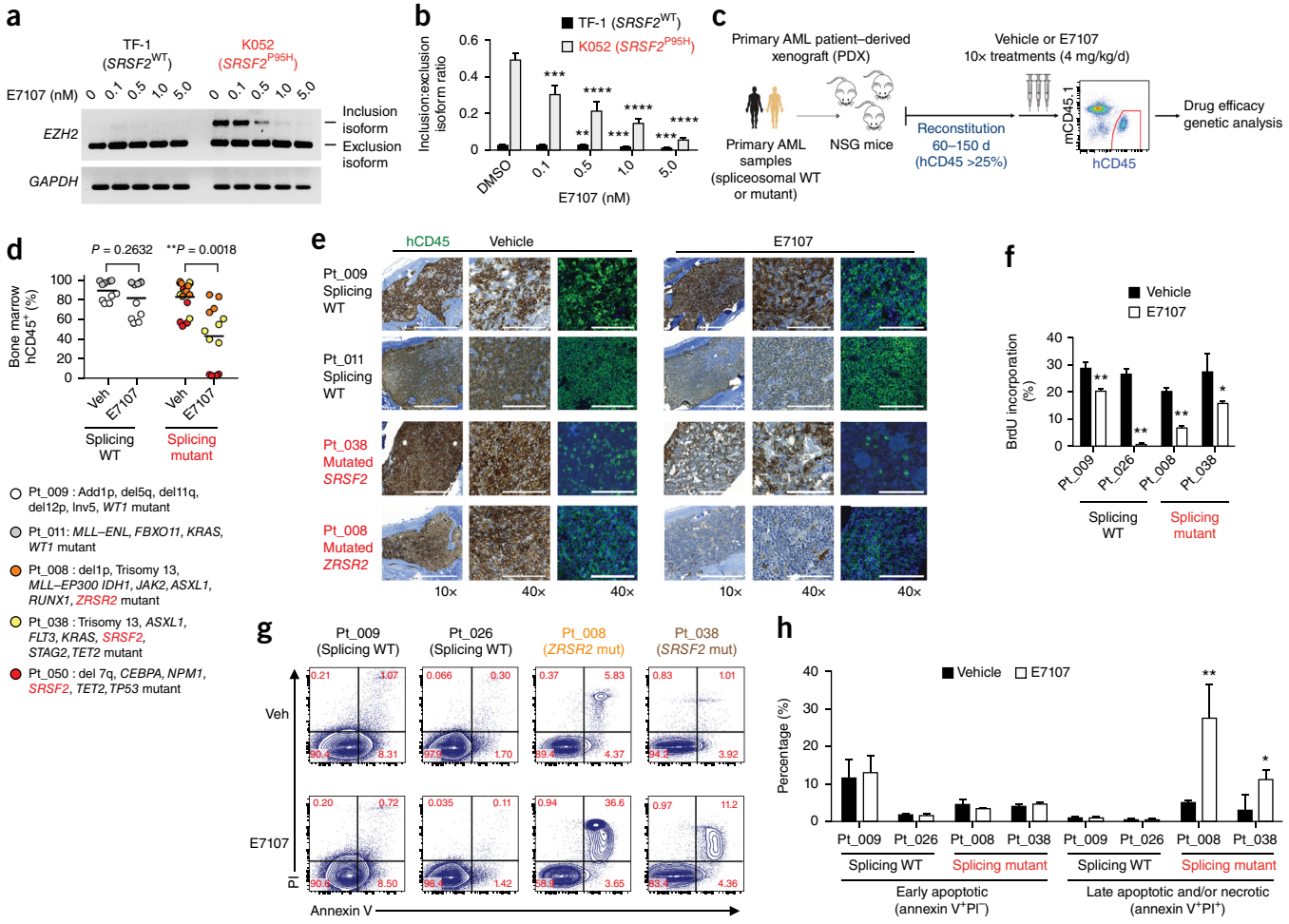

Figure 4 Preferential sensitivity of primary human leukemias to pharmacologic modulation of splicing *in vivo* with E7107. (**a**,**b**) Representative RT–PCR analysis (**a**) and quantification, by qRT–PCR, (**b**) of the effect of E7107 exposure (6 h), relative to DMSO treatment, on expression of a cassette exon inclusion isoform ('poison' exon) of *EZH2* in leukemia cell lines that are either WT (TF-1) or mutated (K052) for *SRSF2*. (**c**) Schema of patient-derived xenograft (PDX) experiments, using engraftment of primary human AML samples (either WT or mutated for spliceosomal genes) into NSG mice. (**d**) Quantification of human CD45 chimerism (hCD45+) (from PDX samples from patients (Pts.) with AML who have (indicated in color) or do not have mutations in spliceosomal genes) in the BM of NSG recipient mice after 10 d of treatment with vehicle or E7107 (4 mg/kg/d). Each circle represents the hCD45 value for an individual NSG mouse, and each color represents the PDX from a specific patient. Mutational data for each patient are listed below the graph. (**e**) Representative immunohistochemical and immunofluorescence analysis for hCD45 in BM sections of recipient mice shown in **d**. Scale bars, 200 µm (10× images) and 50 µm (40× images). (**f**) BM hCD45+ cells in S phase, on the basis of *in vivo* BrdU incorporation after 5 d of treatment with E7107 (4 mg/kg/d) or vehicle. (**g**,**h**) Representative FACS plots of annexin V and propidium iodide (PI) staining of hCD45 cells following 5 d of E1707 (4 mg/kg/d) (bottom) or vehicle (top) treatment *in vivo* (**g**) and quantification of annexin V+PI– or annexin V+PI+ hCD45+ cells (**h**). In **f**,**g**,**h**: for Pt_009, $n = 3$ mice; for Pt_026, $n = 2$ mice; for Pt_008, $n = 4$ mice; for Pt_038, $n = 3$ mice. Throughout, error bars represent mean ± s.d. $^{*}P < 0.05$; $^{**}P < 0.01$; $^{***}P < 0.001$; $^{****}P < 0.0001$; by Student's *t*-test.

a relationship between sensitivity to E7107 and the mutational status of spliceosomal genes in primary AMLs.

Whereas splicing is an essential process required for the normal function of all mammalian cells, here we provide both genetic and pharmacologic evidence that SRSF2-mutant leukemias are preferentially sensitive to splicing modulation *in vivo* relative to SRSF2-WT leukemias. Genomic and biological analyses of cells expressing mutant SRSF2 in the absence of the WT protein indicated that the *SRSF2* mutation, despite being selected for in human leukemia[1,5], is unable to, on its own, support gene expression and splicing patterns required for hematopoiesis. The sensitivity of *SRSF2*-mutated leukemias to loss of the WT *SRSF2* allele was mirrored by the exposure of leukemias bearing heterozygous *SRSF2* mutations to E7107, an inhibitor of splicing[8]. Because mutations affecting the spliceosomal proteins SF3B1 and U2AF1 are also found in an exclusively heterozygous context, it will be important to determine whether the broad range of malignancies carrying diverse spliceosomal gene mutations may prove similarly sensitive to pharmacologic perturbation of normal splicing catalysis.

Given the high frequency of *SRSF2* mutations across myeloid malignancies[1,20,21], the adverse outcome associated with *SRSF2* mutations[20,22,23], and the need for novel therapeutic approaches for these disorders, the data provided here have important therapeutic implications for patients with MDS and AML who have genetic alterations in *SRSF2*. E7107 is one of a host of structurally distinct splicing inhibitors, all of which hinder normal splicing in a similar manner by inhibiting SF3B1 function[24,25]. The only such compound that has been tested in humans to date is E7107, for which there are two completed phase 1 dose-escalation studies for patients with advanced

solid tumors. In patients treated with E7107, inhibition of splicing was observed during dose escalation, and the dose-limiting toxicity was primarily gastrointestinal related; however, visual impairment was reported in 3/66 patients[26,27]. The data presented here demonstrate that SF3B1 inhibition has therapeutic potential for the treatment of malignancies with *SRSF2* mutations; clinical studies with newly identified SF3B1 inhibitors will be essential to define the safety and therapeutic efficacy of this approach in patients. Moreover, ongoing efforts to understand how pharmacological inhibitors of splicing alter the constellation of proteins that directly or indirectly bind to SF3B1, and how mutations affecting splicing factors might alter protein–protein interactions, will facilitate the future development of compounds with heightened specificity for cells with mutant spliceosomes.

METHODS

Methods and any associated references are available in the online version of the paper.

Accession codes. Gene Expression Omnibus: all newly generated RNA-seq data were deposited under accession number GSE74064.

Note: Any Supplementary Information and Source Data files are available in the online version of the paper.

ACKNOWLEDGMENTS

This work was supported by the Leukemia and Lymphoma Society (S.C.-W.L. and O.A.-W.), the US Department of Defense Breast Cancer Research Program grant W81XWH-14-1-0044 (H.D.), the US Department of Defense Bone Marrow Failure Research Program grants BM150092 (O.A.-W.) and W81XWH-12-1-0041 (R.K.B. and O.A.-W.), the Worldwide Cancer Research Fund (E.K.), the Fondation de France (J.-B.M.), the American Society of Hematology (B.H.D. and O.A.-W.), the Edward P. Evans Foundation (R.K.B. and O.A.-W.), the US National Institutes of Health (NIH)-NHLBI grant R01 HL128239 (R.K.B. and O.A.-W.), the NIH–NCI grant 1K08CA160647-01 (O.A.-W.), the Ellison Medical Foundation grant AG-NS-1030-13 (R.K.B.), the Damon Runyon Foundation (R.K.B. and O.A.-W.), the NIH–NIDDK grant R01 DK103854 (R.K.B.), the Starr Foundation grant I8-A8-075 (O.A.-W.), the Josie Robertson Investigator Program (O.A.-W.), the Mr. William H. Goodwin and Mrs. Alice Goodwin Commonwealth Foundation for Cancer Research (O.A.-W.), and the Experimental Therapeutics Center of MSKCC (O.A.-W.).

AUTHOR CONTRIBUTIONS

S.C.-W.L., H.D., E.K., R.K.B., and O.A.-W. designed the study; S.C.-W.L., E.K., H.C., Y.R.C., J.-B.M., B.H.D., A.Y., Y.J.K., C.-W.C., A.P., J.T., X.W., A.K., S.A.A., and O.A.-W. performed experiments; H.D. and R.K.B. performed RNA-seq analysis; M.T., J.P., S.B., and P.G.S. provided E7107 and advice with drug-dosing experiments; and S.C.-W.L., H.D., E.K., C.L., R.K.B., and O.A.-W. prepared the manuscript with help from all co-authors.

COMPETING FINANCIAL INTERESTS

The authors declare competing financial interests: details are available in the online version of the paper.

1. Yoshida, K. *et al.* Frequent pathway mutations of splicing machinery in myelodysplasia. *Nature* **478**, 64–69 (2011).
2. Papaemmanuil, E. *et al.* Somatic *SF3B1* mutation in myelodysplasia with ring sideroblasts. *N. Engl. J. Med.* **365**, 1384–1395 (2011).
3. Graubert, T.A. *et al.* Recurrent mutations in the *U2AF1* splicing factor in myelodysplastic syndromes. *Nat. Genet.* **44**, 53–57 (2012).
4. Shirai, C.L. *et al.* Mutant U2AF1 expression alters hematopoiesis and pre-mRNA splicing *in vivo*. *Cancer Cell* **27**, 631–643 (2015).
5. Kim, E. *et al. SRSF2* mutations contribute to myelodysplasia by mutant-specific effects on exon recognition. *Cancer Cell* **27**, 617–630 (2015).
6. Ilagan, J.O. *et al. U2AF1* mutations alter splice site recognition in hematological malignancies. *Genome Res.* **25**, 14–26 (2015).
7. Folco, E.G., Coil, K.E. & Reed, R. The antitumor drug E7107 reveals an essential role for SF3b in remodeling U2 snRNP to expose the branch point-binding region. *Genes Dev.* **25**, 440–444 (2011).
8. Kotake, Y. *et al.* Splicing factor SF3b as a target of the antitumor natural product pladienolide. *Nat. Chem. Biol.* **3**, 570–575 (2007).
9. Lindsley, R.C. *et al.* Acute myeloid leukemia ontogeny is defined by distinct somatic mutations. *Blood* **125**, 1367–1376 (2015).
10. Genovese, G., Jaiswal, S., Ebert, B.L. & McCarroll, S.A. Clonal hematopoiesis and blood-cancer risk. *N. Engl. J. Med.* **372**, 1071–1072 (2015).
11. Xie, M. *et al.* Age-related mutations associated with clonal hematopoietic expansion and malignancies. *Nat. Med.* **20**, 1472–1478 (2014).
12. Genovese, G. *et al.* Clonal hematopoiesis and blood-cancer risk inferred from blood DNA sequence. *N. Engl. J. Med.* **371**, 2477–2487 (2014).
13. Katz, Y., Wang, E.T., Airoldi, E.M. & Burge, C.B. Analysis and design of RNA sequencing experiments for identifying isoform regulation. *Nat. Methods* **7**, 1009–1015 (2010).
14. Wagenmakers, E.J., Lodewyckx, T., Kuriyal, H. & Grasman, R. Bayesian hypothesis testing for psychologists: a tutorial on the Savage–Dickey method. *Cognit. Psychol.* **60**, 158–189 (2010).
15. Zhang, J. *et al.* Disease-associated mutation in *SRSF2* misregulates splicing by altering RNA-binding affinities. *Proc. Natl. Acad. Sci. USA* **112**, E4726–E4734 (2015).
16. Lavallée, V.P. *et al.* The transcriptomic landscape and directed chemical interrogation of *MLL*-rearranged acute myeloid leukemias. *Nat. Genet.* **47**, 1030–1037 (2015).
17. Daigle, S.R. *et al.* Selective killing of mixed lineage leukemia cells by a potent small-molecule DOT1L inhibitor. *Cancer Cell* **20**, 53–65 (2011).
18. Bernt, K.M. *et al. MLL*-rearranged leukemia is dependent on aberrant H3K79 methylation by DOT1L. *Cancer Cell* **20**, 66–78 (2011).
19. Yokoi, A. *et al.* Biological validation that SF3b is a target of the antitumor macrolide pladienolide. *FEBS J.* **278**, 4870–4880 (2011).
20. Papaemmanuil, E. *et al.* Clinical and biological implications of driver mutations in myelodysplastic syndromes. *Blood* **122**, 3616–3627, quiz 3699 (2013).
21. Bejar, R. *et al.* Validation of a prognostic model and the impact of mutations in patients with lower-risk myelodysplastic syndromes. *J. Clin. Oncol.* **30**, 3376–3382 (2012).
22. Zhang, S.J. *et al.* Genetic analysis of patients with leukemic transformation of myeloproliferative neoplasms shows recurrent *SRSF2* mutations that are associated with adverse outcome. *Blood* **119**, 4480–4485 (2012).
23. Vannucchi, A.M. *et al.* Mutations and prognosis in primary myelofibrosis. *Leukemia* **27**, 1861–1869 (2013).
24. Effenberger, K.A., Urabe, V.K., Prichard, B.E., Ghosh, A.K. & Jurica, M.S. Interchangeable SF3B1 inhibitors interfere with pre-mRNA splicing at multiple stages. *RNA* **22**, 350–359 (2016).
25. Bonnal, S., Vigevani, L. & Valcárcel, J. The spliceosome as a target of novel antitumor drugs. *Nat. Rev. Drug Discov.* **11**, 847–859 (2012).
26. Eskens, F.A. *et al.* Phase 1 pharmacokinetic and pharmacodynamic study of the first-in-class spliceosome inhibitor E7107 in patients with advanced solid tumors. *Clin. Cancer Res.* **19**, 6296–6304 (2013).
27. Hong, D.S. *et al.* A phase 1, open-label, single-arm, dose-escalation study of E7107, a precursor messenger ribonucleic acid (pre-mRNA) splicesome inhibitor, administered intravenously on days 1 and 8 every 21 days to patients with solid tumors. *Invest. New Drugs* **32**, 436–444 (2014).
28. Katz, Y. *et al.* Quantitative visualization of alternative exon expression from RNA-seq data. *Bioinformatics* **31**, 2400–2402 (2015).
29. Thorvaldsdóttir, H., Robinson, J.T. & Mesirov, J.P. Integrative genomics viewer (IGV): high-performance genomics data visualization and exploration. *Brief. Bioinform.* **14**, 178–192 (2013).

ONLINE METHODS

Mice. All mice were housed at Memorial Sloan Kettering Cancer Center (MSKCC). All animal procedures were completed in accordance with the Guidelines for the Care and Use of Laboratory Animals[30] and were approved by the Institutional Animal Care and Use Committees at MSKCC. The number of mice in each experiment was chosen to provide 90% statistical power with a 5% error level. Generation and genotyping of the *Srsf2*$^{P95H/+}$ conditional knock-in mice as well as the *Srsf2* conditional-knockout mice (both on the C57BL/6 background) were as previously described[5,31]. For *MLL–AF9* BM transplantation assays, *Srsf2*$^{P95H/+}$ and littermate control mice were crossed to *Vav-Cre* transgenic mice[32].

Peripheral blood analysis. Blood was collected by retro-orbital bleeding using heparinized microhematocrit capillary tubes (Thermo Fisher Scientific). Automated peripheral blood counts were obtained using an IDEXX ProCyte Dx Hematology Analyzer. Differential blood counts were scored on blood smears stained using Wright–Giemsa stain and visualized using an Axio Observer A1 microscope.

Histological analyses. Mice were euthanized and autopsied, and the dissected tissue samples were fixed in 4% paraformaldehyde, dehydrated, and embedded in paraffin. Paraffin blocks were sectioned at 4 μm and stained with hematoxylin and eosin (H&E). Images were acquired using an Axio Observer A1 microscope (Carl Zeiss) or scanned using a MIRAX Scanner (Zeiss).

Bone marrow (BM) transplantation assays. Freshly dissected femora and tibiae were isolated from *Mx1-Cre*$^{+}$*Srsf2*$^{+/+}$, *Mx1-Cre*$^{+}$*Srsf2*$^{+/fl}$, *Mx1-Cre*$^{+}$*Srsf2*$^{P95H/+}$, or *Mx1-Cre*$^{+}$*Srsf2*$^{P95H/fl}$ CD45.2^{+} mice of both sexes. BM was flushed with a 3-ml insulin syringe into cold PBS (without Ca^{2+} and Mg^{2+}), supplemented with 2% bovine serum albumin, to generate single-cell suspensions. BM cells were pelleted by centrifugation at 1,500 r.p.m. for 5 min, and the red blood cells (RBCs) were lysed in ammonium chloride–potassium bicarbonate lysis (ACK) buffer for 5 min on ice. After centrifugation, cells were resuspended in PBS with 2% BSA, passed through a 40-μm cell strainer, and counted. For competitive transplantation experiments, 0.5×10^6 BM cells from *Mx1-Cre*$^{+}$*Srsf2*$^{+/+}$, *Mx1-Cre*$^{+}$*Srsf2*$^{+/fl}$, *Mx1-Cre*$^{+}$*Srsf2*$^{P95H/+}$, or *Mx1-Cre*$^{+}$*Srsf2*$^{P95H/fl}$ CD45.2^{+} mice were mixed with 0.5×10^6 wild-type CD45.1^{+} support BM and transplanted via tail vein injection into 6-week-old lethally irradiated (900 cGy) female CD45.1^{+} recipient mice. To activate the conditional alleles, mice were treated with three doses of polyinosinic:polycytidylic acid (polyI:C; 12 mg/kg/d; GE Healthcare) every second day via intraperitoneal injection. Peripheral blood chimerism was assessed every 4 weeks by flow cytometry. For noncompetitive transplantation experiments, 1×10^6 total BM cells from *Mx1-Cre*$^{+}$*Srsf2*$^{+/+}$, *Mx1-Cre*$^{+}$*Srsf2*$^{+/fl}$, *Mx1-Cre*$^{+}$*Srsf2*$^{P95H/+}$, or *Mx1-Cre*$^{+}$*Srsf2*$^{P95H/fl}$ CD45.2^{+} mice were injected into lethally irradiated (900 cGy) CD45.1^{+} recipient mice. Peripheral blood chimerism was assessed as described for competitive transplantation experiments. Additionally, for each bleeding, whole-blood cell counts were measured on an automated blood analyzer. Animals that failed to engraft (<1% CD45.2 chimerism in peripheral blood) or were lost due to poly(I:C) toxicity were excluded from analysis.

Xenografts of primary human AML samples. Studies were approved by the Institutional Review Boards of Memorial Sloan Kettering Cancer Center and Fred Hutchinson Cancer Research Center and conducted in accordance to the Declaration of Helsinki protocol. Primary human AML samples derived from whole peripheral blood or BM MNCs were depleted of CD3^{+} T lymphocytes and transplanted via tail vein injection into 6-week-old NOD–Scid *Il2rg*^{null} (NSG) mice (Jackson Laboratory) conditioned with 200 cGy of gamma irradiation. Mice were bled monthly to assess the presence of human CD45^{+} cells in the blood. If hCD45^{+} was >1%, then BM aspiration was performed to assess BM hCD45 chimerism.

Retroviral transduction and transplantation of primary hematopoietic cells. *Vav-Cre*$^{+}$*Srsf2*$^{+/+}$ and *Vav-Cre*$^{+}$*Srsf2*$^{P95H/+}$ mice were treated with a single dose of 5-fluorouracil (150 mg/kg) followed by BM harvest from the femora, tibiae and hip bones 6 d later. RBCs were removed by ACK lysis buffer, and nucleated BM cells were transduced with viral supernatants containing murine stem cell virus (MSCV)-driven *MLL–AF9* fusion oncogene in a construct tagged with *GFP* reported from an internal ribosomal entry site (MSCV-*MLL–AF9*-IRES-*GFP*) for 2 d in Iscove's modified Dulbecco's medium (IMDM) with 15% fetal calf serum (FCS) supplemented with mouse stem cell factor (mSCF) (25 ng/ml), mouse interleukin (IL)-3 (10 ng/ml) and mouse IL-6 (10 ng/ml), followed by injection of ~400,000 cells per recipient mouse via tail vein injection into lethally irradiated (900 cGy) CD45.1 mice. For secondary transplantation experiments, 6-week-old, sublethally irradiated (450 cGy) C57/BL6 recipient mice were injected with 250,000 primary *MLL–AF9* leukemic cells. For *Srsf2* hemizygous rescue experiments, *Srsf2*$^{P95H/fl}$ and *Mx1-Cre*$^{+}$*Srsf2*$^{P95H/fl}$ fetal liver cells (embryonic day (E) 12.5–E14.5) were c-Kit-enriched using CD117 MicroBeads (MACS, Miltenyi Biotec) and transduced with viral supernatants containing MSCV-*MLL–AF9*-IRES-GFP twice for 2 d in IMDM with 15% FCS supplemented with mSCF (100 ng/ml), mouse thrombopoietin (mTPO; 50 ng/ml), mouse FLT3 ligand (mFLT3-L; 5 ng/ml), and mouse IL-6 (10 ng/ml), followed by tail vein injection of ~500,000 cells into lethally irradiated (900 cGy) CD45.1 recipient mice. All cytokines were purchased from R&D Systems.

Flow cytometry analyses and antibodies. Surface marker staining of hematopoietic cells was performed by first lysing cells with ACK lysis buffer and then washing the cells with ice-cold PBS. Cells were stained with antibodies in PBS with 2% BSA for 30 min on ice. For hematopoietic stem and progenitor cell staining, cells were stained with a specific lineage-positive antibody cocktail, including antibodies specific for B220 (RA3-6B2), CD3 (17A2), CD4 (RM4-5), Gr-1 (RB6-8C5), Mac1 (M1/70), NK1.1 (PK136), and Ter119 (all from BioLegend), allowing for mature lineage exclusion from the analysis. Cells were also stained with monoclonal antibodies against c-Kit (2B8), Sca1 (D7), Fc-γRII and Fc-γRIII (2.4G2), CD34 (RAM34), CD45.1 (A20), CD45.2 (104), CD48 (HM48-1), and CD150 (9D1) (all from eBioscience). The composition of mature hematopoietic cell lineages in the BM, spleen and peripheral blood was assessed using a combination of Mac1, Gr-1, B220, CD19, CD4 and CD8 staining. For analysis of human cell populations in mouse xenograft experiments, BM mononuclear cells and peripheral blood mononuclear cells were stained with a combination of antibodies against hCD3 (SK7), hCD19 (HIB19), hCD33 (WM-53), hCD34 (4H11), hCD38 (HIT2), and hCD45 (HI30) (all from eBioscience). Antibodies against mouse CD45.1 (A20) and Ter119 were used to exclude host-derived cells. DAPI was used to exclude dead cells. The final staining volume was 100 μl, and the final concentration for all antibodies used was 1:200, except for CD34 (1:50), c-Kit (1:100), and CD150 (1:100). For *in vivo* apoptosis experiments, BM cells were harvested from NSG mice 3 h after E7107 treatment. Cells were stained with an allophycocyanin (APC)-conjugated annexin V antibody in annexin V binding buffer (BD Pharmingen) to detect cells undergoing apoptosis, according to the manufacturer's instructions. For assessment of the effect of E7107 treatment on cell cycle status *in vivo*, 5-bromo-2′-deoxyuridine (BrdU; 0.1 mg per g body weight (mg/g)) was administered via intraperitoneal injection to NSG mice 24 h before drug treatment. BM cells were harvested 3 h after E7107 treatment, and the detection of BrdU incorporation was performed following the manufacturer's instructions (BD Pharmingen) Propidium iodide (PI) was used as a counter stain in both the annexin V and BrdU experiments. All FACS sorting was performed on FACS Aria, and analysis was performed on an LSRII or LSR Fortessa (BD Biosciences). For western blotting, the following antibodies to the following proteins were used: H3K79me2 (Abcam; Ab-3594), histone H3 (Cell Signaling Technologies; D1-H2), Meis1 (Abcam; Ab-124686), Sf3b1/Sap-155 (MBL; D221-3), Flag-M2 (Sigma-Aldrich; F-1084) and β-actin (Sigma-Aldrich; A-5441). All primary antibodies for western blotting were diluted to a final concentration of 1:1,000, in either 5% BSA (Sigma-Aldrich) in 0.05% TBS–Tween 20 (TBS-T) or 5% skim milk in 0.05% TBS-T.

Administration of spliceosome modulator E7107 *in vitro* and *in vivo*. For all *in vitro* experiments E7107 was dissolved in DMSO. For drug-sensitivity studies, cells were exposed to E7107 from a range of 10 μM to 0.05 nM. For *in vivo* administration, E7107 was dissolved in vehicle (10% ethanol and 4% Tween-80 in sterile PBS) and administered via intravenous (i.v.) injection at

4 mg/kg/d. For drug-efficacy studies, randomization was done by conducting WBC analysis before the start of drug administration and confirming that WBC count averages were equivalent in treatment and vehicle groups. All mice received ten consecutive doses of E7107. No blinding was done in the *in vivo* drug studies or in data analysis. For RNA-seq analysis in the mouse *MLL–AF9* leukemia model, five consecutive doses of E7107 were administered to the mice. The mice were euthanized 3 h after receiving the last dose, and BM Mac1$^+$ GFP$^+$ cells were purified by flow cytometry.

Cell culture. K052 leukemia cells were purchased from the Japanese Collection of Research Bioresources (JCRB) Cell Bank (JCRB0123) and were cultured in RPMI medium (made in-house at MSKCC) with 10% FCS. TF-1 cells were purchased from Deutsche Sammlung von Mikroorganismen und Zellkulturen (DSMZ; ACC344); these cells were cultured in RPMI medium with 10% FCS supplemented with human granulocyte–macrophage colony-stimulating factor (hGM-CSF) (R&D Systems; 5 ng/ml). Primary mouse *MLL–AF9* leukemia cell lines were generated from BM cells of leukemia-bearing mice and maintained in IMDM with 15% FCS, supplemented with L-glutamine, mSCF (20 ng/ml), mouse IL-3 (10 ng/ml), and mouse IL-6 (10 ng/ml). All cell lines have been tested for mycoplasma contamination and authenticated to confirm the status of the *SRSF2* mutation.

MSCV-Flag-Bio-*DOT1L*-Puro, MSCV-*Meis1*-IRES-Puro, and MSCV-IRES-Puro constructs were used for overexpression studies. Retroviral supernatants were produced by transfecting 293 GPII cells (Clontech Laboratories) with cDNA constructs and the packaging plasmid VSV.G using XtremeGene9 (Roche) and were used to transduce *MLL–AF9* leukemic cells in the presence of polybrene (5 μg/ml), followed by puromycin selection (1 μg/ml; Invitrogen) for successfully transduced cells. Cells were treated with E7107 (0.5 nM) or DMSO in 96-well plate format and were changed into fresh medium containing E7107 or DMSO every 2 d. Relative cell growth was assessed on day 6 after E7107 exposure using the LSR Canto.

Overexpression of the *SF3B1*^{WT} or *SF3B1*^{R1074H} allele was introduced into *MLL–AF9*;*Srsf2*$^{P95H/+}$ leukemic cells using the PiggyBac transposon system (**Supplementary Fig. 5e**). 2 μg of PiggyBac Transposase construct (CMV-PB-Transposase-IRES-TK-HSV) and 6 μg of either the *SF3B1*^{WT} (ITR-CAG-Flag-*SF3B1*^{WT}-IRES-Puro-ITR) or the *SF3B1*^{R1074H} (ITR-CAG-Flag-*SF3B1*^{R1074H}-IRES-Puro-ITR) cDNA construct were electroporated into 2 × 10^6 cells (in a 200-μl volume) using the Amaxa Nucleofector Protocol (Program T-003) according to the manufacturer's instructions (Lonza). Puromycin selection (1 μg/ml) was initiated 4 d after electroporation to select for cells that successfully incorporated the constructs. Sanger sequencing was performed to confirm successful integration of the cDNA plasmid using the primers Fwd: TCCAATCAAAGATCTTCTTCCAA and Rev: GAGCAGGTTTCTGCAACGAT.

***In vitro* cell viability assays.** Cells were seeded in white flat-well 96-well plates (Costar) at a density of 10,000 cells per well. ATP luminescence readings were taken 48 h after E7107 treatment using Cell Titer Glo (Promega) according to the manufacturer's instructions.

Semi-quantitative and quantitative RT–PCR. Total RNA was isolated using the RNeasy Mini or Micro Kit (Qiagen). For cDNA synthesis, total RNA was reverse-transcribed with the SuperScript VILO cDNA Synthesis kit (Life Technologies). Primers used in the RT–PCR reactions were: *Dot1l* (exons 11–13), Fwd: ACTTGAGTGACATTGGCACCA, Rev: AGCACCAGAATCCGCGGGG; *Meis1* (exons 7–9), Fwd: CGGCATCCACTCGTTCAG, Rev: TCACTTGAAG GATGGTAAGTCCT; *Gapdh*, Fwd: CCATGACAACTTTGGCATTG, Rev: CCTG CTTCACCACCTTCTTG; *EZH2* (exons 9–10), Fwd: TTTCATGCAACA CCCAACACT, Rev: CCCTGCTTCCCTATCACTGT. The PCR cycling conditions chosen were as follows: 33 cycles of (i) 45 s at 95 °C; (ii) 45 s at 52 °C; (iii) 60 s at 72 °C; with a subsequent 5-min extension at 72 °C. Reaction products were analyzed on 2% agarose gels. The bands were visualized by ethidium bromide staining.

Quantitative RT–PCR (qRT–PCR) analysis was performed on an Applied Biosystems QuantStudio 6 Flex cycler using Power SYBR Green PCR Master Mix (ThermoFisher Scientific). The following primers were used: *EZH2* inclusion, Fwd: CAGCATTTGCCACTCCTACC, Rev: AGAGCAGCAGCAAACTCCTTT; *EZH2* exclusion,c Fwd: CAGCATTTGGAGGGAGCA, Rev: GCTGGGC CTGCTACTGTTATT; 18S rRNA, Fwd: GTAACCCGTTGAACCCCATT, Rev: CCATCCAATCGGTAGTAGCG; *Dot1l* exclusion, Fwd: GCAGGAAC TTGAGTGCTTGAA, Rev: GGCAGCTGCTTTGCTCTC; *Dot1l* inclusion, Fwd: CGGCAGAATCGTATCCTCAA, Rev: AAGTATGGTGCGGTCAATG; *Meis1* exclusion, Fwd: TAACAGCAGTGAGCAAGCAC, Rev: AATAAACCAATTG TTCACTTGAAGG; *Meis1* inclusion, Fwd: AAGGTGATGGCTTGGACAAC, Rev: AGGGTGTGTTAGATGCTGGAA; *Gapdh*, Fwd: TGGAGAAACCT GCCAAGTATG, Rev: GGAGACAACCTGGTCCTCAG.

All samples, including the template controls, were assayed in triplicate. The relative number of target transcripts was normalized to the housekeeping gene found in the same sample. The relative quantification of target gene expression was performed with the standard curve or comparative cycle threshold (C_T) method.

Statistical analyses. Statistical significance was determined by Student's *t*-test or analysis of variance (ANOVA) after testing for normal distribution. For Kaplan–Meier survival analysis, Mantel–Cox log-ranked test was used to determine statistical significance. Data were plotted as mean values with error bars representing s.d. using GraphPad Prism 7 software.

Targeted genomic sequencing using MSKCC IMPACT. Genomic alterations from FACS-purified hCD45$^+$ BM cells from NSG mice of PDX models were profiled using the MSKCC IMPACT assay as described previously[33]. Genomic DNA was extracted using DNeasy Blood and Tissue Kit (Qiagen).

Replicates. RNA-seq was conducted with 3–5 biological replicates from each group. Genetic phenotyping experiments were replicated three times independently. For *in vivo* experiments, the number of animals was chosen to ensure 90% power with 5% error based on observed s.d. Flow cytometric experiments were replicated independently two or three times. Pilot studies were conducted with drug studies, and results were replicated in a larger study to achieve enough statistical power. *In vitro* experiments were replicated two or three times, and viability experiments were completed in triplicate.

mRNA isolation, sequencing, and analysis. RNA was extracted from sorted mouse cell populations using Qiagen RNeasy columns. Poly(A)-selected, unstranded Illumina libraries were prepared with a modified TruSeq protocol. 0.5× AMPure XP beads were added to the sample library to select for fragments <400 bp, followed by addition of 1× beads to select for fragments >100 bp. These fragments were then amplified with PCR (15 cycles) and separated by gel electrophoresis (2% agarose). 300-bp DNA fragments were isolated and sequenced on the Illumina HiSeq 2000 (~100 million 101-bp reads per sample).

Publicly available RNA-seq data. Unprocessed RNA-seq reads from 31 patients with AML (with *MLL* rearrangements) were downloaded from the US National Center for Biotechnology Information (NCBI) sequence read archive (SRA; accession numbers SRP028594, SRP033266, SRP048759, and SRP056295). The data consisted of paired-end 2 × 100-bp libraries, with an average read count of 102 million per sample. The *SRSF2* mutational status of the samples was obtained from Lavallée *et al.*[16].

Genome annotations. To create organism-specific gene and genome annotation files, information was combined across University of California, Santa Cruz (UCSC) and Ensembl databases, using mouse assembly mm10 (NCBI GRCm38) and human assembly hg19 (NCBI GRCh37). To create splice junction annotation files, alternatively spliced cassette exons, competing 5′ or 3′ splice sites, and retained introns were obtained from MISO v2.0 (ref. 13). Constitutively spliced exons and introns were identified based on exon–exon junctions that were not alternatively spliced according to UCSC knownGene[34]. Novel junctions were defined from the UCSC and Ensembl 71 databases[35] using all possible combinations of splice sites, as described previously[36].

RNA-seq read mapping. All human and mouse samples were processed using the same pipeline. (i) The reads were mapped to their respective genome

doi:10.1038/nm.4097

assembly, using Bowtie v1.0.0 (ref. 37) and RSEM v.1.2.4 (ref. 38). The latter was internally modified to call Bowtie with -v 2, and it was run on the gene annotation file with the parameters --bowtie-m 100 --bowtie-chunkmbs 500 --calc-ci --output-genome-bam. (ii) BAM files from step 1 were filtered to remove reads in which the alignment mapq score was 0 and the splice junction overhang was <6 nt. (iii) All remaining unaligned reads were mapped to the splice junction annotation files using TopHat v2.0.8b (refs. 39,40), called with the parameters --bowtie1 --read-mismatches 3 -- read-edit-dist 2 --no-mixed --no-discordant --min-anchor-length 6 --splice-mismatches 0 --min-intron-length 10 --max-intron-length 1000000 --min-isoform-fraction 0.0 --no-novel-juncs --no-novel-indels --raw-juncs. The --mate-inner-dist and --mate-std-dev arguments were calculated using the MISO exon_utils.py script, which maps reads to constitutively spliced exon junctions. (iv) The reads aligned to splice junctions were filtered as in ii. (v) All resulting BAM files were merged to create a combined file of all aligned RNA-seq reads.

Identification and quantification of differential splicing. Isoform ratios for all alternative splicing events were quantified using MISO v2.0 (ref. 13). Constitutively spliced exons and introns were quantified using junction-spanning reads, as previously described[36]. The conditional knock-in and knockout mice were compared in a pair-wise manner, and for each pair the analysis was restricted to splicing events with 20 or more reads supporting either or both isoforms, and for which the event was alternatively spliced in the sample pair. From that subsets of events, those that fulfilled the following criteria were defined as differentially spliced: (i) they had at least 20 relevant reads in both samples, (ii) the change in absolute isoform ratio was ≥ 10%, and (iii) the statistical analysis of isoform ratios had a Bayes factor ≥5, when calculated using Wagenmakers's framework[14]. The human AML samples were analyzed by calculating the median isoform ratios across all 28 *SRSF2*$^{+/+}$ samples and comparing those in a pair-wise manner to each sample with mutated *SRSF2*, using the same methodology as for the knock-in and knockout mice. The *Mx1-Cre*$^{+}$*Srsf2*$^{+/+}$ or *Mx1-Cre*$^{+}$*Srsf2*$^{P95H/+}$ E7107-treated mice were compared in a pair-wise manner against the median isoform ratios of their vehicle-treated counterparts, using the same methodology. For the *MLL–AF9*-AML-transformed mice, there were sufficient numbers of replicates to do a group-based comparison within the *Srsf2*^{P95H} and *Srsf2*$^{+/+}$ genotypes individually ($n = 5$ for each genotype–treatment combination). E7107- and vehicle-treated mice were compared in a two-sided Wilcoxon rank-sum test, using the total number of isoform reads within each treatment group. Events were categorized as being differentially spliced if they fulfilled the following criteria: (i) they had at least 20 relevant reads in both samples, (ii) the change in median absolute isoform ratio was ≥10%, and (iii) they had a P value <0.01.

Gene expression analysis. All comparisons of gene expression levels were performed using RNA-seq read counts normalized with the trimmed mean of M values (TMM) method[41]. The scaling factors were calculated based on protein-coding genes only. For comparisons with fewer than five replicates per group, we used Wagenmakers's Bayesian framework[14] to compare samples in a pair-wise manner, as described above for the analysis of differential splicing. Differentially expressed genes had to have a Bayes factor >100. For the *MLL–AF9* leukemic mouse model, E7107- and vehicle-treated mice within the *Srsf2*$^{+/+}$ or *Srsf2*$^{P95H/+}$ genotype were analyzed using a two-sided Wilcoxon rank-sum test to compare the five replicates within each genotype–treatment group. Differentially expressed genes had to fulfill the following criteria: (i) a difference in abundance greater than a fold change of 2, and (ii) a P value <0.01.

Gene Ontology (GO) enrichment analysis. For each genotype–treatment comparison, we identified genes that were differentially expressed in at least one of the replicates to test for enrichment of GO biological process terms using the R package goseq[42]. All protein-coding genes were included as the background gene set. The 'Wallenius' method was used, and the resulting false-discovery rates were corrected using the Benjamini–Hochberg approach. Only terms with at least two ancestors were tested, and terms with more than 500 genes associated with them were removed to eliminate parent terms associated with generic biological processes.

Motif enrichment and distribution. The relative occurrences of sequence motifs in exons with increased inclusion versus exclusion rates in a given sample comparison were calculated. For the analysis of E7107 treatment in *Srsf2*$^{+/+}$ or *Srsf2*$^{P95H/+}$ mutant mice in the *Mx1-Cre* model, exons with decreased inclusion rates were compared to all exons with no changes in splicing, as the number of exons with increased inclusion rates was insufficient for statistical analysis. The 95% confidence interval for the enrichment ratios were computed based on bootstrapping, using 500 resampling steps for the enrichment ratios, or 100 steps for displaying the spatial distribution of motifs along a meta-exon.

Sample clustering. *MLL–AF9*-AML-transformed mice were clustered using multidimensional scaling (also known as principal coordinates analysis) of distances calculated using the 'canberra' method, $\text{sum}(|x_i - y_i|/|x_i + y_i|)$. For cassette exons and retained introns, only events that were alternatively spliced in the samples and had more than 20 reads in at least one sample were included. For protein-coding genes only genes with normalized expression >10 in at least one sample were included. Hierarchical clustering was performed on z-score-standardized data with the 'ward.D2' method, using the most variable splicing events and genes across samples (s.d. across the 20 mice > 0.25; splicing event or gene could be detected in at least ten mice).

Mouse versus human splicing comparison. For the cumulative distribution function (CDF) comparison of cassette exon-splicing and intron retention in *MLL–AF9* myeloid leukemias following *in vivo* E7107 or vehicle treatment, only cassette exons and introns within mouse homologs of genes containing differentially spliced events in at least one of the human *SRSF2 MLL*-rearranged AML samples were included.

Mouse homologs of the differentially spliced human genes were extracted from the Ensembl database version 81 (ref. 43) using BioMart.

30. National Research Council. *Guide for the Care and Use of Laboratory Animals* 8th edn. (The National Academies Press, 2011).
31. Wang, H.Y., Xu, X., Ding, J.H., Bermingham, J.R. Jr. & Fu, X.D. SC35 plays a role in T cell development and alternative splicing of *CD45*. *Mol. Cell* **7**, 331–342 (2001).
32. Georgiades, P. *et al. Vav-Cre* transgenic mice: a tool for mutagenesis in hematopoietic and endothelial lineages. *Genesis* **34**, 251–256 (2002).
33. Cheng, D.T. *et al.* Memorial Sloan Kettering–integrated mutation profiling of actionable cancer targets (MSK-IMPACT): a hybridization-capture-based next-generation sequencing clinical assay for solid tumor molecular oncology. *J. Mol. Diagn.* **17**, 251–264 (2015).
34. Meyer, L.R. *et al.* The UCSC Genome Browser database: extensions and updates 2013. *Nucleic Acids Res.* **41**, D64–D69 (2013).
35. Flicek, P. *et al.* Ensembl 2013. *Nucleic Acids Res.* **41**, D48–D55 (2013).
36. Hubert, C.G. *et al.* Genome-wide RNAi screens in human brain tumor isolates reveal a novel viability requirement for *PHF5A*. *Genes Dev.* **27**, 1032–1045 (2013).
37. Langmead, B., Trapnell, C., Pop, M. & Salzberg, S.L. Ultrafast and memory-efficient alignment of short DNA sequences to the human genome. *Genome Biol.* **10**, R25 (2009).
38. Li, B. & Dewey, C.N. RSEM: accurate transcript quantification from RNA-seq data with or without a reference genome. *BMC Bioinformatics* **12**, 323 (2011).
39. Kim, D. *et al.* TopHat2: accurate alignment of transcriptomes in the presence of insertions, deletions and gene fusions. *Genome Biol.* **14**, R36 (2013).
40. Trapnell, C., Pachter, L. & Salzberg, S.L. TopHat: discovering splice junctions with RNA-seq. *Bioinformatics* **25**, 1105–1111 (2009).
41. Robinson, M.D. & Oshlack, A. A scaling normalization method for differential expression analysis of RNA-seq data. *Genome Biol.* **11**, R25 (2010).
42. Young, M.D., Wakefield, M.J., Smyth, G.K. & Oshlack, A. Gene ontology analysis for RNA-seq: accounting for selection bias. *Genome Biol.* **11**, R14 (2010).
43. Guberman, J.M. *et al.* BioMart central portal: an open database network for the biological community. *Database* **2011**, bar041 (2011).

Corrigendum: Retinal lipid and glucose metabolism dictates angiogenesis through the lipid sensor Ffar1

Jean-Sébastien Joyal, Ye Sun, Marin L Gantner, Zhuo Shao, Lucy P Evans, Nicholas Saba, Thomas Fredrick, Samuel Burnim, Jin Sung Kim, Gauri Patel, Aimee M Juan, Christian G Hurst, Colman J Hatton, Zhenghao Cui, Kerry A Pierce, Patrick Bherer, Edith Aguilar, Michael B Powner, Kristis Vevis, Michel Boisvert, Zhongjie Fu, Emile Levy, Marcus Fruttiger, Alan Packard, Flavio A Rezende, Bruno Maranda, Przemyslaw Sapieha, Jing Chen, Martin Friedlander, Clary B Clish & Lois E H Smith
***Nat. Med.*; doi:10.1038/nm.4059; corrected 24 March 2016**

In the version of this article initially published online, there were two errors. There was a typographical error in the text, which should have stated that the 'dark current' is an electrochemical gradient required for photon-induced polarization (rather than depolarization, as incorrectly stated). In addition, some funding sources were inadvertently omitted from the Acknowledgments. The errors have been corrected for the print, PDF and HTML versions of this article.

Corrigendum: ROR-γ drives androgen receptor expression and represents a therapeutic target in castration-resistant prostate cancer

Junjian Wang, June X Zou, Xiaoqian Xue, Demin Cai, Yan Zhang, Zhijian Duan, Qiuping Xiang, Joy C Yang, Maggie C Louie, Alexander D Borowsky, Allen C Gao, Christopher P Evans, Kit S Lam, Jianzhen Xu, Hsing-Jien Kung, Ronald M Evans, Yong Xu & Hong-Wu Chen
***Nat. Med.*; doi:10.1038/nm.4070; corrected online 22 April 2016**

In Figure 2a of the version of this article initially published online, one phenyl ring was inadvertently deleted from the chemical structure of compound SR2211. One affiliation of H.-W.C. (Veterans Affairs Northern California Health Care System–Mather, Mather, California, USA) was also inadvertently omitted. These errors have been corrected for the print, PDF and HTML versions of this article.

Corrigendum: Protection against malaria at 1 year and immune correlates following PfSPZ vaccination

Andrew S Ishizuka, Kirsten E Lyke, Adam DeZure, Andrea A Berry, Thomas L Richie, Floreliz H Mendoza, Mary E Enama, Ingelise J Gordon, Lee-Jah Chang, Uzma N Sarwar, Kathryn L Zephir, LaSonji A Holman, Eric R James, Peter F Billingsley, Anusha Gunasekera, Sumana Chakravarty, Anita Manoj, MingLin Li, Adam J Ruben, Tao Li, Abraham G Eappen, Richard E Stafford, Natasha K C, Tooba Murshedkar, Hope DeCederfelt, Sarah H Plummer, Cynthia S Hendel, Laura Novik, Pamela J M Costner, Jamie G Saunders, Matthew B Laurens, Christopher V Plowe, Barbara Flynn, William R Whalen, J P Todd, Jay Noor, Srinivas Rao, Kailan Sierra-Davidson, Geoffrey M Lynn, Judith E Epstein, Margaret A Kemp, Gary A Fahle, Sebastian A Mikolajczak, Matthew Fishbaugher, Brandon K Sack, Stefan H I Kappe, Silas A Davidson, Lindsey S Garver, Niklas K Björkström, Martha C Nason, Barney S Graham, Mario Roederer, B Kim Lee Sim, Stephen L Hoffman, Julie E Ledgerwood & Robert A Seder, for the VRC 312 and VRC 314 Study Teams
***Nat. Med.*; doi:10.1038/nm.4110; corrected online 18 May 2016**

In the version of this article initially published online, the authors omitted a funding source, The Bill and Melinda Gates Foundation (Investment ID: 24922). The error has been corrected for the print, PDF and HTML versions of this article.

Erratum: Modulation of splicing catalysis for therapeutic targeting of leukemia with mutations in genes encoding spliceosomal proteins

Stanley Chun-Wei Lee, Heidi Dvinge, Eunhee Kim, Hana Cho, Jean-Baptiste Micol, Young Rock Chung, Benjamin H Durham, Akihide Yoshimi, Young Joon Kim, Michael Thomas, Camille Lobry, Chun-Wei Chen, Alessandro Pastore, Justin Taylor, Xujun Wang, Andrei Krivtsov, Scott A Armstrong, James Palacino, Silvia Buonamici, Peter G Smith, Robert K Bradley & Omar Abdel-Wahab
***Nat. Med.*; doi:10.1038/nm.4097; corrected 11 May 2016**

In the version of this article initially published online, the graphs in Figure 3b–d were laid out incorrectly and were not consistent with the figure legend and text. The error has been corrected for the print, PDF and HTML versions of this article.

Cancer Cell

Synthetic lethal and convergent biological effects of cancer-associated spliceosomal gene mutations

--Manuscript Draft--

Manuscript Number:	
Full Title:	Synthetic lethal and convergent biological effects of cancer-associated spliceosomal gene mutations
Article Type:	Research Article
Keywords:	Myelodysplastic Syndromes, NF-κB, SF3B1, Splicing, SRSF2, U2AF1
Corresponding Author:	Omar Abdel-Wahab New York, UNITED STATES
First Author:	Omar Abdel-Wahab
Order of Authors:	Omar Abdel-Wahab
	Stanley Chun-Wei Lee
	Khrystyna Dilai
	Eunhee Kim
	Esther Obeng
	Sydney X. Lu
	Bo Liu
	Daichi Inoue
	Akihide Yoshimi
	Michelle Ki
	Xiao Jing Zhang
	Min Kyung Kim
	Young Rock Chung
	Justin Taylor
	Benjamin H. Durham
	James Palacino
	Michael Seiler
	Silvia Buonamici
	Peter G. Smith
	Benjamin L. Ebert
	Robert K. Bradley
Abstract:	Mutations affecting the RNA splicing factors SF3B1, SRSF2, and U2AF1 are the most common class of mutations in patients with myelodysplastic syndromes (MDS) and occur as heterozygous, mutually exclusive mutations. The basis for the mutual exclusivity of these mutations and how they commonly contribute to MDS pathogenesis is not understood. Here we report that different spliceosomal mutations, despite imparting distinct effects on splicing and gene expression, are negatively selected for when co-expressed in the same cell or in a homozygous state. At the same time, each mutation induces aberrant splicing of mRNAs encoding distinct enzymes that independently promote hyperactive NF-κB signaling. These data identify convergent consequences of splicing factor mutations and the basis for their mutual exclusivity and heterozygous nature.

Suggested Reviewers:	Guy Sauvageau guy.sauvageau@umontreal.ca
	Ulrich Steidl ulrich.steidl@einstein.yu.edu
	Mark Dawson Mark.Dawson@petermac.org
	Scott Armstrong Scott_Armstrong@dfci.harvard.edu
	Ari Melnick amm2014@med.cornell.edu
	Ernesto Guccione eguccione@imcb.a-star.edu.sg
Opposed Reviewers:	Timothy Graubert
	Seishi Ogawa
	Jaroslaw Maciejewski
Additional Information:	
Question	**Response**

Thursday, May 11, 2017

Li-Kuo Su,
Editor, *Cancer Cell*

Dear Dr. Su,

It is our pleasure to submit for your consideration our manuscript entitled "Synthetic lethal and convergent biological effects of cancer-associated spliceosomal gene mutations" to *Cancer Cell*.

As you are likely aware mutations within genes encoding RNA splicing factors are now the single most common class of genetic alterations in patients with myelodysplastic syndromes (MDS) in addition to occurring in a number of other forms of leukemia and solid tumors. These mutations primarily occur in the genes encoding *SF3B1, SRSF2,* and *U2AF1* as heterozygous point mutations at highly specific residues. In addition, these mutations occur in a mutually exclusive manner with one another such that patients are rarely found to have more than one splicing factor mutation at a time. Although this genetic configuration suggests that RNA splicing factor mutations may confer a gain-of-function and/or have a synthetic lethal interaction, there is currently no functional evidence to support either possibility. Moreover, several recent studies published in *Cancer Cell* (Obeng *et al. Cancer Cell* 2016; Wang, L *et al. Cancer Cell* 2016; Kim, E, *et al. Cancer Cell* 2015) and other journals, have reported that the effects of mutations in *SF3B1* and *SRSF2* on RNA splicing are quite distinct, making it unclear why these mutations would be mutually exclusive with one another.

In this manuscript, we utilize a combination of mouse genetic analyses and RNA-seq analyses to identify that mutations in RNA splicing factors are mutually exclusive due to both synthetic lethal interactions as well as convergent biological effects. Overall, our work includes the following novel findings:

- Simultaneous expression of two cancer-associated RNA splicing factor mutations in the same cell is not compatible with cell survival. This was identified through the generation of mice that allow conditional expression of cancer-associated mutations in *SF3B1* and *SRSF2* simultaneously in the same cells *in vivo*. These findings were confirmed through the use of two distinct Cre recombinase systems and provide definitive explanation for the mutual exclusivity of RNA splicing factor mutations in cancer.
- Mutations in RNA splicing factors are not tolerated in the homozygous state. This was identified through the generation of mice that allow for conditional homozygous expression of cancer-associated mutations in SRSF2. Again here, these findings provide definitive explanation for the consistent occurrence of mutations in RNA splicing factors in the heterozygous state.
- Despite their mutual exclusivity, mutations in RNA splicing factors each impart distinct mechanistic effects on splicing with few commonly mis-spliced genes. This was identified by RNA-seq analyses of isogenic hematopoietic progenitors from the above mouse models as well as human MDS patient samples.
- In order to understand the mechanistic basis for the synthetic lethal interactions of cancer-associated RNA splicing factor mutations, we performed RNA-seq analysis of cells bearing expression of 2 mutations simultaneously. This revealed that co-expression of these mutations results in additive, rather than synergistic, effects on RNA splicing mechanisms.
- In addition to the synthetic lethal interactions of cancer-associated RNA splicing factor mutations, we identified a shared effect of these mutations on hyper-activation of innate immune signaling. Through genomic and functional analyses, we identify that mutations in SF3B1 and SRSF2 robustly mis-splice the mRNAs encoding distinct enzymes to upregulate NF-kB signaling. Specifically, this includes mutant SF3B1 mis-splicing of the mRNA encoding MAP3K7 and mutant SRSF2 mis-splicing of the mRNA encoding caspase 8. These mis-splicing events resulted in physiologically important effects on response to inflammatory stimuli *in vivo*.

- Of note, we identify and validate a far greater overlap of aberrantly spliced genes between mouse and human cells bearing mutations in RNA splicing factors than previously reported in recent studies, making the results from this manuscript particularly important for the community of researchers interested to utilize these models.

Overall, our results provide the first definitive explanation for the mutual exclusivity of RNA splicing factor mutations, their consistent nature as heterozygous mutations, and convergent biological effects of these mutations. Of note, although there have been several recent excellent studies related to mutant SF3B1 published in *Cancer Cell* as well as other journals, the critical question of how mutations in *SF3B1* relate to other RNA splicing factor mutations to explain their mutual exclusivity and the aberrant splicing events linking SF3B1-induced mis-splicing to MDS pathogenesis have not been addressed. Finally, there are numerous therapeutic implications of these data including potential for use of therapies targeting NF-kB signaling in MDS as well as therapeutic modulation of normal splicing catalysis in splicing factor mutant cancers.

We hope you find this work suitable for review at *Cancer Cell* and would like to suggest the following as potential reviewers given their expertise in the genomics of MDS and leukemia, analysis of transcriptomic data, RNA splicing, and/or mouse genetics: Guy Sauvageau (Université de Montréal), Scott Armstrong (Dana Farber Cancer Institute), Ulrich Steidl (Albert Einstein College of Medicine), Mark Dawson (Peter MacCullum Cancer Centre, Australia), Ari Melnick (Weill Cornell College of Medicine), and Ernesto Guccione (Institute of Molecular and Cell Biology and A*STAR, Singapore).

We would also like to suggest that the following not be considered reviewers: Timothy Graubert (Massachusetts General Hospital), Seishi Ogawa (Kyoto University), and Jaroslaw Maciejewski (Cleveland Clinic). Although these individuals are friends and colleagues, there is an element of competition in this story with these individuals.

We thank you once again for consideration of our manuscript,

Sincerely

Omar Abdel-Wahab and Robert Bradley on behalf of all co-authors

Graphical Abstract

Click here to download Graphical Abstract 2017_05_05 potential graphical abstract.pdf

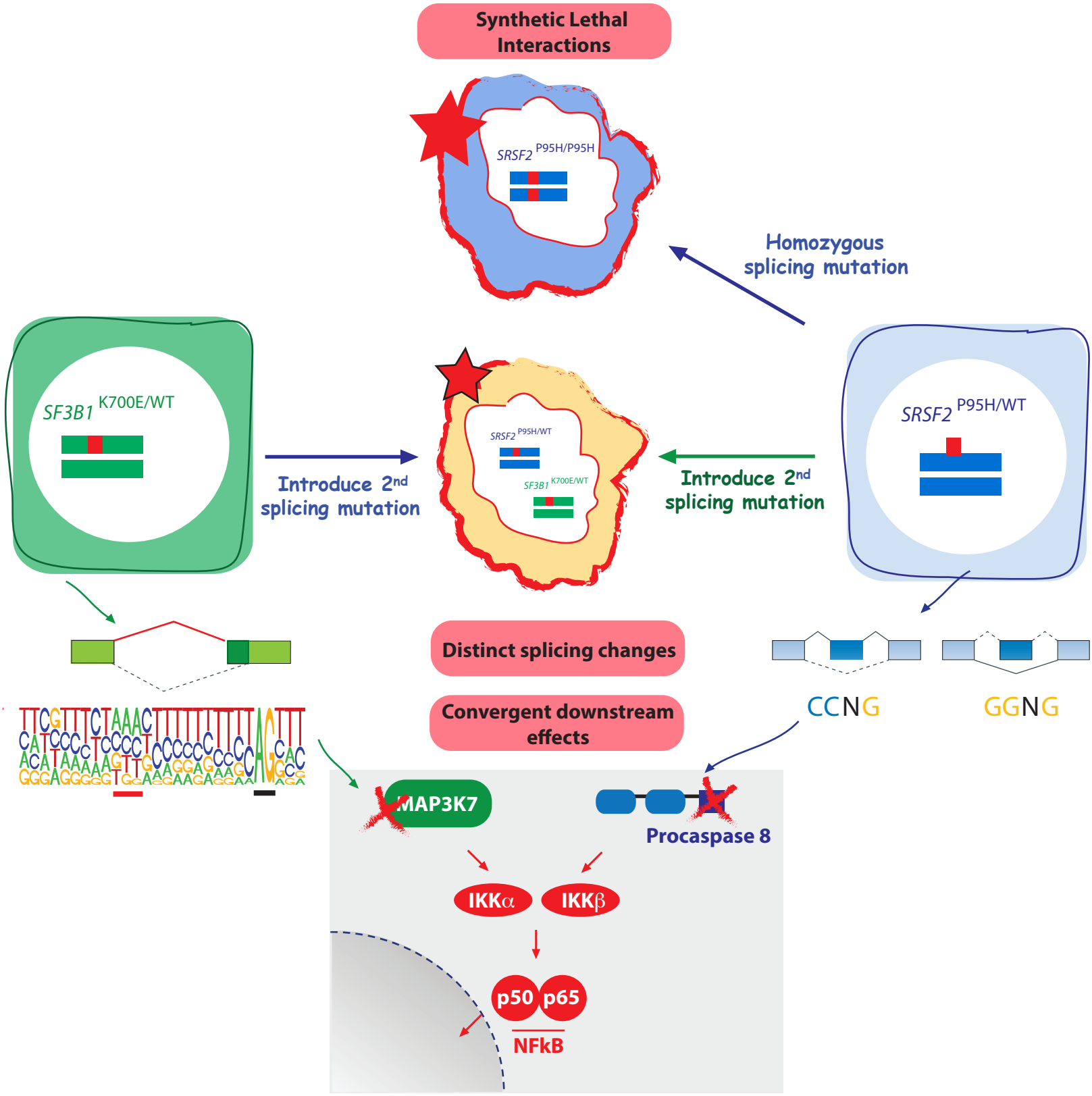

Synthetic lethal and convergent biological effects of cancer-associated spliceosomal gene mutations

Stanley Chun-Wei Lee[1,*], Khrystyna Dilai[2,3,4*], Eunhee Kim[5,*], Esther Obeng[6], Sydney X. Lu[1], Bo Liu[1], Daichi Inoue[1], Akihide Yoshimi[1], Michelle Ki[1], Xiao Jing Zhang[1], Min Kyung Kim[1], Young Rock Chung[1], Justin Taylor[1], Benjamin H. Durham[1], James Palacino[7], Michael Seiler[7], Silvia Buonamici[7], Peter G. Smith[7], Benjamin L. Ebert[4], Robert K. Bradley[2,3,4,*], Omar Abdel-Wahab[1,8,*,**]

Affiliations:
[1]Human Oncology and Pathogenesis Program, Memorial Sloan Kettering Cancer Center, New York, NY, USA
[2]Computational Biology Program, Public Health Sciences Division, Fred Hutchinson Cancer Research Center, Seattle, WA, USA
[3]Basic Sciences Division, Fred Hutchinson Cancer Research Center, Seattle, WA, USA
[4]Department of Genome Sciences, University of Washington, Seattle, WA, USA
[5]School of Life Sciences, Ulsan National Institute of Science and Technology, Ulsan 44919, Republic of Korea
[6]Division of Hematology, Department of Medicine, Brigham and Women's Hospital, Harvard Medical School, Boston, MA 02115, USA; Broad Institute of MIT and Harvard, Cambridge, MA 02142, USA.
[7]H3 Biomedicine, Cambridge, MA 03129, USA
[8]Leukemia Service, Department of Medicine, Memorial Sloan Kettering Cancer Center, New York, NY, USA

***Equal contributors.**

****Lead contact**: Omar Abdel-Wahab

Correspondence:

Robert K. Bradley
Fred Hutchinson Cancer Research Center
1100 Fairview Ave. N.
Mailstop: M1-B514
Seattle, WA 98109-1024
Phone: 206-667-5662
Fax: 206-667-1319
Email: rbradley@fredhutch.org

Omar Abdel-Wahab
Zuckerman 701,
Memorial Sloan Kettering Cancer Center
408 E. 69th Street
New York, NY USA 10065
Phone: 646-888-3487
Fax: 646-422-0890
Email: abdelwao@mskcc.org

Summary
Mutations affecting the RNA splicing factors SF3B1, SRSF2, and U2AF1 are the most common class of mutations in patients with myelodysplastic syndromes (MDS) and occur as heterozygous, mutually exclusive mutations. The basis for the mutual exclusivity of these mutations and how they commonly contribute to MDS pathogenesis is not understood. Here we report that different spliceosomal mutations, despite imparting distinct effects on splicing and gene expression, are negatively selected for when co-expressed in the same cell or in a homozygous state. At the same time, each mutation induces aberrant splicing of mRNAs encoding distinct enzymes that independently promote hyperactive NF-κB signaling. These data identify convergent consequences of splicing factor mutations and the basis for their mutual exclusivity and heterozygous nature.

Keywords: Myelodysplastic Syndromes, NF-κB, SF3B1, Splicing, SRSF2, U2AF1

Significance
Mutual exclusivity of different mutations that affect a single pathway in cancer is commonly thought to indicate convergent effects of these mutations. RNA splicing factor mutations constitute the most common class of alterations in patients with myelodysplastic syndromes (MDS) and are also frequent in several additional cancer types and occur as heterozygous mutations at restricted residues in a mutually exclusive manner. The mutual exclusivity of spliceosomal mutations suggests synthetic lethal and/or convergent biological effects of these mutations; however, there is currently no functional evidence supporting either of these possibilities. Here we report that individual spliceosomal mutations have non-overlapping effects on splicing and are mutually exclusive due to both synthetic lethal interactions and convergent effects on hyperactivation of innate immune signaling.

Highlights
- Mutations in *SF3B1* and *SRSF2* have a synthetic lethal interaction.
- Mutations in RNA splicing factors are not tolerated in a homozygous state.
- Mutations in *SF3B1* and *SRSF2* have distinct and additive effects on mis-splicing.
- Both *SF3B1* and *SRSF2* mutations result in hyperactive innate immune signaling.

INTRODUCTION

Recently, recurrent somatic mutations in genes encoding components of the spliceosome have been identified through large-scale DNA sequencing across multiple cancer types. Spliceosomal mutations most commonly occur in myeloid neoplasms including myelodysplastic syndromes (MDS), chronic myelomonocytic leukemia (CMML), and acute myeloid leukemia (AML) (Graubert et al., 2012; Papaemmanuil et al., 2011; Yoshida et al., 2011), chronic lymphocytic leukemia (CLL) (Quesada et al., 2012; Wang et al., 2011), and uveal melanoma (Harbour et al., 2013; Martin et al., 2013). *SF3B1, U2AF1,* and *SRSF2*, encoding RNA splicing factors that promote recognition of 3' splice sites and exons, are the most commonly mutated genes. Mutations in each of these genes are consistently heterozygous and occur as point mutations at highly restricted residues, suggesting that these are oncogenic gain-of-function alterations. In addition, mutations in splicing factor genes are mutually exclusive with one another, presumably due to either redundant oncogenic effects and/or a limit on cellular tolerance of disrupted spliceosome function.

Despite recent insights into the individual effects of each of these mutations on RNA splicing, gene expression, and hematopoiesis, the mechanistic basis for the mutual exclusivity of these mutations and any functionally convergent effects they may have are currently unknown. For example, recent work has identified that mutations affecting the core RNA splicing factor SF3B1 are associated with cryptic 3’ splice site (ss) selection and altered branchpoint recognition (Alsafadi et al., 2016; Darman et al., 2015; DeBoever et al., 2015; Obeng et al., 2016; Wang et al., 2016). In contrast, mutations affecting SRSF2, an auxiliary splicing factor that binds to exonic splicing enhancers to promote splicing, alter its RNA binding preferences in a sequence-specific manner and thereby alter the efficiency of exon inclusion (Kim et al., 2015; Zhang et al., 2015). Finally, mutations affecting U2AF1, the small subunit of the U2AF heterodimer that binds the AG dinucleotide at the 3' ss, promote or repress 3' ss based on sequences flanking the AG dinucleotide (Fei et al., 2016; Ilagan et al., 2014; Okeyo-Owuor et al., 2015; Shirai et al., 2015). As these reported effects of *SF3B1*, *U2AF1*, and *SRSF2* mutations on splicing mechanisms are distinct, it is unclear why mutations affecting these three factors are mutually exclusive with one another. Moreover, a direct comparison of the effects of these individual mutations on RNA splicing and gene expression in an isogenic manner has not been performed.

Here we directly evaluated the functional basis for the mutually exclusive and heterozygous occurrence of mutations affecting RNA splicing factors with murine models expressing single and/or multiple splicing factor mutations simultaneously. Evaluation of mice with inducible expression of mutations in *Srsf2* or *Sf3b1*, alone or together, definitively demonstrated that each mutation affects RNA splicing in a distinct manner. Nonetheless, these two mutations were not tolerated when co-expressed in the same cell. Remarkably, although mutant SRSF2 and SF3B1 alter RNA splicing through different mechanisms, hematopoietic cells expressing either mutant splicing factor resulted in hyperactivated NF-κB signaling via aberrant splicing of distinct signaling intermediates. These data provide a functional explanation for the genetic spectrum of mutations affecting RNA splicing factors and identify a convergent biological effect of these mutations in a pathway of established relevance to MDS pathogenesis.

RESULTS

Simultaneous expression of cancer-associated mutations in *Srsf2* and *Sf3b1* is incompatible with hematopoiesis

Evaluation of sequencing data from >4,000 patients with MDS and related myeloid neoplasms (Bejar et al., 2012; Damm et al., 2012; Haferlach et al., 2014; Lasho et al., 2012; Makishima et al., 2012; Meggendorfer et al., 2012; Papaemmanuil et al., 2013; Patnaik et al., 2013; Thol et al., 2012; Yoshida et al., 2011; Zhang et al., 2012) revealed that while ~48% of patients (1,935/4,032) have a mutation in an RNA splicing factor, only 2% of MDS patients (86/4,032) have mutations in >1 splicing factor (**Figure 1A** and **Table S1**). To understand the functional basis of this apparent mutual exclusivity of RNA splicing factor mutations, we generated mice to permit inducible heterozygous expression of two of the most common mutations in RNA splicing factors (the *SF3B1*K700E and *SRSF2*P95H mutations) simultaneously (*Mx1*-Cre *Sf3b1*$^{K700E/+}$ *Srsf2*$^{P95H/+}$) (**Figure 1B**). We next performed noncompetitive bone marrow transplantation (BMT), wherein each mutation was induced, either alone or together, following stable engraftment in recipient mice (**Figure 1B**). Bone marrow (BM) cells from mice co-expressing *Sf3b1*^{K700E} and *Srsf2*^{P95H} mutations had severe defects in multi-lineage reconstitution (**Figures 1C-D**). Similarly, in competitive BMT assays (**Figure 2A**), simultaneous expression of *Sf3b1*^{K700E} and *Srsf2*^{P95H} mutations resulted in severe defects in the self-renewal and differentiation of hematopoietic stem and progenitor cells (HSPCs), which were outcompeted by wild-type (WT) and single-mutant HSPCs. Analyses of hematopoietic organs six months post-BMT revealed a near-complete absence of *Sf3b1*$^{K700E/+}$/*Srsf2*$^{P95H/+}$ double-mutant cells, which was distinct from expression of the *Sf3b1*^{K700E} or *Srsf2*^{P95H} mutation alone (**Figures 2B-C** and **Figure S1**). Selection against co-expression of two splicing factor mutations was also strongly supported by the fact that mice with hematopoietic-restricted expression of simultaneous *Sf3b1*^{K700E} and *Srsf2*^{P95H} (*Vav*-Cre *Sf3b1*$^{K700E/+}$ *Srsf2*$^{P95H/+}$) mutations were associated with 100% embryonic lethality, in contrast to control mice with expression of either mutation alone, which were born at the expected Mendelian ratios (**Figure 1E**). These data provide functional evidence that co-expression of these change-of-function mutations affecting RNA splicing factors are not tolerated in the same cell and provide a basis for the mutual exclusivity of these mutations in patients.

Expression of cancer-associated RNA splicing factor mutations in a homozygous or hemizygous state is incompatible with hematopoiesis

Prior data from epithelial and hematopoietic cells identified that cells bearing mutant splicing factors require the WT allele for survival (Fei et al., 2016; Lee et al., 2016; Zhou et al., 2015). While these observations potentially explain the heterozygous nature of RNA splicing factor mutations in patients, the copy number of the RNA splicing factor was not maintained in these experiments. To unambiguously test whether these mutations can exist in a homozygous state, we generated mice with conditional homozygous expression of the *SRSF2*^{P95H} mutation (*Mx1*-Cre *Srsf2*$^{P95H/P95H}$). In BMT assays, HSPCs from these mice showed severe defects in self-renewal as well as multi-lineage reconstitution relative to heterozygous mutant (*Mx1*-Cre *Srsf2*$^{P95H/+}$) or control (*Mx1*-Cre *Srsf2*$^{+/+}$) HSPCs, analogous to the defects seen with hemizygous *Srsf2*^{P95H} expression *(Mx1*-Cre *Srsf2*$^{P95H/fl}$) (**Figures 2D-E** and **Figure S2**). These data firmly establish that neither hemizygous nor homozygous expression of splicing factor mutations is tolerated by hematopoietic cells, further highlighting the unique dependency of spliceosome-mutant cells on residual function of WT spliceosome components.

Srsf2 and *Sf3b1* mutations have largely distinct effects on gene expression

To understand the mechanistic basis for mutual exclusivity of *SF3B1* and *SRSF2* mutations, we performed RNA-seq on lineage$^-$ c-Kit$^+$ (LK) cells from *Mx1*-Cre *Sf3b1*$^{K700E/+}$/*Srsf2*$^{P95H/+}$ mice, as well as the respective single-mutant and WT control cells, two weeks after conditionally expressing each mutation alone or together (**Figure 3A**). The mean allelic ratio of *Sf3b1*^{K700E} and *Srsf2*^{P95H} expressed in double-mutant mice was 20.7% and 33.5%, markedly lower than the near 50% expression seen in single-mutant controls, illustrating the intolerability of combined *SF3B1* and *SRSF2* mutations (**Figure 3B**). We therefore focused the majority of our subsequent gene expression and splicing analyses on the replicate with highest allelic expression of both *Sf3b1*^{K700E} and *Srsf2*^{P95H}. Expression of either

mutation resulted in dysregulation of hundreds of coding genes, with the most marked dysregulation exhibited by double-mutant (*Sf3b1*$^{K700E/+}$/*Srsf2*$^{P95H/+}$) cells (**Figure 3C-E** and **Table S2**). Double-mutant cells shared a greater proportion of differentially expressed genes with each single-mutant genotype than single-mutants shared with one another. Gene Ontology (GO) enrichment analysis of coding genes that were differentially expressed within each genotype relative to WT control revealed strong signatures of impaired hematopoiesis in double-mutant cells, consistent with the multi-lineage defects in hematopoiesis evident in these cells noted above (**Figure 3D**).

We next tested whether mutations in *SF3B1* and *SRSF2* likely have additive or synergistic effects on gene expression by comparing the sets of differentially expressed genes in single- and double-mutant cells. *Sf3b1*$^{K700E/+}$/*Srsf2*$^{P95H/+}$ cells recapitulated approximately 80% and 40% of gene dysregulation present in *Sf3b1*$^{K700E/+}$ and *Srsf2*$^{P95H/+}$ cells expressing single splicing factor mutations (**Figure 3E** and **Table S2**). A subset of genes was dysregulated in cells expressing either mutation, including *Plk2* and *Trib1*, consistent with the possibility of convergent effects of distinct spliceosomal mutations (**Figure 3F**). As double-mutant cells exhibited only moderately more differentially expressed genes than did single-mutant cells, we conclude that *SF3B1* and *SRSF2* mutations likely have additive, rather than synergistic, effects on gene expression.

***Srsf2* and *Sf3b1* mutations have distinct and additive effects on RNA splicing**

We next assessed the consequences of single versus double mutations in *SF3B1* and *SRSF2* on RNA splicing (**Table S3**). Mutations in *SF3B1* have been proposed to preferentially alter 3' splice site recognition (Alsafadi et al., 2016; Darman et al., 2015; DeBoever et al., 2015). In contrast, mutations in *SRSF2* alter exon recognition via preferential recognition of C-rich exonic splicing enhancer (ESE) motifs relative to G-rich ESEs, while WT SRSF2 recognizes both classes of ESEs (Kim et al., 2015; Zhang et al., 2015). Our current understanding of *SF3B1* and *SRSF2* mutations therefore indicates that they induce distinct changes in RNA splicing. However, the consequences of these mutations for splicing have not yet been compared in an isogenic context.

We used our double-mutant system to directly compare the consequences of *SF3B1* and *SRSF2* mutations on RNA splicing mechanisms. Consistent with prior studies (Alsafadi et al., 2016; Darman et al., 2015; DeBoever et al., 2015; Kim et al., 2015; Zhang et al., 2015), *SF3B1* and *SRSF2* mutations preferentially affected 3' splice site and cassette exon recognition, respectively (**Figure 4A**-**B**). We observed a modest enrichment of adenosines upstream of intron-proximal 3' splice sites promoted by the *Sf3b1*K700E mutation, independent of the presence or absence of *Srsf2*P95H. This enrichment was absent from cells expressing *Srsf2*P95H alone (**Figure S3A**). Cassette exons that were promoted versus repressed in cells expressing *Srsf2*P95H were respectively enriched for the CCNG and GGNG ESEs, independent of the presence or absence of *Sf3b1*K700E, but were absent from cells expressing *Sf3b1*K700E alone (**Figure 4C** and **Figure S3B**). These sequence analyses are consistent with previous reports that *SF3B1* and *SRSF2* mutations affect branchpoint recognition and ESE preference, respectively, and furthermore demonstrate that these changes in splicing mechanisms are specific to *SF3B1* and *SRSF2* mutations.

As *SF3B1* and *SRSF2* mutations cause distinct changes in splicing mechanisms, even when simultaneously present in a cell, we hypothesized that *SF3B1* and *SRSF2* mutations likely interacted additively rather than synergistically to alter splicing. Consistent with this hypothesis, we did not observe signs of widespread decreases in splicing efficiency, such as increased retention of constitutive introns, in double-mutant cells (**Figure S3C**). Instead, *Sf3b1*$^{K700E/+}$/*Srsf2*$^{P95H/+}$ cells exhibited only modest increases in the number of mis-spliced genes relative to cells bearing single mutations in *Sf3b1* or *Srsf2*. Consistent with additivity, *Sf3b1*$^{K700E/+}$/*Srsf2*$^{P95H/+}$ cells recapitulated approximately 40% and 32% of splicing dysregulation driven by expression of the single mutations *Sf3b1*K700E and *Srsf2*P95H (**Figure 4D**-**E** and **Figure S3B** and **S3D**). We identified only seven genes that were mis-spliced in both single-mutant as well as double-mutant cells, and only six genes that were mis-spliced in both single-mutant but not double-mutant cells. Such genes might represent cases where mutant SF3B1 and SRSF2 have opposing or convergent consequences for splicing. However, these genes were ten-fold less abundant than genes that were shared between either single-mutant and the double-mutant cells. We therefore conclude that *SF3B1* and *SRSF2* mutations typically have distinct and additive, rather than synergistic, consequences on RNA splicing.

SF3B1 mutations promote mis-splicing of *MAP3K7*, resulting in hyperactivation of NF-κB signaling

The above results provide a compelling explanation for the mutual exclusivity of RNA splicing factor mutations in MDS, but they do not explain why mutations affecting distinct RNA splicing factors are enriched in the same disease. *SF3B1* and *SRSF2* mutations clearly induce distinct changes in RNA splicing with almost no shared mis-spliced genes. We therefore wondered whether *SF3B1* and *SRSF2* mutations might induce convergent downstream molecular pathologies despite causing virtually non-overlapping changes in splicing. To test this hypothesis, we returned to our GO enrichment analysis of differentially expressed genes in single- and double-mutant cells. In addition to impaired hematopoiesis (**Figure 3D**), our GO analysis revealed a strong signature of immune signaling that was augmented in double- relative to single-mutant cells (**Figure 5A**). As innate immune signaling has been implicated in MDS pathogenesis (Basiorka et al., 2016; Fang et al., 2014; Fang et al., 2017; Varney et al., 2015; Wei et al., 2013), we explored the possibility that *SF3B1* and *SRSF2* mutations activated convergent immune signaling pathways.

We first focused on events that were aberrantly mis-spliced within *SF3B1*-mutant hematopoietic cells in both human and mouse (**Table S4**). Although recent studies reported very few such shared mis-spliced genes (Mupo et al., 2016; Obeng et al., 2016), we identified 205 genes that were mis-spliced in both *Sf3b1*-mutant murine hematopoietic cells and *SF3B1*-mutant MDS patient samples (**Figure 5B**). One of the most dramatically mis-spliced genes in MDS patients with *SF3B1* mutations was *MAP3K7* (also known as TAK1; TGFβ-activated kinase 1), for which an intron-proximal 3' splice site was promoted by mutant SF3B1 in both human and mouse hematopoietic cells. This same aberrant isoform of *MAP3K7* has been previously noted in *SF3B1*-mutant chronic lymphocytic leukemia (CLL) (DeBoever et al., 2015) and uveal melanoma (Darman et al., 2015) patient samples. Our re-analysis of RNA-seq data from these cohorts and isogenic human leukemia cell lines with endogenous mutations in *SF3B1*, as well as directed RT-PCR and Sanger sequencing of cDNA from *SF3B1*-mutant cells, validated this aberrant isoform (**Figures 5C-D** and **Figure S4A**). This aberrant 3' splice site occurred in exon five of *MAP3K7*, which encodes part of the kinase domain, and is predicted to result in an out-of-frame transcript that undergoes nonsense-mediated decay (NMD; **Figure S4B**). Consistent with induction of NMD, we observed reduced MAP3K7 protein levels in isogenic cell lines expressing *SF3B1*K700E from the endogenous *SF3B1* locus (**Figure 5E**). MAP3K7 encodes a kinase that mediates TNFα, IL-1β, lipopolysaccharide (LPS), TRAIL, and TLR signaling through the NF-κB, JNK, and p38 MAPK pathways. The biological effects of MAP3K7 loss have been extensively studied across a variety of immune cell types and can result in either loss or promotion of inflammatory signaling depending on the cellular context (Ajibade et al., 2012; Lamothe et al., 2012; Sato et al., 2005; Tang et al., 2008; Vink et al., 2013; Xin et al., 2017). Here, we observed that *SF3B1*$^{K700E/+}$ human lymphoid leukemia cells (NALM-6) stimulated with LPS or TNFα exhibited enhanced NF-κB transcriptional activation and phosphorylation of p65 compared with *SF3B1* WT and silent mutant (*SF3B1*$^{K700K/+}$) isogenic controls (**Figures 5F-H**). We next assessed whether hyperactive NF-κB signaling in *SF3B1*-mutant cells resulted in the induction of known NF-κB target genes that are associated with inflammatory responses. As expected, quantitative RT-PCR (qRT-PCR) analysis revealed marked induction in NF-κB target genes IL-1β and TNF in response to LPS stimulation in *SF3B1*K700E mutant knockin NALM-6 cells relative to parental and *SF3B1*K700K cells (**Figure 5G**). This same effect hyperactivated response in NF-κB transcriptional activity could be seen in *SF3B1*K700E mutant cells in response to LPS and TNFα using an NF-κB transcriptional reporter assay (DeDiego et al., 2014; Hernandez et al., 2015; Simoes et al., 2015) (**Figure 5H**). Similarly, hyperactive NF-κB signaling could be seen with shRNA mediated downregulation of *MAP3K7* in NALM-6 parental cells (**Figure 5H** and **Figure S4C**), suggesting that the effects of *SF3B1*K700E mutation on induction of NF-κB signaling are indeed, in part, mediated through MAP3K7 reduction.

SRSF2 mutations promote aberrant splicing of *caspase-8* (*CASP8*), resulting in expression of a truncated protein that hyperactivates NF-κB signaling

Consistent with the distinct effects of *SF3B1* and *SRSF2* mutations on splicing, *MAP3K7* aberrant splicing was restricted to *SF3B1*-mutant cells and not seen in *SRSF2*-mutant cells (**Figure S5A**). We therefore searched for aberrant splicing events in *SRSF2*-mutant cells that might impact NF-κB signaling. One such event was mutant SRSF2-associated aberrant splicing of *caspase-8* (*CASP8*), which was recurrently mis-spliced in AML and CMML patients with *SRSF2* mutations, but not in cells bearing *SF3B1* mutations (**Figure 6A** and **Figure S5B**). Caspase-8 is a cysteine protease that initiates death receptor-mediated apoptosis (Shu et al., 1997; Thome et al., 1997) in addition to playing a role in necroptosis (reviewed recently (Kearney and Martin, 2017; Weinlich et al., 2017)) and serving as a key activator of NF-κB during the early response to antigenic stimuli (Chaudhary et al., 2000; Hu et al., 2000; Shikama et al., 2003). *SRSF2* mutations repressed a cassette exon of *CASP8*, as was evident by RNA-seq, RT-PCR, qRT-PCR, and direct sequencing of cDNA from cell lines and primary patient samples bearing endogenous mutations in *SRSF2* (**Figures 6A-B** and **Figures S6A-C**). Exclusion of this cassette exon results in an mRNA encoding a truncated caspase-8 protein lacking the C-terminal catalytic domains, which was readily detectable in *SRSF2*-mutant cells by immunoblotting using an N-terminal anti-caspase-8 antibody (**Figure 6C**). *CASP8* normally encodes a 54/55 kDa protein of 480 amino acids containing two death-effector domains (DED) at the N-terminus and a C-terminal catalytic protease domain. Although several caspase-8 isoforms have been described which lack the C-terminal catalytic domain (Xu et al., 2009; Yuan et al., 2012), the specific isoform of *CASP8* detected in *SRSF2*-mutant cells is distinct from those previously described.

Previously described DED-only forms of caspase-8 have been suggested to serve either as competitive inhibitors or promoters of apoptosis (Xu et al., 2009; Yuan et al., 2012). Given this, we first tested the effect of expressing this *SRSF2*-mutant-specific truncated isoform (herein referred to as *CASP8 TR*) in a *SRSF2* WT cell line (K562 cells) on the induction of cell death in response to TRAIL, a potent agonist of death-receptor mediated cell death. Overexpression of both *CASP8* full-length (*CASP8 FL*) and *CASP8 TR* isoforms resulted in the robust expression of caspase-8 proteins at the expected size (**Figure 6D**) with no apparent effect on growth of K562 cells (**Figure S6D**). Moreover, both isoforms promoted TRAIL-mediated cell death in K562 cells, suggesting that the truncated isoform did not impart a clear differential effect of modulating cell death relative to the *CASP8 FL* isoform (**Figure S6E**). Given this, we next evaluated the effect of overexpressing *CASP8 TR* relative to *CASP8 FL* or an empty vector control on NF-κB transcriptional activity. In cells with endogenous *CASP8* expression, overexpression of the *CASP8 TR*, but not the *CASP8 FL* isoform, resulted in the robust induction of NF-κB activity upon increasing concentration of TRAIL exposure. This was demonstrated in both K562 and HAP1 (a near-haploid cell line derived from chronic myeloid leukemia cells KBM7 (Carette et al., 2011)) cells (**Figure 6E** and **Figures S6F**). To rule out the effect of the endogenous caspase-8 in K562 and HAP1 cells, we next assessed the effect of *CASP8 TR* on the cell death and NF-κB activity in *CASP8* knockout (*CASP8* KO) HAP1 cells. Consistent with the lack of the catalytic domain, *CASP8* knockout HAP1 cells expressing *CASP8 TR* isoform were unable to undergo TRAIL-mediated cell death (**Figure S6G-H**); however, the *CASP8 TR* isoform was able to induce robust NF-κB signaling in the absence of WT caspase-8, evidenced by elevated NF-κB transcriptional activity, increased phospho-p65 and a concomitant decrease in total IκBα level (**Figure 6G** and **Figure S6I**). Finally, this enhanced response to inflammatory stimuli across *Srsf2* and *Sf3b1* mutant genotypes was evident *in vivo* upon exposure to LPS-induced sepsis. Intraperitoneal injection of adult primary *Mx1*-Cre control, *Mx1*-Cre *Sf3b1*$^{K700E/+}$, and *Mx1*-Cre *Srsf2*$^{P95H/+}$ mice with LPS 8 weeks following induction of mutant allele expression resulted in accelerated death in both *Srsf2*- and *Sf3b1*-mutant mice relative to WT controls (**Figure 6H-I**).

DISCUSSION

Mutations affecting RNA splicing factors are the most common genetic alterations in patients with MDS (Graubert et al., 2012; Papaemmanuil et al., 2011; Yoshida et al., 2011) but the biological basis for their significant enrichment in this disease remains largely unexplained. Here we identify that two of the most commonly mutated RNA splicing factors in MDS converge on activation of innate immune signaling through aberrant splicing of mRNAs encoding distinct enzymes. These findings were identified using genetically engineered mouse models to evaluate the effect of expressing each RNA splicing factor mutation in an isogenic context, and by comparing the effects of each mutation on splicing across mouse and human cells.

Multiple lines of evidence implicate the role of innate immune signaling in MDS pathogenesis (Basiorka et al., 2016; Fang et al., 2014; Fang et al., 2017; Varney et al., 2015; Wei et al., 2013), including experiments demonstrating that increased innate immune signaling contributes to MDS development *in vivo* (Fang et al., 2017; Varney et al., 2015). In particular, increased activation of toll-like receptor (TLR) and interleukin-1 receptor (IL-1R) signaling with downstream activation of the MAPK and NF-κB pathways is widely reported in MDS, but studies of the mechanistic basis for this activation have mostly been restricted to MDS with deletion of chromosome 5q (Fang et al., 2014; Fang et al., 2017; Starczynowski, 2014; Varney et al., 2015). Here we provide data identifying a mechanism for hyperactivated NF-κB signaling in a wider spectrum of MDS patients carrying mutations in *SF3B1* and *SRSF2*.

Although recent studies have evaluated the effects of *SF3B1*K700E mutations on RNA splicing across mouse and human cells (Mupo et al., 2016; Obeng et al., 2016), we identified here a much greater overlap of aberrantly spliced genes shared across mouse and human hematopoietic cells with an *SF3B1*K700E mutation than has been previously reported. This includes aberrant splicing of *MAP3K7* through the use of an alternative 3' ss promoted by mutant SF3B1, an event that was conserved between mouse and human cells and not identified in prior studies of *Sf3b1* mutant mice (Mupo et al., 2016; Obeng et al., 2016). As partial downregulation of *Map3k7* within myeloid cells *in vivo* has been previously shown to promote development of myeloid neoplasms (Ajibade et al., 2012; Eftychi et al., 2012; Lamothe et al., 2012; Vink et al., 2013), this finding is likely to be relevant to the role of mutant SF3B1 in MDS pathogenesis. For example, downregulation of *Map3k7* through shRNA knockdown *in vivo* resulted in splenomegaly, myeloproliferation, extramedullary hematopoiesis as well as increased immune activation that was exacerbated by LPS challenge (Vink et al., 2013). Similarly, myeloid-specific deletion of *Map3k7* results in heightened response to inflammatory stimuli and these mice succumb to a clonal myeloid leukemia (Ajibade et al., 2012; Eftychi et al., 2012; Lamothe et al., 2012; Xin et al., 2017). Interestingly, the pro-inflammatory and leukemogenic effects of Map3k7 loss appear to be restricted to the myeloid lineages (Ajibade et al., 2012), which is in stark contrast to pan-hematopoietic-deletion of *Map3k7* which results in complete failure of hematopoiesis (Tang et al., 2008). Exactly how *Map3k7* loss results in cell-type specific effects on signaling and cell survival is currently not defined.

While aberrant splicing of *MAP3K7* and consequent downregulation of MAP3K7 expression was specific to cells expressing mutant SF3B1, cells expressing mutant SRSF2 shared a similar transcriptional profile of elevated innate immune signaling and heightened sensitivity to LPS-induced inflammation as *SF3B1* mutant cells. This led us to identify a novel gain-of-function effect of *SRSF2* mutations through the generation of a novel *CASP8* isoform that promotes NF-κB signaling. This observation can be partly attributed to a specific splicing aberration in *CASP8*, whereby mutant SRSF2 promoted a cassette exon exclusion event resulting in the production of a previously unannotated transcript that stably expresses a truncated form of caspase-8 lacking the C-terminal effector domains. This is consistent with prior work showing that N-terminal prodomain-only containing isoforms of procaspase-8 activate NF-κB signaling through interactions with upstream regulators of NF-κB, a function not mediated by the canonical full-length caspase-8 (Chaudhary et al., 2000; Hu et al., 2000; Shikama et al., 2003). While the experiments here are focused on mutations in *SF3B1* and *SRSF2*, it is also noteworthy that mutations in *U2AF1* also drive *CASP8* mis-splicing (Ilagan et al., 2014).

Together, our data demonstrate that different splicing factor mutations alter an entirely distinct set of targets at the level of pre-mRNA splicing that nonetheless converge on the same downstream signaling node to drive hyperactive innate immune signaling, a phenomenon that has been previously

implicated in MDS pathogenesis. In addition to identifying the functional basis for the mutual exclusivity and convergent consequences of splicing factor mutations, our study also highlights new avenues for potential therapeutic development. The universal requirement for the expression of the WT allele of a splicing factor in cells with an existing spliceosomal mutation motivated the use of compounds that inhibit basal splicing catalysis to specifically target mutant cells (Fei et al., 2016; Lee et al., 2016; Obeng et al., 2016; Shirai et al., 2017; Zhou et al., 2015). The identification that hematopoietic cells with expression of either of two mutated splicing factors simultaneously or in the homozygous state, further reinforces the requirement of WT splicing catalysis in cells with heterozygous expression of a mutant RNA splicing factor.

In addition to therapeutic implications regarding targeting RNA splicing, it is important to note that while partial downregulation of *Map3k7* can drive the development of myeloid neoplasms in murine models, complete *Map3k7* loss across hematopoietic cells results in eradication of hematopoiesis (Tang et al., 2008). Thus, we speculate that the convergent effects downstream of splicing factor mutations on immune signaling may suggest new therapeutic opportunities through inhibition of residual MAP3K7 function in *SF3B1*-mutant cells or NF-κB signaling in *SF3B1*- or *SRSF2*-mutant cells. In particular, efforts to develop potent and specific small-molecule inhibitors of MAP3K7 may be especially important to study in the context of spliceosomal mutant cancers (Bosman et al., 2014; Kilty and Jones, 2015; McNew et al., 2016; Singh et al., 2012). Finally, this study also highlights the advantage of functionally interrogating aberrantly spliced transcripts to identify the potentially pathogenic events that can be targeted by novel strategies. The use of oligonucleotide-based approaches to target aberrant splicing choices mediated by mutant splicing factors or specific mRNAs encoding aberrant isoforms, such as the *CASP8 TR* isoform, may be another therapeutic avenue for targeting cells bearing RNA splicing factor mutations.

Acknowledgements
This work was supported by the Leukemia and Lymphoma Society (S.C.-W.L., D.I., O.A.-W.), Aplastic Anemia and MDS International Foundation (A.Y.), Lauri Strauss Leukemia Foundation (A.Y.), U.S. Dept. of Defense Bone Marrow Failure Research Program grant W81XWH-12-1-0041 (R.K.B., O.A.-W.), the Worldwide Cancer Research Fund (E.K.), the American Society of Hematology (J.T., B.H.D., O.A.-W.), the Edward P. Evans Foundation (R.K.B., O.A.-W.), the Taub Foundation (O.A.-W.), grant R01 HL128239 (R.K.B., O.A.-W.), the Ellison Medical Foundation grant AG-NS-1030-13 (R.K.B.), grant R01 DK103854 (R.K.B.), the Starr Foundation grant I8-A8-075 and I9-A9-059 (O.A.-W.), the Mr. William H. Goodwin and Mrs. Alice Goodwin Commonwealth Foundation for Cancer Research (O.A.-W.), and The Experimental Therapeutics Center of MSKCC (O.A.-W.).

Author Contributions
S.C.-W.L., K.D., E.K., R.K.B, and O.A.-W. designed the study. S.C.-W.L., K.D., S.X.L., E.K., B.L., D.I., A.Y., M.K., X.Z., M.K.K., Y.R.C., J.T., and B.H.D. performed experiments and analyzed data. K.D., J.P., M.S., S.B., P.G.S, and R.K.B. performed RNA-seq analysis. E.O. and B.L.E. provided SF3B1 mutant mice and advice with experiments. S.C.-W.L., K.D., R.K.B, and O.A.-W. prepared the manuscript with help from all co-authors.

Competing financial interests
J.P., M.S., S.B., and P.G.S. are employees of H3 Biomedicine, Inc.

References

Ajibade, A. A., Wang, Q., Cui, J., Zou, J., Xia, X., Wang, M., Tong, Y., Hui, W., Liu, D., Su, B.*, et al.* (2012). TAK1 negatively regulates NF-kappaB and p38 MAP kinase activation in Gr-1+CD11b+ neutrophils. Immunity *36*, 43-54.

Alsafadi, S., Houy, A., Battistella, A., Popova, T., Wassef, M., Henry, E., Tirode, F., Constantinou, A., Piperno-Neumann, S., Roman-Roman, S.*, et al.* (2016). Cancer-associated SF3B1 mutations affect alternative splicing by promoting alternative branchpoint usage. Nat Commun *7*, 10615.

Basiorka, A. A., McGraw, K. L., Eksioglu, E. A., Chen, X., Johnson, J., Zhang, L., Zhang, Q., Irvine, B. A., Cluzeau, T., Sallman, D. A.*, et al.* (2016). The NLRP3 inflammasome functions as a driver of the myelodysplastic syndrome phenotype. Blood *128*, 2960-2975.

Bejar, R., Stevenson, K. E., Caughey, B. A., Abdel-Wahab, O., Steensma, D. P., Galili, N., Raza, A., Kantarjian, H., Levine, R. L., Neuberg, D.*, et al.* (2012). Validation of a prognostic model and the impact of mutations in patients with lower-risk myelodysplastic syndromes. Journal of clinical oncology : official journal of the American Society of Clinical Oncology *30*, 3376-3382.

Bosman, M. C., Schepers, H., Jaques, J., Brouwers-Vos, A. Z., Quax, W. J., Schuringa, J. J., and Vellenga, E. (2014). The TAK1-NF-kappaB axis as therapeutic target for AML. Blood *124*, 3130-3140.

Carette, J. E., Raaben, M., Wong, A. C., Herbert, A. S., Obernosterer, G., Mulherkar, N., Kuehne, A. I., Kranzusch, P. J., Griffin, A. M., Ruthel, G.*, et al.* (2011). Ebola virus entry requires the cholesterol transporter Niemann-Pick C1. Nature *477*, 340-343.

Chaudhary, P. M., Eby, M. T., Jasmin, A., Kumar, A., Liu, L., and Hood, L. (2000). Activation of the NF-kappaB pathway by caspase 8 and its homologs. Oncogene *19*, 4451-4460.

Damm, F., Kosmider, O., Gelsi-Boyer, V., Renneville, A., Carbuccia, N., Hidalgo-Curtis, C., Della Valle, V., Couronné, L., Scourzic, L., Chesnais, V.*, et al.* (2012). Mutations affecting mRNA splicing define distinct clinical phenotypes and correlate with patient outcome in myelodysplastic syndromes. Blood *119*, 3211-3218.

Darman, R. B., Seiler, M., Agrawal, A. A., Lim, K. H., Peng, S., Aird, D., Bailey, S. L., Bhavsar, E. B., Chan, B., Colla, S.*, et al.* (2015). Cancer-Associated SF3B1 Hotspot Mutations Induce Cryptic 3? Splice Site Selection through Use of a Different Branch Point. Cell reports *13*, 1033-1045.

DeBoever, C., Ghia, E. M., Shepard, P. J., Rassenti, L., Barrett, C. L., Jepsen, K., Jamieson, C. H., Carson, D., Kipps, T. J., and Frazer, K. A. (2015). Transcriptome sequencing reveals potential mechanism of cryptic 3' splice site selection in SF3B1-mutated cancers. PLoS computational biology *11*, e1004105.

DeDiego, M. L., Nieto-Torres, J. L., Regla-Nava, J. A., Jimenez-Guardeno, J. M., Fernandez-Delgado, R., Fett, C., Castano-Rodriguez, C., Perlman, S., and Enjuanes, L. (2014). Inhibition of NF-kappaB-mediated inflammation in severe acute respiratory syndrome coronavirus-infected mice increases survival. J Virol *88*, 913-924.

Dolatshad, H., Pellagatti, A., Fernandez-Mercado, M., Yip, B. H., Malcovati, L., Attwood, M., Przychodzen, B., Sahgal, N., Kanapin, A. A., Lockstone, H.*, et al.* (2015). Disruption of SF3B1 results in deregulated expression and splicing of key genes and pathways in myelodysplastic syndrome hematopoietic stem and progenitor cells. Leukemia *29*, 1092-1103.

Dvinge, H., Ries, R. E., Ilagan, J. O., Stirewalt, D. L., Meshinchi, S., and Bradley, R. K. (2014). Sample processing obscures cancer-specific alterations in leukemic transcriptomes. Proc Natl Acad Sci U S A *111*, 16802-16807.

Eftychi, C., Karagianni, N., Alexiou, M., Apostolaki, M., and Kollias, G. (2012). Myeloid TAKI [corrected] acts as a negative regulator of the LPS response and mediates resistance to endotoxemia. PloS one *7*, e31550.

Fang, J., Barker, B., Bolanos, L., Liu, X., Jerez, A., Makishima, H., Christie, S., Chen, X., Rao, D. S., Grimes, H. L.*, et al.* (2014). Myeloid malignancies with chromosome 5q deletions acquire a dependency on an intrachromosomal NF-kappaB gene network. Cell reports *8*, 1328-1338.

Fang, J., Bolanos, L. C., Choi, K., Liu, X., Christie, S., Akunuru, S., Kumar, R., Wang, D., Chen, X., Greis, K. D.*, et al.* (2017). Ubiquitination of hnRNPA1 by TRAF6 links chronic innate immune signaling with myelodysplasia. Nat Immunol *18*, 236-245.

Fei, D. L., Motowski, H., Chatrikhi, R., Prasad, S., Yu, J., Gao, S., Kielkopf, C. L., Bradley, R. K., and Varmus, H. (2016). Wild-Type U2AF1 Antagonizes the Splicing Program Characteristic of U2AF1-Mutant Tumors and Is Required for Cell Survival. PLoS Genet *12*, e1006384.
Fellmann, C., Hoffmann, T., Sridhar, V., Hopfgartner, B., Muhar, M., Roth, M., Lai, D. Y., Barbosa, I. A., Kwon, J. S., Guan, Y.*, et al.* (2013). An optimized microRNA backbone for effective single-copy RNAi. Cell reports *5*, 1704-1713.
Flicek, P., Ahmed, I., Amode, M. R., Barrell, D., Beal, K., Brent, S., Carvalho-Silva, D., Clapham, P., Coates, G., Fairley, S.*, et al.* (2013). Ensembl 2013. Nucleic acids research *41*, D48-55.
Graubert, T. A., Shen, D., Ding, L., Okeyo-Owuor, T., Lunn, C. L., Shao, J., Krysiak, K., Harris, C. C., Koboldt, D. C., Larson, D. E.*, et al.* (2012). Recurrent mutations in the U2AF1 splicing factor in myelodysplastic syndromes. Nat Genet *44*, 53-57.
Haferlach, T., Nagata, Y., Grossmann, V., Okuno, Y., Bacher, U., Nagae, G., Schnittger, S., Sanada, M., Kon, A., Alpermann, T.*, et al.* (2014). Landscape of genetic lesions in 944 patients with myelodysplastic syndromes. Leukemia *28*, 241-247.
Harbour, J. W., Roberson, E. D., Anbunathan, H., Onken, M. D., Worley, L. A., and Bowcock, A. M. (2013). Recurrent mutations at codon 625 of the splicing factor SF3B1 in uveal melanoma. Nature genetics *45*, 133-135.
Hernandez, L., Kim, M. K., Noonan, A. M., Sagher, E., Kohlhammer, H., Wright, G., Lyle, L. T., Steeg, P. S., Anver, M., Bowtell, D. D.*, et al.* (2015). A dual role for Caspase8 and NF-kappaB interactions in regulating apoptosis and necroptosis of ovarian cancer, with correlation to patient survival. Cell Death Discov *1*, 15053.
Hu, W. H., Johnson, H., and Shu, H. B. (2000). Activation of NF-kappaB by FADD, Casper, and caspase-8. The Journal of biological chemistry *275*, 10838-10844.
Huber, W., Carey, V. J., Gentleman, R., Anders, S., Carlson, M., Carvalho, B. S., Bravo, H. C., Davis, S., Gatto, L., Girke, T.*, et al.* (2015). Orchestrating high-throughput genomic analysis with Bioconductor. Nature methods *12*, 115-121.
Hubert, C. G., Bradley, R. K., Ding, Y., Toledo, C. M., Herman, J., Skutt-Kakaria, K., Girard, E. J., Davison, J., Berndt, J., Corrin, P.*, et al.* (2013). Genome-wide RNAi screens in human brain tumor isolates reveal a novel viability requirement for PHF5A. Genes Dev *27*, 1032-1045.
Ilagan, J. O., Ramakrishnan, A., Hayes, B., Murphy, M. E., Zebari, A. S., Bradley, P., and Bradley, R. K. (2014). U2AF1 mutations alter splice site recognition in hematological malignancies. Genome research.
Katz, Y., Wang, E. T., Airoldi, E. M., and Burge, C. B. (2010). Analysis and design of RNA sequencing experiments for identifying isoform regulation. Nature methods *7*, 1009-1015.
Kearney, C. J., and Martin, S. J. (2017). An Inflammatory Perspective on Necroptosis. Molecular cell *65*, 965-973.
Kilty, I., and Jones, L. H. (2015). TAK1 selective inhibition: state of the art and future opportunities. Future Med Chem *7*, 23-33.
Kim, E., Ilagan, J. O., Liang, Y., Daubner, G. M., Lee, S. C., Ramakrishnan, A., Li, Y., Chung, Y. R., Micol, J. B., Murphy, M. E.*, et al.* (2015). SRSF2 Mutations Contribute to Myelodysplasia by Mutant-Specific Effects on Exon Recognition. Cancer cell *27*, 617-630.
Lamothe, B., Lai, Y., Hur, L., Orozco, N. M., Wang, J., Campos, A. D., Xie, M., Schneider, M. D., Lockworth, C. R., Jakacky, J.*, et al.* (2012). Deletion of TAK1 in the myeloid lineage results in the spontaneous development of myelomonocytic leukemia in mice. PloS one *7*, e51228.
Langmead, B., Trapnell, C., Pop, M., and Salzberg, S. L. (2009). Ultrafast and memory-efficient alignment of short DNA sequences to the human genome. Genome biology *10*, R25.
Lasho, T. L., Jimma, T., Finke, C. M., Patnaik, M., Hanson, C. A., Ketterling, R. P., Pardanani, A., and Tefferi, A. (2012). SRSF2 mutations in primary myelofibrosis: significant clustering with IDH mutations and independent association with inferior overall and leukemia-free survival. Blood *120*, 4168-4171.
Lee, S. C., Dvinge, H., Kim, E., Cho, H., Micol, J. B., Chung, Y. R., Durham, B. H., Yoshimi, A., Kim, Y. J., Thomas, M.*, et al.* (2016). Modulation of splicing catalysis for therapeutic targeting of leukemia with mutations in genes encoding spliceosomal proteins. Nature medicine *22*, 672-678.
Li, B., and Dewey, C. N. (2011). RSEM: accurate transcript quantification from RNA-Seq data with or without a reference genome. BMC bioinformatics *12*, 323.

Makishima, H., Visconte, V., Sakaguchi, H., Jankowska, A. M., Abu Kar, S., Jerez, A., Przychodzen, B., Bupathi, M., Guinta, K., Afable, M. G.*, et al.* (2012). Mutations in the spliceosome machinery, a novel and ubiquitous pathway in leukemogenesis. Blood *119*, 3203-3210.
Martin, M., Masshofer, L., Temming, P., Rahmann, S., Metz, C., Bornfeld, N., van de Nes, J., Klein-Hitpass, L., Hinnebusch, A. G., Horsthemke, B.*, et al.* (2013). Exome sequencing identifies recurrent somatic mutations in EIF1AX and SF3B1 in uveal melanoma with disomy 3. Nature genetics *45*, 933-936.
McNew, K. L., Whipple, W. J., Mehta, A. K., Grant, T. J., Ray, L., Kenny, C., and Singh, A. (2016). MEK and TAK1 Regulate Apoptosis in Colon Cancer Cells with KRAS-Dependent Activation of Proinflammatory Signaling. Molecular cancer research : MCR *14*, 1204-1216.
Meggendorfer, M., Roller, A., Haferlach, T., Eder, C., Dicker, F., Grossmann, V., Kohlmann, A., Alpermann, T., Yoshida, K., Ogawa, S.*, et al.* (2012). SRSF2 mutations in 275 cases with chronic myelomonocytic leukemia (CMML). Blood *120*, 3080-3088.
Meyer, L. R., Zweig, A. S., Hinrichs, A. S., Karolchik, D., Kuhn, R. M., Wong, M., Sloan, C. A., Rosenbloom, K. R., Roe, G., Rhead, B.*, et al.* (2013). The UCSC Genome Browser database: extensions and updates 2013. Nucleic acids research *41*, D64-69.
Mupo, A., Seiler, M., Sathiaseelan, V., Pance, A., Yang, Y., Agrawal, A. A., Iorio, F., Bautista, R., Pacharne, S., Tzelepis, K.*, et al.* (2016). Hemopoietic-specific Sf3b1-K700E knock-in mice display the splicing defect seen in human MDS but develop anemia without ring sideroblasts. Leukemia.
Obeng, E. A., Chappell, R. J., Seiler, M., Chen, M. C., Campagna, D. R., Schmidt, P. J., Schneider, R. K., Lord, A. M., Wang, L., Gambe, R. G.*, et al.* (2016). Physiologic Expression of Sf3b1(K700E) Causes Impaired Erythropoiesis, Aberrant Splicing, and Sensitivity to Therapeutic Spliceosome Modulation. Cancer cell *30*, 404-417.
Okeyo-Owuor, T., White, B. S., Chatrikhi, R., Mohan, D. R., Kim, S., Griffith, M., Ding, L., Ketkar-Kulkarni, S., Hundal, J., Laird, K. M.*, et al.* (2015). U2AF1 mutations alter sequence specificity of pre-mRNA binding and splicing. Leukemia *29*, 909-917.
Papaemmanuil, E., Cazzola, M., Boultwood, J., Malcovati, L., Vyas, P., Bowen, D., Pellagatti, A., Wainscoat, J. S., Hellstrom-Lindberg, E., Gambacorti-Passerini, C.*, et al.* (2011). Somatic SF3B1 mutation in myelodysplasia with ring sideroblasts. N Engl J Med *365*, 1384-1395.
Papaemmanuil, E., Gerstung, M., Malcovati, L., Tauro, S., Gundem, G., Van Loo, P., Yoon, C. J., Ellis, P., Wedge, D. C., Pellagatti, A.*, et al.* (2013). Clinical and biological implications of driver mutations in myelodysplastic syndromes. Blood *122*, 3616-3627; quiz 3699.
Patnaik, M. M., Lasho, T. L., Finke, C. M., Hanson, C. A., Hodnefield, J. M., Knudson, R. A., Ketterling, R. P., Pardanani, A., and Tefferi, A. (2013). Spliceosome mutations involving SRSF2, SF3B1, and U2AF35 in chronic myelomonocytic leukemia: prevalence, clinical correlates, and prognostic relevance. Am J Hematol *88*, 201-206.
Quesada, V., Conde, L., Villamor, N., Ordóñez, G., Jares, P., Bassaganyas, L., Ramsay, A., Beà, S., Pinyol, M., Martínez-Trillos, A.*, et al.* (2012). Exome sequencing identifies recurrent mutations of the splicing factor SF3B1 gene in chronic lymphocytic leukemia. Nature genetics *44*, 47-52.
Robinson, M. D., and Oshlack, A. (2010). A scaling normalization method for differential expression analysis of RNA-seq data. Genome biology *11*, R25.
Sato, S., Sanjo, H., Takeda, K., Ninomiya-Tsuji, J., Yamamoto, M., Kawai, T., Matsumoto, K., Takeuchi, O., and Akira, S. (2005). Essential function for the kinase TAK1 in innate and adaptive immune responses. Nat Immunol *6*, 1087-1095.
Shikama, Y., Yamada, M., and Miyashita, T. (2003). Caspase-8 and caspase-10 activate NF-kappaB through RIP, NIK and IKKalpha kinases. Eur J Immunol *33*, 1998-2006.
Shirai, C. L., Ley, J. N., White, B. S., Kim, S., Tibbitts, J., Shao, J., Ndonwi, M., Wadugu, B., Duncavage, E. J., Okeyo-Owuor, T.*, et al.* (2015). Mutant U2AF1 Expression Alters Hematopoiesis and Pre-mRNA Splicing In Vivo. Cancer cell *27*, 631-643.
Shirai, C. L., White, B. S., Tripathi, M., Tapia, R., Ley, J. N., Ndonwi, M., Kim, S., Shao, J., Carver, A., Saez, B.*, et al.* (2017). Mutant U2AF1-expressing cells are sensitive to pharmacological modulation of the spliceosome. Nat Commun *8*, 14060.
Shu, H. B., Halpin, D. R., and Goeddel, D. V. (1997). Casper is a FADD- and caspase-related inducer of apoptosis. Immunity *6*, 751-763.

Simoes, A. E., Pereira, D. M., Gomes, S. E., Brito, H., Carvalho, T., French, A., Castro, R. E., Steer, C. J., Thibodeau, S. N., Rodrigues, C. M., and Borralho, P. M. (2015). Aberrant MEK5/ERK5 signalling contributes to human colon cancer progression via NF-kappaB activation. Cell Death Dis *6*, e1718.
Singh, A., Sweeney, M. F., Yu, M., Burger, A., Greninger, P., Benes, C., Haber, D. A., and Settleman, J. (2012). TAK1 inhibition promotes apoptosis in KRAS-dependent colon cancers. Cell *148*, 639-650.
Starczynowski, D. T. (2014). Errant innate immune signaling in del(5q) MDS. Blood *124*, 669-671.
Tang, M., Wei, X., Guo, Y., Breslin, P., Zhang, S., Zhang, S., Wei, W., Xia, Z., Diaz, M., Akira, S., and Zhang, J. (2008). TAK1 is required for the survival of hematopoietic cells and hepatocytes in mice. The Journal of experimental medicine *205*, 1611-1619.
Thol, F., Kade, S., Schlarmann, C., Loffeld, P., Morgan, M., Krauter, J., Wlodarski, M. W., Kolking, B., Wichmann, M., Gorlich, K.*, et al.* (2012). Frequency and prognostic impact of mutations in SRSF2, U2AF1, and ZRSR2 in patients with myelodysplastic syndromes. Blood *119*, 3578-3584.
Thome, M., Schneider, P., Hofmann, K., Fickenscher, H., Meinl, E., Neipel, F., Mattmann, C., Burns, K., Bodmer, J. L., Schroter, M.*, et al.* (1997). Viral FLICE-inhibitory proteins (FLIPs) prevent apoptosis induced by death receptors. Nature *386*, 517-521.
Trapnell, C., Pachter, L., and Salzberg, S. L. (2009). TopHat: discovering splice junctions with RNA-Seq. Bioinformatics *25*, 1105-1111.
Varney, M. E., Niederkorn, M., Konno, H., Matsumura, T., Gohda, J., Yoshida, N., Akiyama, T., Christie, S., Fang, J., Miller, D.*, et al.* (2015). Loss of Tifab, a del(5q) MDS gene, alters hematopoiesis through derepression of Toll-like receptor-TRAF6 signaling. The Journal of experimental medicine *212*, 1967-1985.
Vink, P. M., Smout, W. M., Driessen-Engels, L. J., de Bruin, A. M., Delsing, D., Krajnc-Franken, M. A., Jansen, A. J., Rovers, E. F., van Puijenbroek, A. A., Kaptein, A.*, et al.* (2013). In vivo knockdown of TAK1 accelerates bone marrow proliferation/differentiation and induces systemic inflammation. PloS one *8*, e57348.
Wagenmakers, E. J., Lodewyckx, T., Kuriyal, H., and Grasman, R. (2010). Bayesian hypothesis testing for psychologists: a tutorial on the Savage-Dickey method. Cognitive psychology *60*, 158-189.
Wang, L., Brooks, A. N., Fan, J., Wan, Y., Gambe, R., Li, S., Hergert, S., Yin, S., Freeman, S. S., Levin, J. Z.*, et al.* (2016). Transcriptomic Characterization of SF3B1 Mutation Reveals Its Pleiotropic Effects in Chronic Lymphocytic Leukemia. Cancer cell *30*, 750-763.
Wang, L., Lawrence, M., Wan, Y., Stojanov, P., Sougnez, C., Stevenson, K., Werner, L., Sivachenko, A., DeLuca, D., Zhang, L.*, et al.* (2011). SF3B1 and other novel cancer genes in chronic lymphocytic leukemia. The New England journal of medicine *365*, 2497-2506.
Wei, Y., Dimicoli, S., Bueso-Ramos, C., Chen, R., Yang, H., Neuberg, D., Pierce, S., Jia, Y., Zheng, H., Wang, H.*, et al.* (2013). Toll-like receptor alterations in myelodysplastic syndrome. Leukemia *27*, 1832-1840.
Weinlich, R., Oberst, A., Beere, H. M., and Green, D. R. (2017). Necroptosis in development, inflammation and disease. Nat Rev Mol Cell Biol *18*, 127-136.
Xin, J., Breslin, P., Wei, W., Li, J., Gutierrez, R., Cannova, J., Ni, A., Ng, G., Schmidt, R., Chen, H.*, et al.* (2017). Necroptosis in spontaneously-mutated hematopoietic cells induces autoimmune bone marrow failure in mice. Haematologica *102*, 295-307.
Xu, Z., Tang, K., Wang, M., Rao, Q., Liu, B., and Wang, J. (2009). A new caspase-8 isoform caspase-8s increased sensitivity to apoptosis in Jurkat cells. J Biomed Biotechnol *2009*, 930462.
Yoshida, K., Sanada, M., Shiraishi, Y., Nowak, D., Nagata, Y., Yamamoto, R., Sato, Y., Sato-Otsubo, A., Kon, A., Nagasaki, M.*, et al.* (2011). Frequent pathway mutations of splicing machinery in myelodysplasia. Nature *478*, 64-69.
Young, M. D., Wakefield, M. J., Smyth, G. K., and Oshlack, A. (2010). Gene ontology analysis for RNA-seq: accounting for selection bias. Genome biology *11*, R14.
Yuan, R. T., Young, S., Liang, J., Schmid, M. C., Mielgo, A., and Stupack, D. G. (2012). Caspase-8 isoform 6 promotes death effector filament formation independent of microtubules. Apoptosis *17*, 229-235.
Zhang, J., Lieu, Y. K., Ali, A. M., Penson, A., Reggio, K. S., Rabadan, R., Raza, A., Mukherjee, S., and Manley, J. L. (2015). Disease-associated mutation in SRSF2 misregulates splicing by altering RNA-binding affinities. Proc Natl Acad Sci U S A *112*, E4726-4734.

Zhang, S. J., Rampal, R., Manshouri, T., Patel, J., Mensah, N., Kayserian, A., Hricik, T., Heguy, A., Hedvat, C., Gonen, M.*, et al.* (2012). Genetic analysis of patients with leukemic transformation of myeloproliferative neoplasms shows recurrent SRSF2 mutations that are associated with adverse outcome. Blood *119*, 4480-4485.
Zhou, Q., Derti, A., Ruddy, D., Rakiec, D., Kao, I., Lira, M., Gibaja, V., Chan, H., Yang, Y., Min, J.*, et al.* (2015). A chemical genetics approach for the functional assessment of novel cancer genes. Cancer research *75*, 1949-1958.

Figure Legends

Figure 1. Simultaneous expression of cancer-associated mutations in *Srsf2* and *Sf3b1* is incompatible with hematopoiesis. (A) Heatmap representation of the four most commonly mutated genes encoding pre-mRNA splicing factors across 11 sequencing studies in patients with myeloid malignancies(Bejar et al., 2012; Damm et al., 2012; Haferlach et al., 2014; Lasho et al., 2012; Makishima et al., 2012; Meggendorfer et al., 2012; Papaemmanuil et al., 2013; Patnaik et al., 2013; Thol et al., 2012; Yoshida et al., 2011; Zhang et al., 2012). Each column represents a single patient, and each colored bar represents the presence of the specified mutation in an RNA splicing factor. **(B)** Experimental schema of noncompetitive transplantation experiment using bone marrow mononuclear cells (BM MNCs) from 8-12 week old *Mx1*-Cre, *Mx1*-Cre/*Srsf2*$^{P95H/+}$, *Mx1*-Cre/*Sf3b1*$^{K700E/+}$ and *Mx1*-Cre/*Srsf2*$^{P95H/+}$/*Sf3b1*$^{K700E/+}$ mice. Polyinosinic-polycytidylic acid (pIpC) was administered to recipient mice 4-weeks post-transplantation to induce expression of mutant alleles. **(C)** Percentage of CD45.2^{+} (donor-derived) chimerism in the peripheral blood of CD45.1 recipient mice (n=8-10 mice per genotype) in noncompetitive BM transplantation. **(D)** Representative FACS plots of CD45.2^{+} (donor-derived) cells in the peripheral blood of CD45.1 recipient mice 52 weeks post pIpC administration. Error bars represent means ± standard deviation. One-way analysis of variance followed by Tukey's post-hoc test was used to compare differences between groups. * p<0.05, *** p<0.001 versus control group; ^^p<0.01 versus *Mx1*-Cre/*Sf3b1*$^{K700E/+}$ mice; $^{\#\#}p$<0.01 versus *Mx1*-Cre/*Srsf2*$^{P95H/+}$ mice. **(E)** Number of mice born per genotype from crossing *Sf3b1*$^{K700E/+}$ x *Vav*-Cre *Srsf2*$^{P95H/+}$ or *Srsf2*$^{P95H/+}$ x *Vav*-Cre *Sf3b1*$^{K700E/+}$ mice. A two-sided Chi-square test was used to calculate statistical significance. *p < 0.05. See also **Figure S1** and **Table S1**.

Figure 2. Severe disadvantage of hematopoietic stem cells with simultaneous expression of two cancer-associated mutations in RNA splicing factors or expression of a single RNA splicing factor mutation in the homozygous state. (A) Experimental schema of competitive (1:10) bone marrow (BM) transplantation experiment from 8-12 week old *Mx1*-Cre, *Mx1*-Cre/*Srsf2*$^{P95H/+}$, *Mx1*-Cre/*Sf3b1*$^{K700E/+}$, *Mx1*-Cre/*Srsf2*$^{P95H/+}$/*Sf3b1*$^{K700E/+}$, *Mx1*-Cre/*Srsf2*$^{P95H/P95H}$ and *Mx1*-Cre/*Srsf2*$^{P95H/fl}$ mice. Bone marrow mononuclear cells (BM MNCs) from aged-matched CD45.1 mice were used as the competitor. **(B)** Percentage of CD45.2^{+} (donor-derived) chimerism in the peripheral blood of CD45.1 recipient mice (n=10 mice per genotype) in competitive BM transplantation from *Mx1*-Cre, *Mx1*-Cre/*Srsf2*$^{P95H/+}$, *Mx1*-Cre/*Sf3b1*$^{K700E/+}$, *Mx1*-Cre/*Srsf2*$^{P95H/+}$/*Sf3b1*$^{K700E/+}$ mice. **(C)** Analysis of CD45.2 chimerism in the BM, spleen, thymus and blood 20 weeks post-pIpC administration. **(D)** Percentage of CD45.2^{+} (donor-derived) chimerism in the peripheral blood of CD45.1 recipient mice (n= 5-10 mice per genotype) in competitive BM transplantation from *Mx1*-Cre, *Mx1*-Cre/*Srsf2*$^{P95H/+}$, *Mx1*-Cre/*Srsf2*$^{P95H/P95H}$ and *Mx1*-Cre/*Srsf2*$^{P95H/fl}$ mice. **(E)** Analysis of CD45.2 chimerism in the BM, spleen, thymus, and blood 20 weeks post pIpC administration. Error bars represent means ± standard deviation. One-way analysis of variance followed by Tukey's post-hoc test was used to compare differences between groups. *p<0.05, *** p<0.001 versus control group; ^p<0.05, ^^p<0.01 and ^^^p<0.001 versus *Mx1*-Cre/*Sf3b1*$^{K700E/+}$ mice; $^{\#\#}p$<0.01 and $^{\#\#\#}p$<0.001 versus *Mx1*-Cre/*Srsf2*$^{P95H/+}$ mice. See also **Figure S2**.

Figure 3. *Srsf2* and *Sf3b1* mutations have distinct and additive effects on gene dysregulation. (A) Experimental schema of sample collection for RNA-seq. Samples were collected in biological triplicate. **(B)** Expression of *Srsf2*^{P95H} and *Sf3b1*^{K700E} alleles as percentage of mRNAs expressed from *Srsf2* and *Sf3b1*. Color indicates genotype; the three biological replicates are A-C from left to right. **(C)** Scatter plots comparing coding gene expression in *Mx1*-Cre/*Srsf2*$^{P95H/+}$, *Mx1*-Cre/*Sf3b1*$^{K700E/+}$, and *Mx1*-Cre/*Srsf2*$^{P95H/+}$/*Sf3b1*$^{K700E/+}$ cells relative to wild-type *Mx1*-Cre/*Srsf2*$^{+/+}$/*Sf3b1*$^{+/+}$ cells for replicate B. Red and blue indicate coding genes that were significantly up- or down-regulated in mutant relative to wild-type cells. TPM, transcripts per million (TMM-normalized). **(D)** Gene Ontology (GO) enrichment analysis of *Mx1*-Cre/*Srsf2*$^{P95H/+}$, *Mx1*-Cre/*Sf3b1*$^{K700E/+}$, and *Mx1*-Cre/*Srsf2*$^{P95H/+}$/*Sf3b1*$^{K700E/+}$ cells relative to wild-type *Mx1*-Cre/*Srsf2*$^{+/+}$/*Sf3b1*$^{+/+}$ cells for replicate B. Circle size indicates the magnitude of the *p*-value for each term and genotype comparison. **(E)** Venn diagram showing the overlap between coding genes that were significantly dysregulated in *Mx1*-Cre/*Srsf2*$^{P95H/+}$, *Mx1*-Cre/*Sf3b1*$^{K700E/+}$, and *Mx1*-

Cre/*Srsf2*$^{P95H/+}$/*Sf3b1*$^{K700E/+}$ cells relative to wild-type *Mx1*-Cre/*Srsf2*$^{+/+}$/*Sf3b1*$^{+/+}$ cells for replicate B. **(F)** Expression of *Plk2* and *Trib1*. TPM, transcripts per million (TMM-normalized). See also **Table S2**.

Figure 4. *Srsf2* and *Sf3b1* mutations have distinct and additive effects on RNA splicing. **(A)** Scatter plots of cassette exon inclusion in *Mx1*-Cre/*Srsf2*$^{P95H/+}$, *Mx1*-Cre/*Sf3b1*$^{K700E/+}$, and *Mx1*-Cre/*Srsf2*$^{P95H/+}$/*Sf3b1*$^{K700E/+}$ cells relative to wild-type *Mx1*-Cre/*Srsf2*$^{+/+}$/*Sf3b1*$^{+/+}$ cells for replicate B. Axes indicate the fraction of mRNAs containing each cassette exon in the indicated sample. Red and blue indicate cassette exons whose inclusion is promoted and repressed in mutant relative to wild-type cells. **(B)** As (a), but for competing 3' splice site events. Axes indicate the fraction of mRNAs which use the intron-proximal 3' splice site in the indicated sample. Red and blue indicate intron-proximal 3' splice sites whose usage is promoted and repressed in mutant relative to wild-type cells. **(C)** Plots illustrating the spatial distribution of the CCNG and GGNG (N = any nucleotide) exonic splicing enhancers adjacent to differentially spliced cassette exons that are promoted versus repressed in mutant relative to wild-type cells. Vertical axis indicates the relative frequency of each motif, averaged over all promoted versus repressed cassette exons for the indicated genotype comparisons. **(D)** Venn diagram showing the overlap between splicing events that were significantly dysregulated in *Mx1*-Cre/*Srsf2*$^{P95H/+}$, *Mx1*-Cre/*Sf3b1*$^{K700E/+}$, and *Mx1*-Cre/*Srsf2*$^{P95H/+}$/*Sf3b1*$^{K700E/+}$ cells relative to wild-type *Mx1*-Cre/*Srsf2*$^{+/+}$/*Sf3b1*$^{+/+}$ cells for replicate B. Example genes illustrated below are indicated with arrows. **(E)** RNA-seq read coverage across the genomic loci containing the illustrated differentially spliced events in *Wdr73*, *Wdfy1*, and *Ppig* for all genotypes. Yellow indicates the differentially spliced sequence for each event. See also **Figure S3** and **Table S3**.

Figure 5. *SF3B1* mutations promote mis-splicing of *MAP3K7*, resulting in hyperactivation of NF-κB signaling. (A) Gene Ontology (GO) analysis of mouse hematopoietic stem and progenitor cells (HSPCs) revealed that differentially expressed genes were enriched for innate immune and inflammatory pathways in *Sf3b1*$^{K700E/+}$, *Srsf2*$^{P95H/+}$ and *Sf3b1*$^{K700E/+}$/*Srsf2*$^{P95H/+}$ cells relative to wild-type control. **(B)** Venn diagram illustrating the overlap of differentially spliced genes across murine bone marrow hematopoietic progenitors (lineage^{-} c-Kit^{+}) in *Sf3b1*$^{K700E/+}$ versus *Sf3b1*$^{+/+}$ mice and MDS patient samples that were mutant versus wild-type for *SF3B1*. **(C)** From top to bottom, exon-intron structure of *MAP3K7,* conservation of mouse and human sequences adjacent to the competing 3' splice site affected by *SF3B1* mutations, and RNA-seq coverage plots of this region in human and mouse samples with or without *SF3B1* mutations. **(D)** RT-PCR of the *MAP3K7* competing 3' splice site in isogenic mouse and human cells as well as primary patient MDS samples with or without *SF3B1* mutations. **(E)** Immunoblot analysis of MAP3K7 using a C-terminal anti-MAP3K7 antibody in isogenic NALM-6 leukemia cells expressing wild-type or mutant SF3B1 from its endogenous locus. **(F)** Analysis of phosphorylated p65 (phospho-p65) levels by intracellular flow cytometry in NALM-6 cells with or without *SF3B1*K700E mutation following stimulation with lipopolysaccharide (LPS) or TNFα. **(G)** Quantitative RT-PCR (qRT-PCR) analysis of NF-κB target genes IL-1β and TNF 8 hours post LPS stimulation in NALM-6 *SF3B1*-isogenic cells. **(H)** Heatmap representation of NF-kB luciferase reporter signal in SF3B1 mutant knockin NALM6 cells (left two panels) or parental NALM6 cells with anti-*MAP3K7* shRNA (right two panels) following stimulation with LPS or TNFα. See also **Figure S4** and **Table S4.**

Figure 6. *SRSF2* mutations promote aberrant splicing of *caspase-8* (*CASP8*), resulting in expression of a truncated protein that hyperactivates NF-κB signaling. (A) RNA-seq coverage plots of *CASP8* splicing in chronic myelomonocytic leukemia (CMML) and acute myeloid leukemia (AML) patients wild-type or mutant for *SRSF2*. *SRSF2* mutations repress the illustrated *CASP8* cassette exon. AML and CMML RNA-seq data are from Kim *et al* (Kim et al., 2015). **(B)** RT-PCR analysis of the *CASP8* splicing event in human leukemia cell lines wild-type (TF1 and K562) or mutant (K052) for *SRSF2* and a diagram of the corresponding *CASP8* isoforms. **(C)** Immunoblot analysis of caspase-8 using an N-terminal anti-caspase-8 antibody in human leukemia cells (left panel) and primary AML patient samples (right panel) wild-type or mutant for *SRSF2.* **(D)** Immunoblot analysis of caspase-8 expression in K562 cells (left panel) and *CASP8* knockout (KO) HAP1 cells (right panel) expressing cDNA constructs encoding empty vector (EV), full-length *CASP8* (*CASP8*^{FL}), or the

aberrantly spliced *caspase-8* truncated isoform (*CASP8*^{TR}). Heatmap representation of NF-κB luciferase reporter signal following TRAIL stimulation in **(E)** K562, **(F)** HAP1, or **(G)** *CASP8* KO HAP1 cells expressing cDNA constructs encoding empty vector, full-length *caspase-8* (*CASP8*^{FL}), or the aberrantly spliced *caspase-8* truncated isoform (*CASP8*^{TR}). **(H)** Experimental schema of LPS administration (15 mg/kg) *in vivo* in wild-type control, *Srsf2*$^{P95H/+}$ and *Sf3b1*$^{K700E/+}$ mice. **(I)** Kaplan-Meier survival analysis of wild-type control, *Srsf2*$^{P95H/+}$ and *Sf3b1*$^{K700E/+}$ mice following *in vivo* LPS challenge. See also **Figures S5-6.**

STAR Methods

CONTACT FOR REAGENT AND RESOURCE SHARING

Further information and requests for resources and reagents should be directed to and will be fulfilled by the Lead Contact, Omar Abdel-Wahab (abdelwao@mskcc.org).

EXPERIMENTAL MODEL AND SUBJECT DETAILS

Animals

All animals were housed at Memorial Sloan Kettering Cancer Center (MSKCC). All animal procedures were completed in accordance with the Guidelines for the Care and Use of Laboratory Animals and were approved by the Institutional Animal Care and Use Committees at MSKCC. The number of mice in each experiment was chosen to provide 90% statistical power with a 5% error level. Generation and genotyping of the *Srsf2*$^{P95H/+}$, *Sf3b1*$^{K700E/+}$ and *Srsf2*$^{fl/+}$ as well as the *Mx1*-Cre and *Vav*-Cre transgenic mice have been previously described (Kim et al., 2015; Obeng et al., 2016). 6-week-old *Mx1-cre* mice (both males and females) on a C57BL/6J background were used for all experiments except where 6-week-old female CD45.1 C57BL/6J mice were used as recipients for bone marrow transplantation assays.

Primary human MDS and CLL samples

Studies were approved by the Institutional Review Boards of Memorial Sloan Kettering Cancer Center and conducted in accordance to the Declaration of Helsinki protocol. Primary human de-identified MDS and CLL samples derived from whole peripheral blood or BM mononuclear cells were utilized.

Cell lines

The NALM-6 isogenic cell lines (NALM-6 cells engineered to express the single mutations *SF3B1*K700E or *SF3B1*K700K from the endogenous locus) were cultured in RPMI/10% FCS, and the HAP1 and *CASP8-KO* HAP1 cells were cultured in IMDM/10% FCS. These cell lines were obtained from Horizon Discovery. K562 cells were obtained from ATCC.

METHOD DETAILS

Peripheral blood analysis

Blood was collected by submandibular bleeding using heparinized microhematocrit capillary tubes (Thermo Fisher Scientific). Automated peripheral blood counts were obtained using a ProCyte Dx Hematology Analyzer (IDEXX).

Bone marrow transplantation assays

Primary bone marrow (BM) cells were isolated from *Mx1*-Cre, *Mx1*-Cre/*Srsf2*$^{P95H/+}$, *Mx1*-Cre/*Sf3b1*$^{K700E/+}$, *Mx1*-Cre/*Srsf2*$^{P95H/+}$/*Sf3b1*$^{K700E/+}$, *Mx1*-Cre/*Srsf2*$^{P95H/fl}$ or *Mx1*-Cre/*Srsf2*$^{P95H/P95H}$ mice (aged 8-12 weeks) into cold PBS (without Ca^{2+} and Mg^{2+}) supplemented with 2% bovine serum albumin (BSA) to generate single cell suspensions. Red blood cells (RBCs) were removed using ammonium chloride-potassium bicarbonate (ACK) lysis buffer, resuspended in PBS/2% BSA, and filtered through a 40μm cell strainer. Total nucleated cells were quantified by the Vi-Cell XR cell counter (Beckman Coulter). For competitive transplantation experiments, a total of 1.8 x 10^6 BM cells from *Mx1*-Cre, *Mx1*-Cre/*Srsf2*$^{P95H/+}$, *Mx1*-Cre/*Sf3b1*$^{K700E/+}$, *Mx1*-Cre/*Srsf2*$^{P95H/+}$/*Sf3b1*$^{K700E/+}$ or *Mx1*-Cre/*Srsf2*$^{P95H/P95H}$ CD45.2$^+$ mice were mixed with 0.2 x 10^6 wild-type CD45.1$^+$ support BM and transplanted via tail vein injection into 8-week old lethally irradiated (2x 450 cGy; 4 hours apart) CD45.1$^+$ recipient mice. For noncompetitive transplantation experiments, 2 x 10^6 total BM cells from *Mx1*-Cre, *Mx1*-Cre/*Srsf2*$^{P95H/+}$, *Mx1*-Cre/*Sf3b1*$^{K700E/+}$, *Mx1*-Cre/*Srsf2*$^{P95H/+}$/*Sf3b1*$^{K700E/+}$, *Mx1*-Cre/*Srsf2*$^{P95H/fl}$ or *Mx1*-Cre/*Srsf2*$^{P95H/P95H}$ mice were injected into lethally irradiated (2 x 450 cGy) CD45.1$^+$ recipient mice. To activate the conditional alleles, mice were treated with 3 doses of polyinosinic:polycytidylic acid (pIpC; 12mg/kg/day; GE Healthcare) every other day via intraperitoneal injection. Peripheral blood chimerism of mature blood cell lineages was assessed routinely by flow cytometry.

***In vivo* LPS stimulation experiment**
For *in vivo* LPS stimulation, *Escherichia coli* 055:B4 LPS (Sigma Aldrich) was used.

Flow cytometry analyses
Cells were incubated with antibodies in PBS/2% BSA (without Ca^{2+} and Mg^{2+}) for 30-45 minutes on ice. For hematopoietic stem and progenitor cell staining, cells were stained with a lineage cocktail of monoclonal antibodies including B220 (RA3-6B2), CD19 (1D3), CD3 (17A2), CD4 (GK1.5), CD8a (53-6.7), Gr-1 (RB6-8C5), Mac-1 (M1/70), NK1.1 (PK136) and Ter119, allowing for mature lineage exclusion from the analysis. Cells were also stained with antibodies against c-Kit (2B8), Sca-1 (D7), FcγRII/III (93), CD34 (RAM34), CD45.1 (A20), CD45.2 (104), CD48 (HM48-1) and CD150 (9D1). DAPI was used to exclude dead cells. The composition of mature hematopoietic cell lineages in the bone marrow, spleen, thymus and peripheral blood was assessed using a combination of antibodies against Mac-1, Gr-1, B220, CD19, CD3, CD4, CD8a, CD25 (PC61.5), CD44 (IM7), IgM (Il/41), CD43 (S11). All FACS sorting was performed on FACS Aria, and analysis was performed on an LSR Fortessa (BD Biosciences). Intracellular flow cytometry for phospho-p65/NF-κB-Ser536 (CST) was performed using the Transcription Factor Staining Buffer Set (eBiosciences 00-5523) following the manufacturer instructions.

Immunoblot
For immunoblotting, the following antibodies were used: NF-κB/p65 (CST; 8242), phospho NF-κB/p65-Ser536 (CST; 3033), IκBα (CST; 9242), TAK1/MAP3K7 (CST; 5206), RIP (CST; D94C12), Caspase-8, N-terminal (Abcam; clone E6), Caspase-8, C-terminal (Enzo Life Science; clone 12F5), phospho-IRAK1 Thr209 (Assay Biotech), phospho-IRAK4 Thr345 (AbboMax), total IRAK1 (CST), total IRAK4 (CST), β-actin (Sigma-Aldrich; A-5441).

Caspase 8 constructs
MSCV-Flag-CASP8^{FL}-IRES-GFP and MSCV-Flag-CASP8^{TR}-IRES-GFP, and MSCV-IRES-GFP empty vector constructs were used for overexpression studies. Retroviral supernatants were produced by transfecting 293 GPII cells with cDNA constructs and the packaging plasmid VSV.G using XtremeGene9 (Roche), and were used to transduce HAP1, *CASP8* KO HAP1 and K562 leukemic cells in the presence of polybrene (5 μg/mL; Millipore). Successfully transduced cells expressing GFP were purified by flow cytometry. Cells were stimulated with TRAIL (PeproTech).

Luciferase reporter assay
We generated K562, NALM-6 *SF3B1* isogenic cells, HAP1 and *CASP8* knockout (KO) HAP1 cells expressing the luciferase reporter for NF-κB response elements by following the manufacturer instructions (Cignal^{TM} Reporter Assay, Qiagen). Cells were stimulated with LPS, TNFα or TRAIL as described above, and NF-κB activity was assessed by luciferase intensity using the Dual-Luciferase Reporter Assay System (Promega) according to the manufacturer instructions.

RT-PCR and quantitative RT-PCR (qRT-PCR)
Total RNA was isolated using RNeasy Mini kit (Qiagen). For cDNA synthesis, total RNA was reverse transcribed to cDNA with SuperScript VILO cDNA synthesis kit (Life Technologies). The resulting cDNA was diluted 10-20 fold prior to use. Quantitative RT-PCR (qRT-PCR) was performed in 10 μL reactions with either SYBR Green PCR Master Mix or Taqman Gene Expression Master Mix with AmpErase (ThermoFisher Scientific). All qRT-PCR analysis was performed on an Applied Biosystems QuantStudio 6 Flex Cycler (ThermoFisher Scientific). Relative gene expression levels of TNF and IL-1β in LPS- or TNFα-treated versus pre-stimulated cells were calculated using the comparative CT method.

Primers used in RT-PCR reactions were:
MAP3K7 (human) – Fwd: GATGGAATATGCTGAAGGGG, Rev: CACTCCTTGGGAACACTGTA
Map3k7 (mouse) – Fwd: GATGGAATATGCAGAGGGGG, Rev: CACTCCTTGGGAACACTGTA
CASP8 (human) – Fwd: GAACTTCAGACACCAGGC, Rev: CTTTGTCCAAAGTCTTTGCTG

Primers used in qRT-PCR reactions were:
CASP8 exclusion isoform (aberrant):
Fwd: GATGAATTTTCAAATGACTTTGGAC,
Rev: TGATCAGACAGTATCCCCGAG

CASP8 inclusion isoform (canonical):
Fwd: TGATGAATTTTCAAATGGGGAGGA
Rev: ATCCTGTTCTCTTGGAGAGTCC

Taqman probes were used for gene expression analysis of TNF (Hs00174128_m1), IL-1β (Hs01555410_m1) and GAPDH (Hs02786624_g1).

shRNA experiments
NALM-6 parental cells carrying the NF-κB luciferase reporter were transduced with a doxycycline-inducible lentiviral vector, T3G-dsRED-mirE-PGK-Neo-IRES-rtTA3 (Fellmann et al., 2013), expressing shRNAs for *MAP3K7* or a non-targeting luciferase control. Transduced cells were selected with G418 (0.5 mg/mL; ThermoFisher Scientific), and the short hairpins were induced with the addition of doxycycline (2.0 µg/mL; Sigma Aldrich).

The short hairpin sequences are:
MAP3K7.748: TTAGGTAAATTTTTTATCAGTG
MAP3K7.1041: TTTTCAACAATTTTGATTCTAA
Luciferase control: TTAATCAGAGACTTCAGGCGGT

QUANTIFICATION AND STATISTICAL ANALYSIS
Statistical analyses
Statistical significance was determined by unpaired Student's t-test or analysis of variance (ANOVA) after testing for normal distribution and equal variance, unless indicated otherwise. For Kaplan Meier survival analysis, Mantel-Cox log-ranked test was used to determine statistical significance. For offspring frequency analysis, a Chi-Square test was performed to test the difference between observed and expected frequencies from different genotypes. Data were plotted using GraphPad Prism 7 software as mean values, error bars represent standard deviation.

mRNA isolation, sequencing, and analysis
RNA was extracted from sorted mouse cell populations using Qiagen RNeasy columns. Poly(A)-selected, unstranded Illumina libraries were prepared with a modified TruSeq protocol. 0.5X AMPure XP beads were added to the sample library to select for fragments <400 bp, followed by 1X beads to select for fragments >100 bp. These fragments were then amplified with PCR (15 cycles) and separated by gel electrophoresis (2% agarose). 300 bp DNA fragments were isolated and sequenced on the Illumina HiSeq 2000 (~100M 101 bp reads per sample).

Genome annotations
Genome annotations for the human (NCBI GRCh37/UCSC hg19) and mouse (NCBI GRCm38/UCSC mm10) genomes were created as previously described (Dvinge et al., 2014). Genome annotations from the Ensembl (Flicek et al., 2013) and UCSC (Meyer et al., 2013) databases were merged with splicing event annotations from MISO v2.0 (Katz et al., 2010). An additional annotation of all possible combinations of annotated 5' and 3' splice sites found in the merged annotation was created for read mapping. Constitutive introns were defined as those whose associated 5' and 3' splice sites were alternatively spliced in the UCSC annotation.

RNA-seq read mapping
RNA-seq reads were sequentially mapped to the transcriptome and genome as previously described (Dvinge et al., 2014). Reads were first mapped to the transcriptome using Bowtie v1.0.0 (Langmead et

al., 2009) and RSEM v1.2.4 (Li and Dewey, 2011). The resulting read alignments were then filtered to require that reads spanning splice junctions overlapped the flanking exons by at least six nt. The remaining unaligned reads were then mapped to the genome and splice junctions using TopHat v2.0.8b(Trapnell et al., 2009), where reads were only allowed to align to the splice junctions present in the file of all possible combinations of annotated 5' and 3' splice sites described above. The resulting read alignments were then merged with the output of RSEM's alignment to create a final file of aligned reads.

Differential gene expression analysis

Gene expression analysis was performed using the gene expression estimates computed by RSEM in units of transcripts per million (TPM). Those estimates were then further normalized using the TMM method (Robinson and Oshlack, 2010), with a reference set of all protein-coding genes. Differentially expressed genes were defined as those with an associated Bayes factor ≥ 100 (computed using Wagenmakers's Bayesian framework (Wagenmakers et al., 2010)) and an associated fold-change ≥ 1.5.

Differential splicing analysis

Isoform ratios for annotated splicing events (cassette exons, competing 5' and 3' splice sites, and annotated retained introns) were calculated using MISO v2.0 (Katz et al., 2010). Splicing of constitutively spliced introns and junctions was quantified using only junction-spanning reads, as previously described (Hubert et al., 2013). Differential splicing in the murine data was identified by comparing samples from different genotypes for a single replicate in a pairwise fashion. The analysis was restricted to splicing events with at least 20 informative reads, where an informative read is defined as a read that distinguishes between isoforms. Differentially spliced events were defined as those with an associated Bayes factor was ≥ 5 (computed using Wagenmakers's Bayesian framework (Wagenmakers et al., 2010)) and absolute change in isoform ratio of ≥ 10%. Differential splicing in the human patient cohorts was identified using a group statistical test to identify differences between patient samples with or without defined splicing factor mutations. Differentially spliced events were defined as those with an associated *p*-value ≤ 0.05 (computed using the Wilcoxon rank-sum test) and an absolute change in median per-group isoform ratio of ≥10%.

Gene Ontology (GO) enrichment analysis

GO enrichment analysis was performed using the GOseq method (Young et al., 2010) to correct for sequencing depth biases. The background set of genes was defined as all protein-coding genes. False discovery rates were calculated using the Wallenius method and corrected using the Benjamini-Hochberg method. We restricted reporting of enriched terms to those with at least two ancestors and fewer than 500 associated genes.

Motif enrichment analysis and sequence logos

The relative enrichment of different ESEs was computed by comparing motif occurrence within and adjacent to cassette exons that were promoted versus repressed in cells or samples with versus without defined splicing factor mutations. These analyses were performed using all cassette exons that were differentially spliced in at least one mouse replicate for a given genotype comparison. 95% confidence intervals were calculated by bootstrapping with 500 resampling steps. Sequence logos centered on intron-proximal or intron-distal 3' splice sites were created using all competing 3' splice sites that were differentially spliced in at least one mouse replicate for a given genotype comparison. The analysis was restricted to events with canonical GT and AG dinucleotides at the 5' and 3' splice sites. These analyses relied upon the GenomicRanges package in Bioconductor (Huber et al., 2015).

DATA AND SOFTWARE AVAILABILITY

Publicly available RNA-seq data

FASTQ files from published RNA-seq studies of patients with MDS (Dolatshad et al., 2015) and CLL (Darman et al., 2015) were downloaded from GEO series GSE63569 and GSE72790.

Accession codes
Gene Expression Omnibus: All newly generated RNA-seq data are deposited into the GEO database (accession number GSE97452).

KEY RESOURCES TABLE
See separate document.

Table S1: Mutational analysis of *SF3B1, SRSF2, U2AF1,* and *ZRSR2* in patients with myelodysplastic syndromes and related myeloid neoplasms.

Table S2: Differentially expressed genes in spliceosomal mutant mouse hematopoietic progenitors.

Table S3: Percent spliced in (Psi) values for differentially spliced events across all replicates.

Table S4: Human splicing events corresponding to differentially spliced genes in both human and mouse samples with a mutation in *SF3B1*.

Figure S1. Severe self-renewal disadvantage of hematopoietic stem cells from *Srsf2*$^{P95H/+}$/*Sf3b1*$^{K700E/+}$ double-mutant mice. (A) Representative FACS plots of CD45.2^{+} (donor-derived) cells of both lymphoid and myeloid lineages in the peripheral blood of CD45.1 recipient mice reconstituted with bone marrow (BM) mononuclear cells (MNCs) from *Mx1*-Cre, *Mx1*-Cre/*Srsf2*$^{P95H/+}$, *Mx1*-Cre/*Sf3b1*$^{K700E/+}$ and *Mx1*-Cre/*Srsf2*$^{P95H/+}$/*Sf3b1*$^{K700E/+}$ mice 20 weeks post pIpC administration. **(B)** Percentage of CD45.2 (donor-derived) chimerism in the B-, T- or myeloid lineages in peripheral blood of CD45.1 recipient mice (n=10 mice per genotype) in competitive BM transplantation. **(C)** Analysis of CD45.2 chimerism in the various cellular lineages in the bone marrow, spleen and thymus 20 weeks post pIpC administration in CD45.1 recipient mice. Error bars represent means ± standard deviation. One-way analysis of variance followed by Tukey's post-hoc test was used to compare differences between groups. *p<0.05, **p< 0.01 and ***p< 0.001 versus control group; ^p<0.05, ^^p<0.01 and ^^^p<0.001 versus *Mx1*-Cre/*Sf3b1*$^{K700E/+}$ mice; $^{\#}p$< 0.05, $^{\#\#}p$< 0.01 and $^{\#\#\#}p$< 0.001 versus *Mx1*-Cre/*Srsf2*$^{P95H/+}$ mice.

Figure S2. Severe self-renewal disadvantage of hematopoietic stem cells from *Srsf2*$^{P95H/P95H}$ homozygous mutant mice. (A) Representative FACS plots of CD45.2^{+} (donor-derived) cells of both lymphoid and myeloid lineages in the peripheral blood of CD45.1 recipient mice reconstituted with bone marrow (BM) mononuclear cells (MNCs) from *Mx1*-Cre, *Mx1*-Cre/*Srsf2*$^{P95H/+}$, *Mx1*-Cre/*Srsf2*$^{P95H/P95H}$ and *Mx1*-Cre/*Srsf2*$^{P95H/fl}$ mice 20 weeks post pIpC administration. **(B)** Percentage of CD45.2 (donor-derived) chimerism in the B-, T- or myeloid lineages in peripheral blood of CD45.1 recipient mice (n=5-10 mice per genotype) in competitive BM transplantation. **(C)** Analysis of CD45.2 chimerism in the various cellular lineages in the bone marrow, spleen and thymus 20 weeks post pIpC administration in CD45.1 recipient mice. Error bars represent means ± standard deviation. One-way analysis of variance followed by Tukey's post-hoc test was used to compare differences between groups. *p< 0.05, **p< 0.01 and ***p< 0.001 versus control group; $^{\#}p$< 0.05, $^{\#\#}p$< 0.01 and $^{\#\#\#}p$< 0.001 versus *Mx1*-Cre/*Srsf2*$^{P95H/+}$ mice.

Figure S3. Co-occurring *Srsf2* and *Sf3b1* mutations do not cause global splicing failure. (A) Sequence logos associated with competing 3' splice sites that are differentially spliced in *Mx1*-Cre/*Srsf2*$^{P95H/+}$, *Mx1*-Cre/*Sf3b1*$^{K700E/+}$, and *Mx1*-Cre/*Srsf2*$^{P95H/+}$/*Sf3b1*$^{K700E/+}$ cells relative to wild-type *Mx1*-Cre/*Srsf2*$^{+/+}$/*Sf3b1*$^{+/+}$ cells in any replicate. The left- and right-hand columns contain sequence logos created for the intron-proximal and intron-distal 3' splice sites. **(B)** Bar plots illustrating enrichment of different variants of the SSNG (S = C or G; N = any nucleotide) exonic splicing enhancer in *Mx1*-Cre/*Srsf2*$^{P95H/+}$, *Mx1*-Cre/*Sf3b1*$^{K700E/+}$, and *Mx1*-Cre/*Srsf2*$^{P95H/+}$/*Sf3b1*$^{K700E/+}$ cells relative to wild-type *Mx1*-Cre/*Srsf2*$^{+/+}$/*Sf3b1*$^{+/+}$ cells. Enrichment computed using the alternatively spliced sequence for cassette exons that are differentially spliced in the indicated genotype comparisons. **(C)** Scatter plots of constitutive intron splicing in *Mx1*-Cre/*Srsf2*$^{P95H/+}$, *Mx1*-Cre/*Sf3b1*$^{K700E/+}$, and *Mx1*-Cre/*Srsf2*$^{P95H/+}$/*Sf3b1*$^{K700E/+}$ cells relative to wild-type *Mx1*-Cre/*Srsf2*$^{+/+}$/*Sf3b1*$^{+/+}$ cells for replicate B. Axes indicate the fraction of mRNAs for which each constitutive intron is removed. Red and blue indicate constitutive introns that are preferentially spliced and retained in mutant relative to wild-type cells. **(D)** As Figure 4d, but with different genes highlighted. **(E)** RNA-seq read coverage across the genomic loci containing the illustrated differentially spliced events in *Smg7*, *A230046K03Rik*, and *Wsb1* for all genotypes. Yellow indicates the differentially spliced sequence for each event.

Figure S4. *SF3B1* mutations promote mis-splicing of *MAP3K7*. (A) RT-PCR analysis and Sanger sequencing traces of the normal and aberrantly spliced *MAP3K7* isoforms in NALM6 *SF3B1* isogenic cells. **(B)** Protein diagram of MAP3K7 indicating region of aberrant 3' splice site usage in *SF3B1* mutant cells. **(C)** Western blot of MAP3K7 in parental NALM6 cells treated with NF-κB reporter construct, anti-*MAP3K7* shRNAs, and/or control shRNAs.

Figure S5. *MAP3K7* and *CASP8* aberrant splicing events are specific to mutant SF3B1 and SRSF2, respectively. (A) RNA-seq coverage plots of *MAP3K7* in acute myeloid leukemia (AML) and chronic myelomonocytic leukemia (CMML) patient samples wild-type (WT) or mutant (MUT) for *SRSF2*. **(B)** RNA-seq coverage plots of *CASP8* in normal human bone marrow (BM) cells as well as the NALM-6 cell line and cells from myelodysplastic syndrome (MDS) and chronic lymphocytic leukemia (CLL) patients wild-type (WT) or mutant (MUT) for *SF3B1.*

Figure S6. *SRSF2* mutations promote aberrant splicing of *caspase-8* (*CASP8)* resulting in expression of a stable truncated protein that hyperactivates NF-κB signaling. (A) RT-PCR of the *CASP8* splicing event in human leukemia cell lines and primary human AML patient samples wild-type or mutant for *SRSF2* with diagram of predicted effects of *CASP8* mRNA. The red box highlights the *CASP8* isoform promoted by mutant SRSF2. **(B)** Sanger sequencing traces of the aberrant *CASP8* isoform (*CASP8 TR*) in *SRSF2*-mutant leukemia cell line (K052) and *SRSF2*-mutant primary AML patient samples. **(C)** Quantitative RT-PCR analysis of the aberrant *CASP8* isoform expression in *SRSF2* wild-type and *SRSF2* mutant patient AML samples. **(D)** Growth assay of K562 cells overexpressing empty vector control (EV), full-length *caspase-8* (*CASP8 FL*) and the aberrant *caspase-8* truncated isoform (*CASP8 TR*). **(E)** Cell viability assay using CellTiter-Glo in K562 cells expressing empty vector control (EV), *CASP8 FL*, and *CASP8 TR* isoforms 48 hours post-TRAIL stimulation. **(F)** Analysis of NF-κB signaling following TRAIL stimulation (50 ng/mL) in K562 cells overexpressing EV, *CASP8 FL*, and *CASP8 TR* isoforms. Cell viability assay using CellTiter-Glo in **(G)** *CASP8* wild-type (WT) and **(H)** *CASP8* knockout (KO) HAP1 cells expressing EV control, *CASP8 FL*, and *CASP8 TR* isoforms 48 hours post TRAIL stimulation. **(I)** Analysis of NF-κB signaling following TRAIL stimulation (50 ng/mL) in *CASP8* KO HAP1 cells expressing EV, *CASP8 FL*, and *CASP8 TR* isoforms.

Figure 1

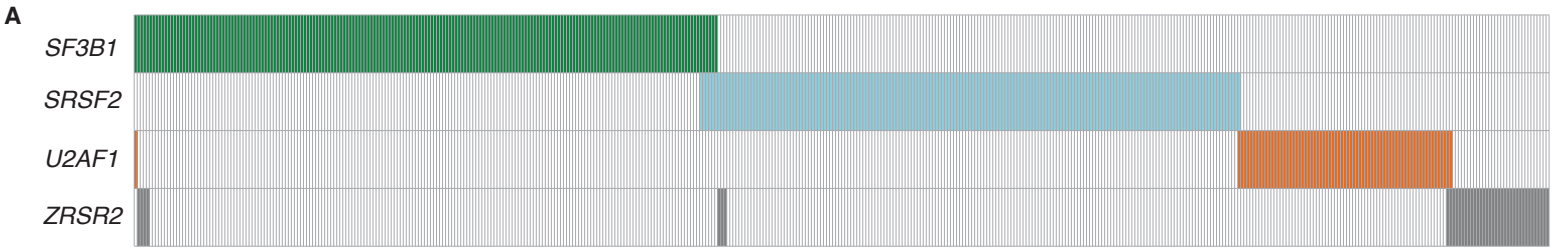

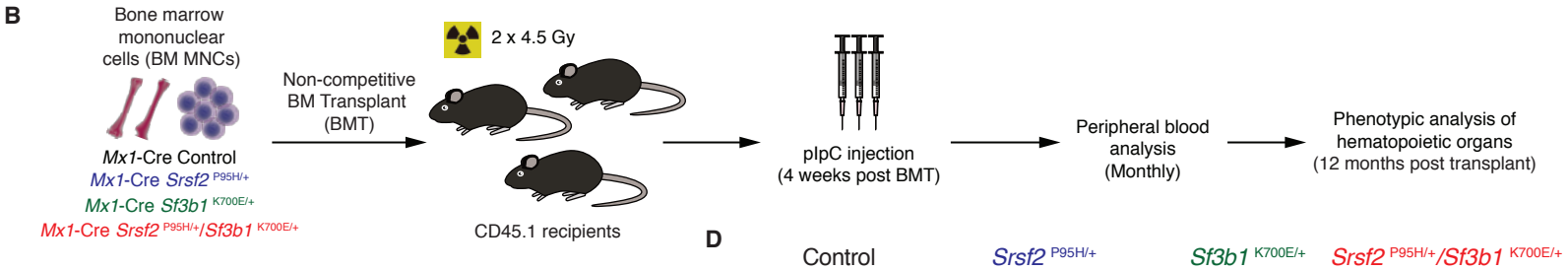

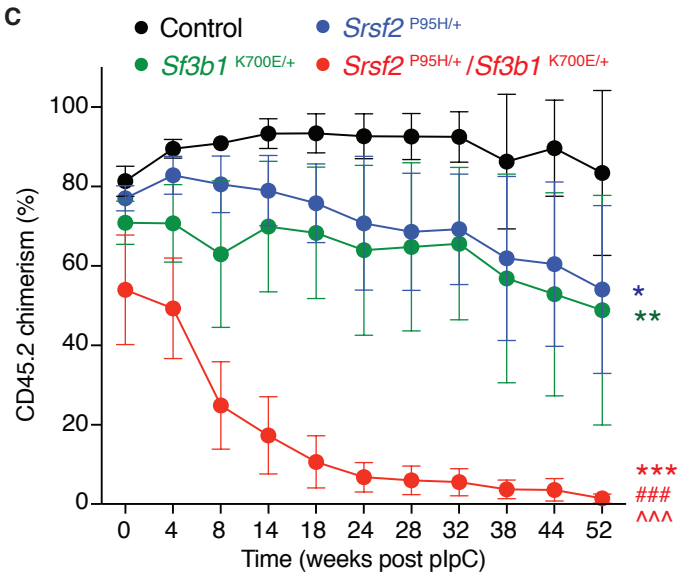

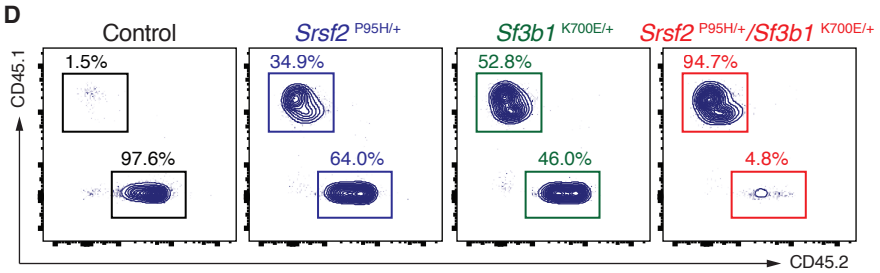

E

♂ 1. *Srsf2* P95H/+ x ♀ *Vav*-Cre *Sf3b1* K700E/+

♂ 2. *Sf3b1* K700E/+ x ♀ *Vav*-Cre *Srsf2* P95H/+

Total live births (n = 78)	*Vav*-Cre negative	*Vav*-Cre positive
Srsf2 +/+ / *Sf3b1* +/+	16.7% (13/78)	17.9% (14/78)
Srsf2 P95H/+ / *Sf3b1* +/+	10.3% (8/78)	14.1% (11/78)
Srsf2 +/+ / *Sf3b1* K700E/+	17.9% (14/78)	10.3% (8/78)
Srsf2 P95H/+ / *Sf3b1* K700E/+	12.8% (10/78)	0% (0/78) *

* $p = 0.0144$

Figure 2

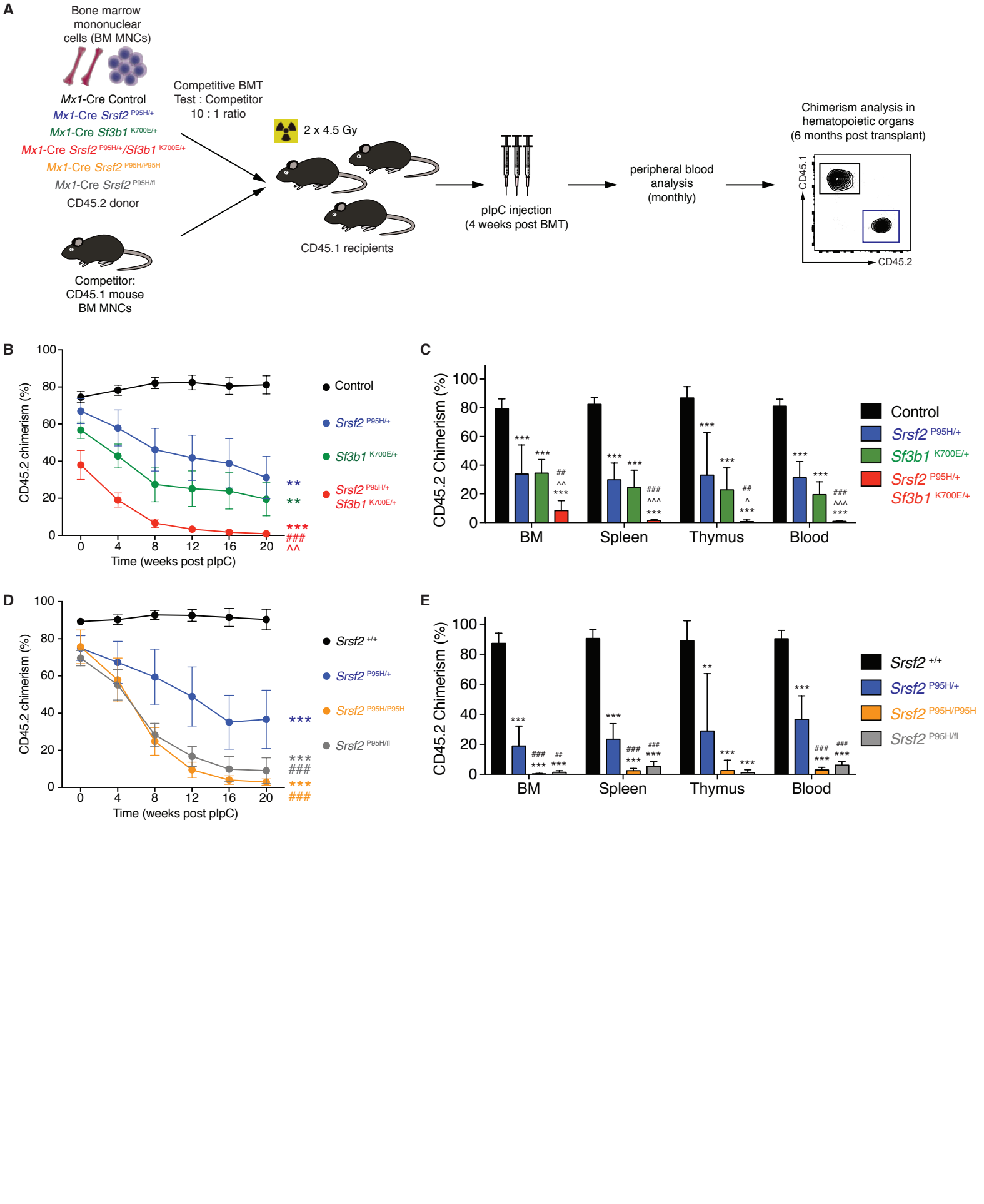
A
Bone marrow mononuclear cells (BM MNCs)
Mx1-Cre Control
Mx1-Cre Srsf2 P95H/+
Mx1-Cre Sf3b1 K700E/+
Mx1-Cre Srsf2 P95H/+/Sf3b1 K700E/+
Mx1-Cre Srsf2 P95H/P95H
Mx1-Cre Srsf2 P95H/fl
CD45.2 donor
Competitive BMT
Test : Competitor
10 : 1 ratio
2 x 4.5 Gy
CD45.1 recipients
Competitor: CD45.1 mouse BM MNCs
pIpC injection (4 weeks post BMT)
peripheral blood analysis (monthly)
Chimerism analysis in hematopoietic organs (6 months post transplant)
CD45.1
CD45.2
B
CD45.2 chimerism (%)
Time (weeks post pIpC)
Control
Srsf2 P95H/+
Sf3b1 K700E/+
Srsf2 P95H/+ Sf3b1 K700E/+
C
CD45.2 Chimerism (%)
BM
Spleen
Thymus
Blood
Control
Srsf2 P95H/+
Sf3b1 K700E/+
Srsf2 P95H/+ Sf3b1 K700E/+
D
CD45.2 chimerism (%)
Time (weeks post pIpC)
Srsf2 +/+
Srsf2 P95H/+
Srsf2 P95H/P95H
Srsf2 P95H/fl
E
CD45.2 Chimerism (%)
BM
Spleen
Thymus
Blood
Srsf2 +/+
Srsf2 P95H/+
Srsf2 P95H/P95H
Srsf2 P95H/fl

Figure 3

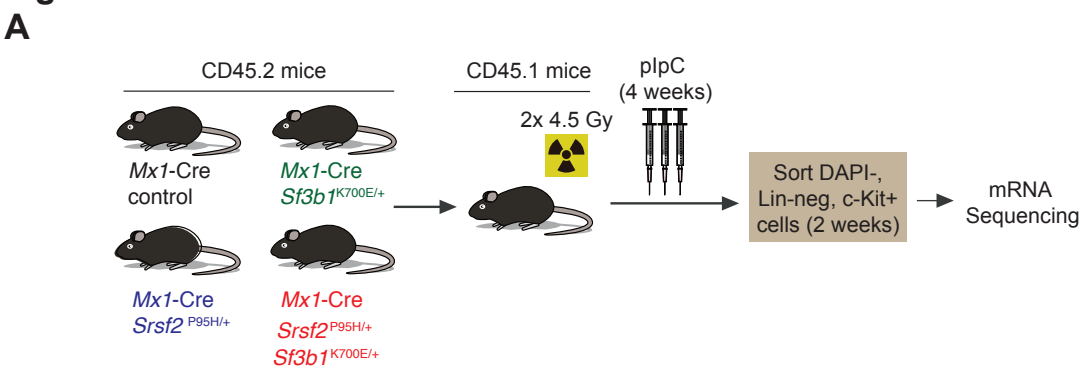
A
CD45.2 mice
CD45.1 mice
pIpC
(4 weeks)
2x 4.5 Gy
Mx1-Cre
control
Mx1-Cre
Sf3b1 K700E/+
Mx1-Cre
Srsf2 P95H/+
Mx1-Cre
Srsf2 P95H/+
Sf3b1 K700E/+
Sort DAPI-,
Lin-neg, c-Kit+
cells (2 weeks)
mRNA
Sequencing

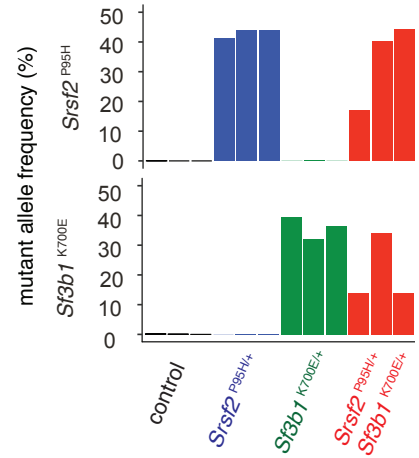
B
mutant allele frequency (%)
Srsf2 P95H
Sf3b1 K700E
control
Srsf2 P95H/+
Sf3b1 K700E/+
Srsf2 P95H/+
Sf3b1 K700E/+

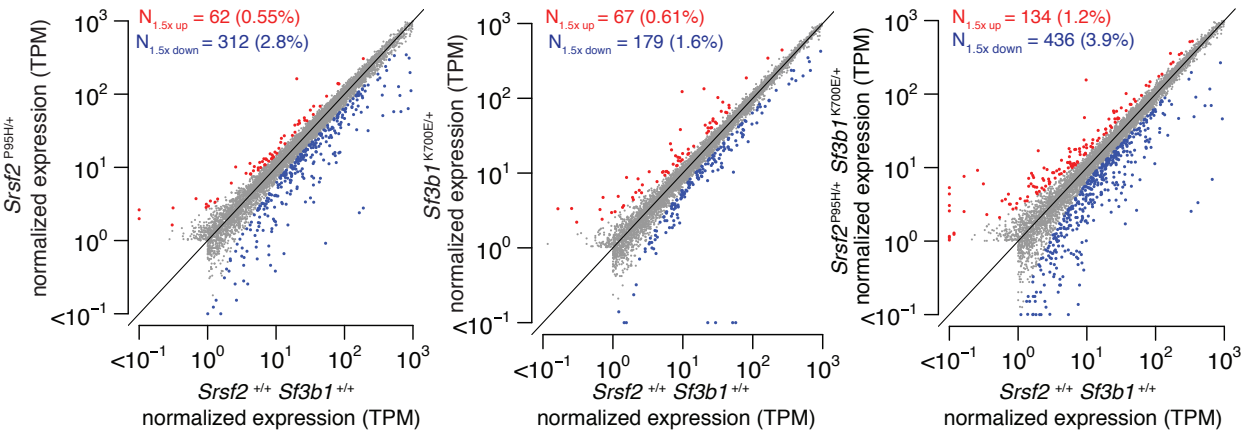
C
N1.5x up = 62 (0.55%)
N1.5x down = 312 (2.8%)
Srsf2 P95H/+ normalized expression (TPM)
Srsf2 +/+ Sf3b1 +/+ normalized expression (TPM)
N1.5x up = 67 (0.61%)
N1.5x down = 179 (1.6%)
Sf3b1 K700E/+ normalized expression (TPM)
Srsf2 +/+ Sf3b1 +/+ normalized expression (TPM)
N1.5x up = 134 (1.2%)
N1.5x down = 436 (3.9%)
Srsf2 P95H/+ Sf3b1 K700E/+ normalized expression (TPM)
Srsf2 +/+ Sf3b1 +/+ normalized expression (TPM)

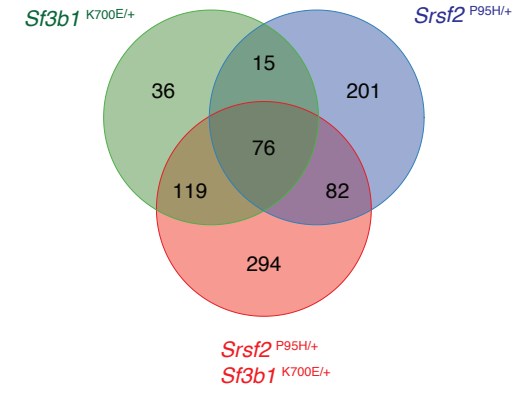
E
Sf3b1 K700E/+
Srsf2 P95H/+
36
15
201
76
119
82
294
Srsf2 P95H/+
Sf3b1 K700E/+

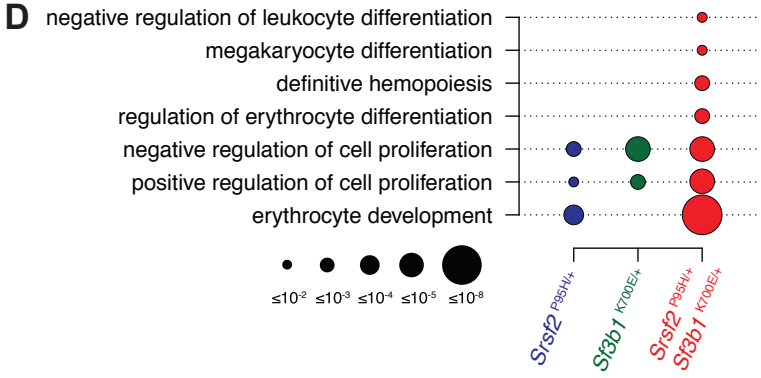
D
negative regulation of leukocyte differentiation
megakaryocyte differentiation
definitive hemopoiesis
regulation of erythrocyte differentiation
negative regulation of cell proliferation
positive regulation of cell proliferation
erythrocyte development
≤10-2 ≤10-3 ≤10-4 ≤10-5 ≤10-8
Srsf2 P95H/+
Sf3b1 K700E/+
Srsf2 P95H/+
Sf3b1 K700E/+

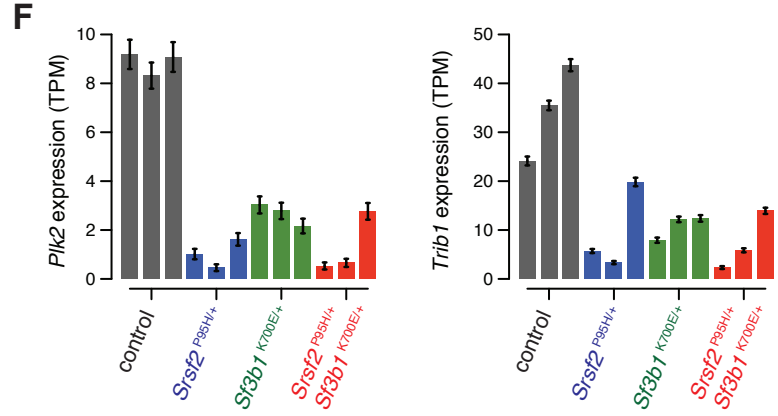
F
Plk2 expression (TPM)
Trib1 expression (TPM)
control
Srsf2 P95H/+
Sf3b1 K700E/+
Srsf2 P95H/+
Sf3b1 K700E/+

Figure 4

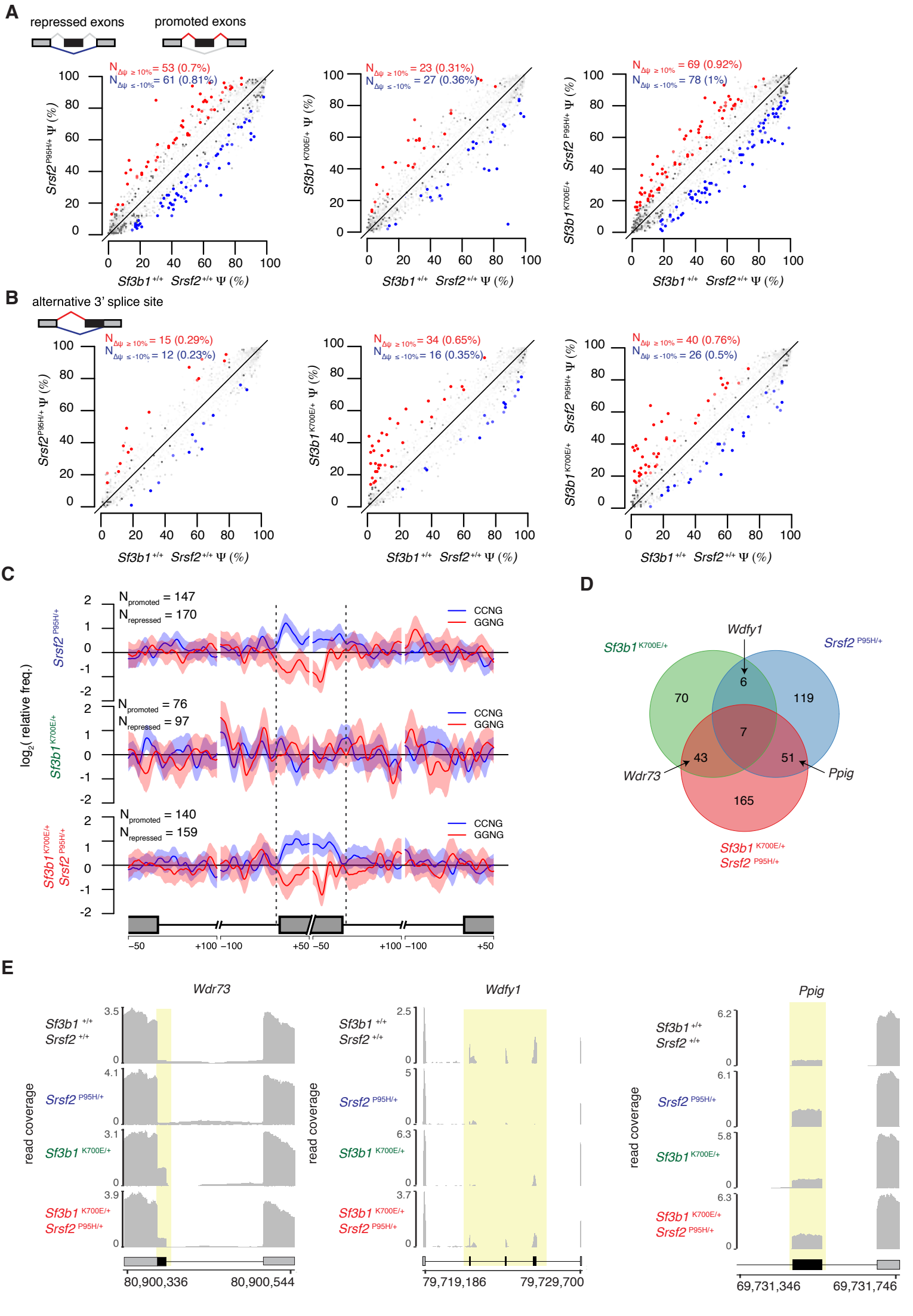
A
repressed exons
promoted exons
N Δψ ≥ 10% = 53 (0.7%)
N Δψ ≤ -10% = 61 (0.81%)
Srsf2 P95H/+ Ψ (%)
Sf3b1 +/+ Srsf2 +/+ Ψ (%)
N Δψ ≥ 10% = 23 (0.31%)
N Δψ ≤ -10% = 27 (0.36%)
Sf3b1 K700E/+ Ψ (%)
N Δψ ≥ 10% = 69 (0.92%)
N Δψ ≤ -10% = 78 (1%)
Sf3b1 K700E/+ Srsf2 P95H/+ Ψ (%)
B
alternative 3' splice site
N Δψ ≥ 10% = 15 (0.29%)
N Δψ ≤ -10% = 12 (0.23%)
N Δψ ≥ 10% = 34 (0.65%)
N Δψ ≤ -10% = 16 (0.35%)
N Δψ ≥ 10% = 40 (0.76%)
N Δψ ≤ -10% = 26 (0.5%)
C
log2 (relative freq.)
N promoted = 147
N repressed = 170
N promoted = 76
N repressed = 97
N promoted = 140
N repressed = 159
CCNG
GGNG
−50
+100
−100
+50
D
Wdfy1
Sf3b1 K700E/+
Srsf2 P95H/+
70
6
119
7
43
51
Wdr73
Ppig
165
E
Wdr73
Wdfy1
Ppig
read coverage
80,900,336
80,900,544
79,719,186
79,729,700
69,731,346
69,731,746

Figure 5

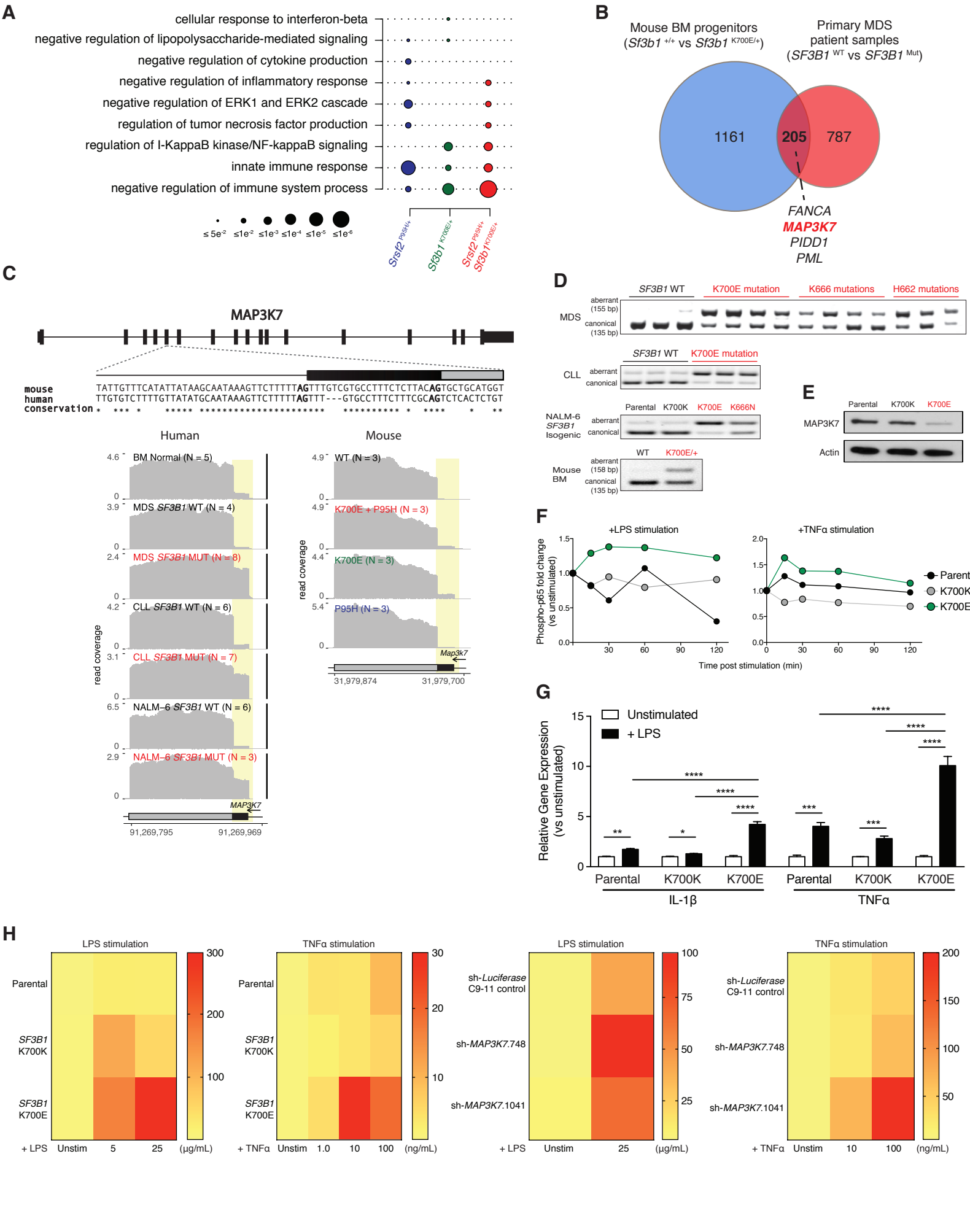
A
cellular response to interferon-beta
negative regulation of lipopolysaccharide-mediated signaling
negative regulation of cytokine production
negative regulation of inflammatory response
negative regulation of ERK1 and ERK2 cascade
regulation of tumor necrosis factor production
regulation of I-KappaB kinase/NF-kappaB signaling
innate immune response
negative regulation of immune system process
≤ 5e-2 ≤1e-2 ≤1e-3 ≤1e-4 ≤1e-5 ≤1e-6
Srsf2 P95H/+
Sf3b1 K700E/+
Srsf2 P95H/+
Sf3b1 K700E/+
B
Mouse BM progenitors (Sf3b1 +/+ vs Sf3b1 K700E/+)
Primary MDS patient samples (SF3B1 WT vs SF3B1 Mut)
1161
205
787
FANCA
MAP3K7
PIDD1
PML
C
MAP3K7
mouse
human
conservation
Human
Mouse
BM Normal (N = 5)
MDS SF3B1 WT (N = 4)
MDS SF3B1 MUT (N = 8)
CLL SF3B1 WT (N = 6)
CLL SF3B1 MUT (N = 7)
NALM-6 SF3B1 WT (N = 6)
NALM-6 SF3B1 MUT (N = 3)
read coverage
MAP3K7
91,269,795
91,269,969
WT (N = 3)
K700E + P95H (N = 3)
K700E (N = 3)
P95H (N = 3)
Map3k7
31,979,874
31,979,700
D
SF3B1 WT
K700E mutation
K666 mutations
H662 mutations
MDS
aberrant (155 bp)
canonical (135 bp)
CLL
NALM-6 SF3B1 Isogenic
Parental
K700K
K700E
K666N
Mouse BM
WT
K700E/+
aberrant (158 bp)
E
MAP3K7
Actin
F
+LPS stimulation
+TNFα stimulation
Phospho-p65 fold change (vs unstimulated)
Time post stimulation (min)
Parental
K700K
K700E
G
Unstimulated
+ LPS
Relative Gene Expression (vs unstimulated)
IL-1β
TNFα
H
LPS stimulation
TNFα stimulation
Parental
SF3B1 K700K
SF3B1 K700E
+ LPS
Unstim
5
25
(μg/mL)
+ TNFα
1.0
10
100
(ng/mL)
sh-Luciferase C9-11 control
sh-MAP3K7.748
sh-MAP3K7.1041

Figures 6

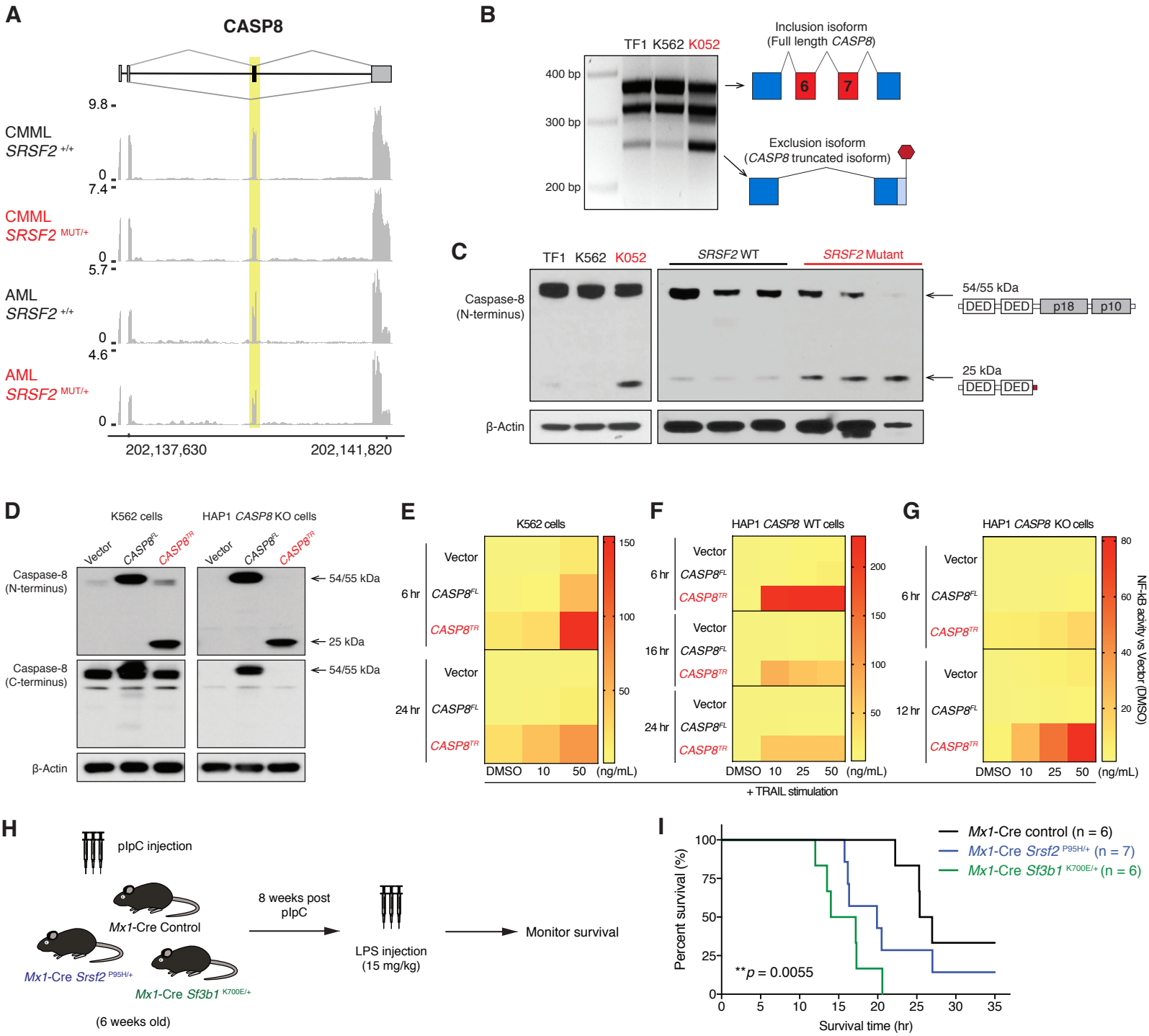
A
CASP8
CMML SRSF2 +/+
CMML SRSF2 MUT/+
AML SRSF2 +/+
AML SRSF2 MUT/+
9.8
7.4
5.7
4.6
0
202,137,630
202,141,820
B
TF1 K562 K052
400 bp
300 bp
200 bp
Inclusion isoform (Full length CASP8)
Exclusion isoform (CASP8 truncated isoform)
6
7
C
TF1 K562 K052
SRSF2 WT
SRSF2 Mutant
Caspase-8 (N-terminus)
β-Actin
54/55 kDa
25 kDa
DED
p18
p10
D
K562 cells
HAP1 CASP8 KO cells
Vector
Caspase-8 (N-terminus)
Caspase-8 (C-terminus)
54/55 kDa
25 kDa
E
K562 cells
F
HAP1 CASP8 WT cells
G
HAP1 CASP8 KO cells
6 hr
16 hr
24 hr
12 hr
DMSO 10 25 50 (ng/mL)
+ TRAIL stimulation
NF-kB activity vs Vector (DMSO)
H
pIpC injection
Mx1-Cre Control
Mx1-Cre Srsf2 P95H/+
Mx1-Cre Sf3b1 K700E/+
(6 weeks old)
8 weeks post pIpC
LPS injection (15 mg/kg)
Monitor survival
I
Mx1-Cre control (n = 6)
Mx1-Cre Srsf2 P95H/+ (n = 7)
Mx1-Cre Sf3b1 K700E/+ (n = 6)
Percent survival (%)
**p = 0.0055
Survival time (hr)

KEY RESOURCES TABLE

REAGENT or RESOURCE	SOURCE	IDENTIFIER
Antibodies		
Anti-B220 Alexa Fluor 700 (RA3-6B2)	eBioscience	Cat# 56-0452-82
Anti-CD19 PECy7 (1D3)	eBioscience	Cat# 25-0193-82
Anti-CD3 BV605 (17A2)	BioLegend	Cat# 100237
Anti-CD4 BV711 (GK1.5)	BioLegend	Cat# 100447
Anti-CD8a PerCP/Cy5.5 (53-6.7)	BioLegend	Cat# 100734
Anti-Gr-1 PECy7 (RB6-8C5)	eBioscience	Cat# 25-5931-82
Anti-Mac-1 PE (M1/70)	eBioscience	Cat# 12-0112-82
Anti-NK1.1 APCCy7 (PK136)	BioLegend	Cat# 108724
Anti-Ter119	BioLegend	Cat# 116223
Anti-c-Kit APC (2B8)	eBioscience	Cat# 17-1171-82
Anti-Sca-1 PECy7 (D7)	eBioscience	Cat# 25-5981-82
Anti-FcγRII/III Alexa Fluor 700 (93)	eBioscience	Cat# 56-0161-82
Anti-CD34 FITC (RAM34)	eBioscience	Cat# 11-0341-82
Anti-CD45.1 PerCP/Cy5.5 (A20)	BioLegend	Cat# 110728
Anti-CD45.2 BV605 (104)	BioLegend	Cat# 109841
Anti-CD48 PerCP/Cy5.5 (HM48-1)	BioLegend	Cat# 103422
Anti-CD150 PE (9D1)	eBioscience	Cat# 12-1501-82
Anti-CD44 FITC (IM7)	eBioscience	Cat# 11-0441-82
Anti-IgM PE (II/41)	eBioscience	Cat# 12-5790-82
Anti-CD25 PE (PC61.5)	eBioscience	Cat # 12-0251-82
Anti-CD43 FITC (S11)	BioLegend	Cat# 143204
Anti-NF-κB/p65 (D14E12)	Cell Signaling Technology	Cat# 8242
Anti-phospho NF-κB/p65-Ser536 (93H1)	Cell Signaling Technology	Cat# 3033
Anti-phospho-IRAK1-Thr209, rabbit polyclonal	Assay Biotech	Cat# A1074

Anti-IRAK1 (D51G7), rabbit monoclonal	Cell Signaling Technology	Cat# 4504
Anti-phospho-IRAK4-Thr345 (A8A8), mouse monoclonal	AbboMax	Cat# 600-560
Anti-IRAK4, rabbit polyclonal	Cell Signaling Technology	Cat# 4363
Anti-IκBα, rabbit polyclonal	Cell Signaling Technologies	Cat# 9242
Anti-TAK1/MAP3K7 (D94D7), rabbit monoclonal	Cell Signaling Technologies	Cat# 5206
Anti-Caspase-8, N-terminal (E6), rabbit monoclonal	Abcam	Cat# ab32125
Anti-Caspase-8, C-terminal (12F5), mouse monoclonal	Enzo Life Science	Cat# ALX-804-242-C100
Anti-β-actin (AC-15), mouse monoclonal	Sigma-Aldrich	Cat# A5441
Bacterial and Virus Strains		
None		
Biological Samples		
MDS and CLL primary patient samples	MSKCC	
Chemicals, Peptides, and Recombinant Proteins		
Escherichia coli 0111:B4 LPS	Sigma Aldrich	Cat# L2630
Polybrene	Millipore	Cat# TR-1003-G
Recombinant TRAIL (soluble, human)	Enzo Life Science	Cat# ALX-201-073-3020
Recombinant TNF-α	PeproTech	Cat# 300-01A
Critical Commercial Assays		
NF-κB Cignal^{TM} Reporter Assay	Qiagen	Cat# CCS-013L
Deposited Data		
RNAseq data	This paper	GSE97452
Experimental Models: Cell Lines		
Human: K562 cells	ATCC	Cat# CCL-243

Human: NALM-6 cells, Parental, SF3B1K700K/+, SF3B1K700E/+, SF3B1K666N/+	Horizon Discovery	Cat# N/A
Human: HAP1 Parental cells	Horizon Discovery	Cat# C631
Human: HAP1 *CASP8* knockout cells	Horizon Discovery	Cat# HZGHC001511c007
Human: 293 GPII cells	Clontech	Cat# 631530
Experimental Models: Organisms/Strains		
Mice: *Mx1*-cre transgenic mice (C.Cg-Tg(Mx1-cre)1Cgn/J)	The Jackson Laboratory	Cat# JAX: 005673
Mice: *Vav*-cre transgenic mice (B6.Cg-Tg(Vav1-icre)A2Kio/J)	The Jackson Laboratory	Cat# JAX: 008610
Mice: *Srsf2*$^{P95H/+}$ (B6J.B6NTac(SJL)-*Srsf2tm1.1Oaw*/J)	Kim et al. 2015	
Mice: *Srsf2*$^{fl/fl}$ (B6;129S4-*Srsf2*^{tm1Xdfu}/J)	The Jackson Laboratory	Cat# JAX: 018019
Mice: *Sf3b1*$^{K700E/+}$	Obeng et al. 2016	
Oligonucleotides		
RT-PCR *MAP3K7* (human) Fwd: GATGGAATATGCTGAAGGGG		
RT-PCR *MAP3K7* (human) Rev: CACTCCTTGGGAACACTGTA		
RT-PCR *Map3k7* (mouse) Fwd: GATGGAATATGCAGAGGGGG		
RT-PCR *Map3k7* (mouse) Rev: CACTCCTTGGGAACACTGTA		
RT-PCR *CASP8* (human) Fwd: GAACTTCAGACACCAGGC		
RT-PCR *CASP8* (human) Rev: CTTTGTCCAAAGTCTTTGCTG		
qRT-PCR CASP8 Exclusion isoform Fwd: GATGAATTTTCAAATGACTTTGGAC		
qRT-PCR CASP8 Exclusion isoform Rev: TGATCAGACAGTATCCCCGAG		
qRT-PCR CASP8 Inclusion isoform Fwd: TGATGAATTTTCAAATGGGGAGGA		
qRT-PCR CASP8 Inclusion isoform Rev: ATCCTGTTCTCTTGGAGAGTCC		
Taqman probe: TNF-α (human)	ThermoFisher Scientific	Cat# Hs00174128_m1

Taqman probe: IL-1β (human)	ThermoFisher Scientific	Cat# Hs01555410_m1
Taqman probes for gene expression analysis of GAPDH	ThermoFisher Scientific	Cat# Hs02786624_g1
sh.*MAP3K7*.748: TTAGGTAAATTTTTTATCAGTG		
sh.*MAP3K7*.1041: TTTTCAACAATTTTGATTCTAA		
sh.Luci control: TTAATCAGAGACTTCAGGCGGT		
Recombinant DNA		
pVSV.G	Addgene	Cat# 12259
pxPAX2	Addgene	Cat# 12260
MSCV-IRES-GFP empty vector	Addgene	Cat# 52107
MSCV-Flag-CASP8^{FL}-IRES-GFP	This paper	
MSCV-Flag-CASP8^{TR}-IRES-GFP	This paper	
T3G-dsRED-mirE-PGK-Neo-IRES-rtTA3 (LT3RENIR)	Fellmann et al., 2013	
Software and Algorithms		
Bowtie v1.0.0	Langmead et al. 2009	
RSEM v1.2.4	Li and Dewey 2001	
TopHat v2.0.8b	Trapnell et al. 2009	
TMM method	Robinson and Oshlack 2010	
Wagenmakers's Bayesian framework	Wagenmakers et al. 2010	
MISO v2.0	Katz et al. 2010	
GOseq	Young et al. 2010	
Bioconductor	Huber et al. 2015	
Other		
FASTQ files from published RNA-seq studies of patients with MDS	Dolatshad et al. 2015	GSE63569
FASTQ files from published RNA-seq studies of patients with CLL	Darman et al. 2015	GSE72790

Supplemental Text & Figures

Figure S1

Click here to download Supplemental Text & Figures Supp Figures 1-6 reduced_05112017.pdf

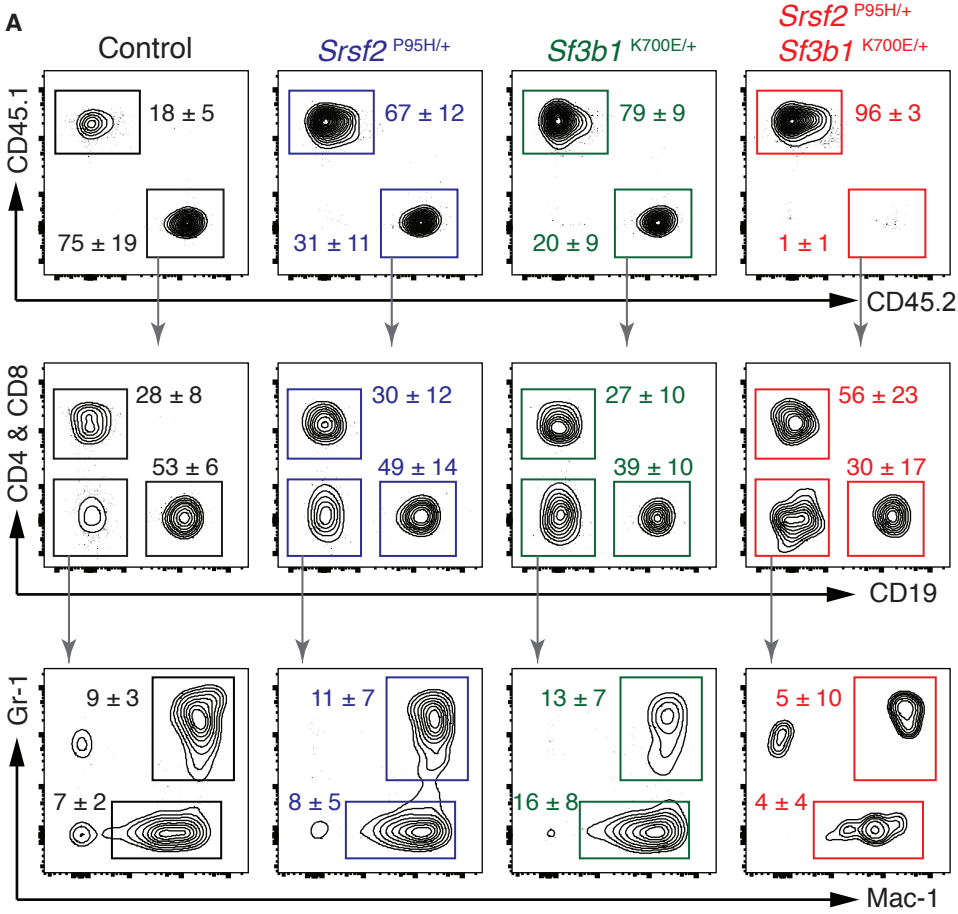

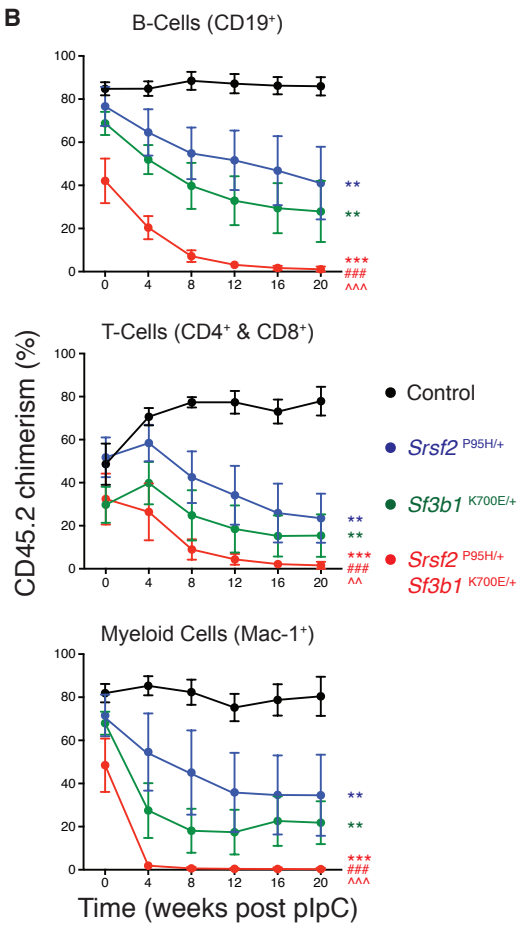

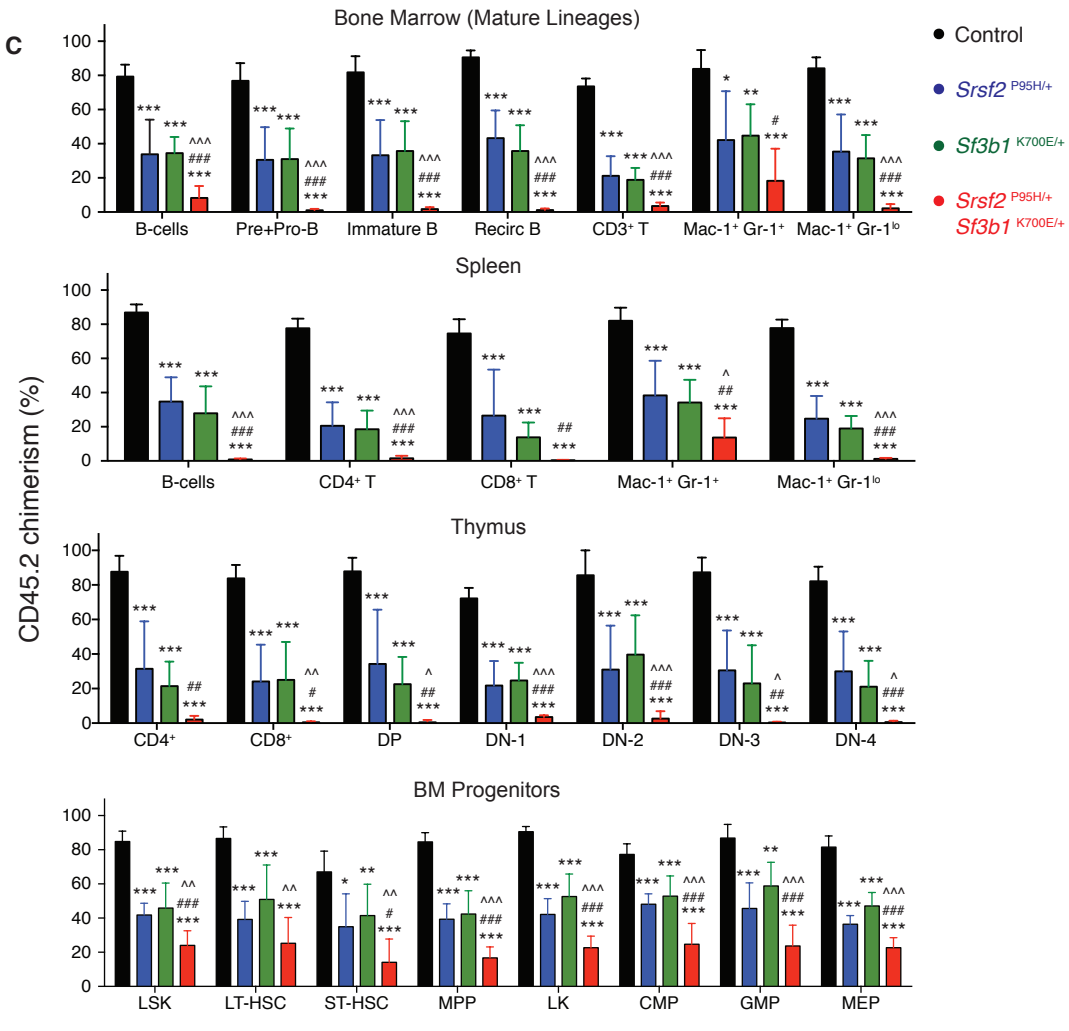

Figure S2

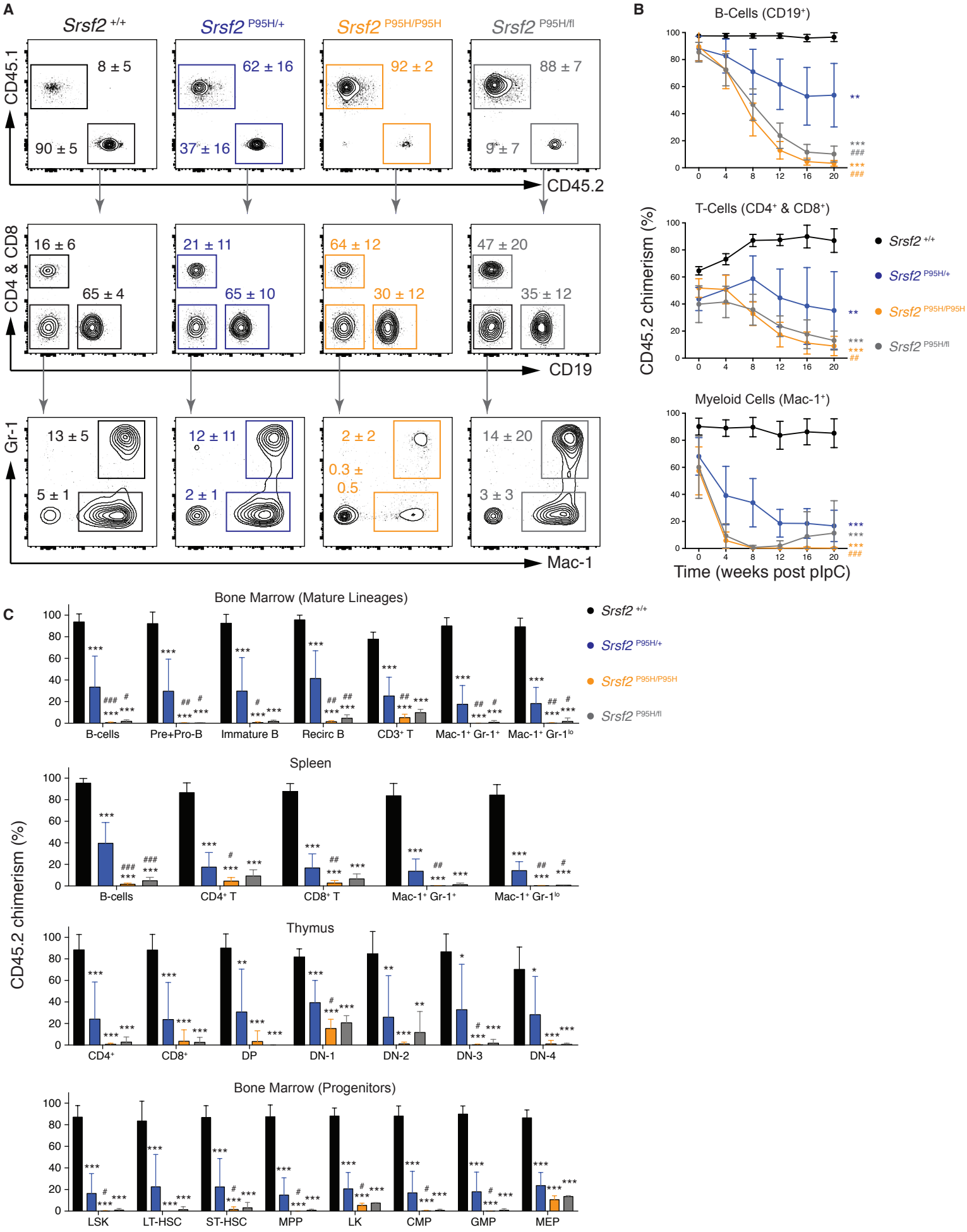
A
Srsf2 +/+
Srsf2 P95H/+
Srsf2 P95H/P95H
Srsf2 P95H/fl
CD45.1
CD45.2
8 ± 5
90 ± 5
62 ± 16
37 ± 16
92 ± 2
88 ± 7
9 ± 7
CD4 & CD8
CD19
16 ± 6
65 ± 4
21 ± 11
65 ± 10
64 ± 12
30 ± 12
47 ± 20
35 ± 12
Gr-1
Mac-1
13 ± 5
5 ± 1
12 ± 11
2 ± 1
2 ± 2
0.3 ± 0.5
14 ± 20
3 ± 3
B
B-Cells (CD19⁺)
T-Cells (CD4⁺ & CD8⁺)
Myeloid Cells (Mac-1⁺)
CD45.2 chimerism (%)
Time (weeks post pIpC)
Srsf2 +/+
Srsf2 P95H/+
Srsf2 P95H/P95H
Srsf2 P95H/fl
C
Bone Marrow (Mature Lineages)
B-cells
Pre+Pro-B
Immature B
Recirc B
CD3⁺ T
Mac-1⁺ Gr-1⁺
Mac-1⁺ Gr-1lo
Spleen
CD4⁺ T
CD8⁺ T
Thymus
CD4⁺
CD8⁺
DP
DN-1
DN-2
DN-3
DN-4
Bone Marrow (Progenitors)
LSK
LT-HSC
ST-HSC
MPP
LK
CMP
GMP
MEP

Figure S3

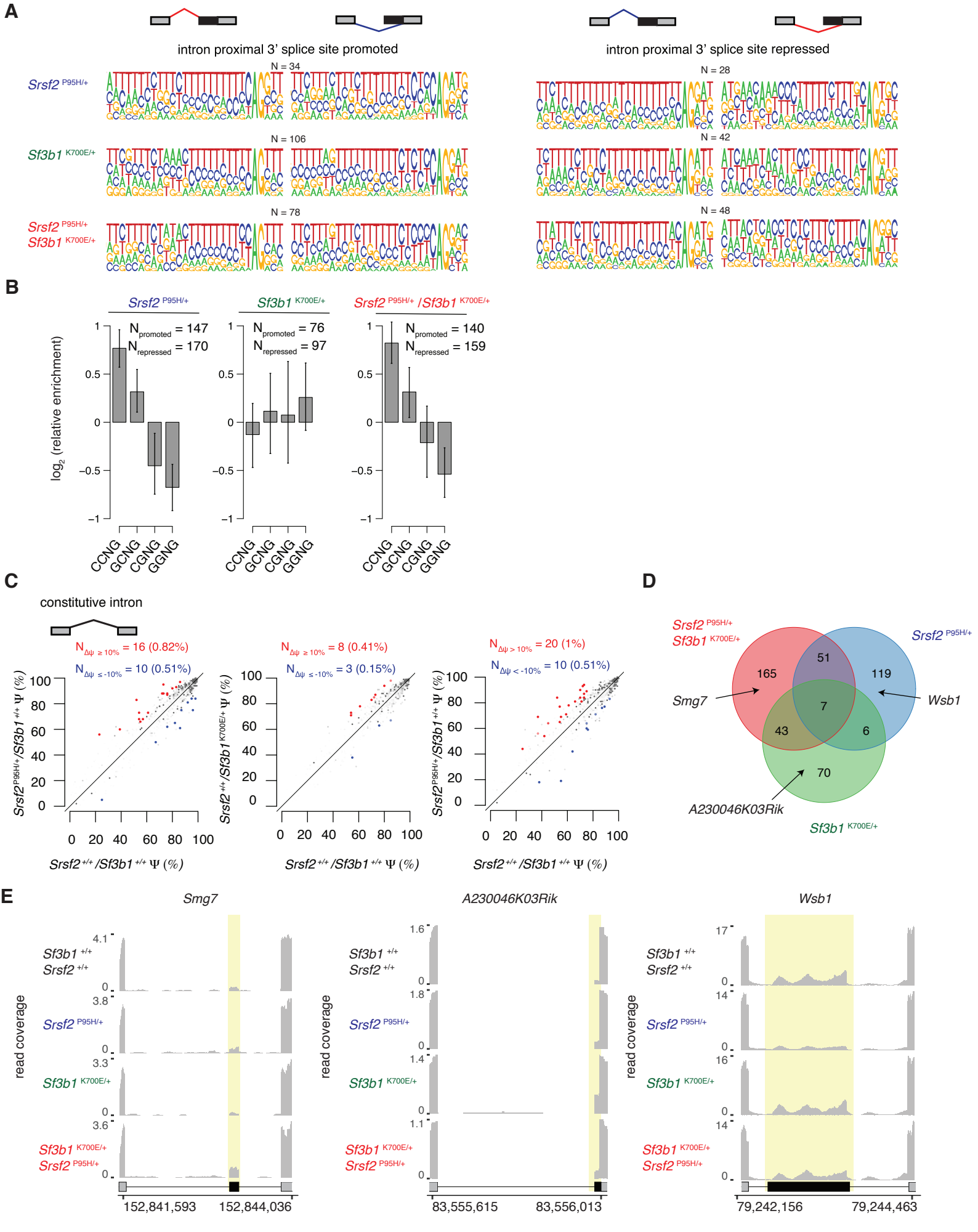
A
intron proximal 3' splice site promoted
intron proximal 3' splice site repressed
Srsf2 P95H/+
Sf3b1 K700E/+
Srsf2 P95H/+ Sf3b1 K700E/+
N = 34
N = 106
N = 78
N = 28
N = 42
N = 48
B
Srsf2 P95H/+
Sf3b1 K700E/+
Srsf2 P95H/+ /Sf3b1 K700E/+
log2 (relative enrichment)
N promoted = 147
N repressed = 170
N promoted = 76
N repressed = 97
N promoted = 140
N repressed = 159
CCNG
GCNG
CGNG
GGNG
C
constitutive intron
N Δψ ≥ 10% = 16 (0.82%)
N Δψ ≤ -10% = 10 (0.51%)
N Δψ ≥ 10% = 8 (0.41%)
N Δψ ≤ -10% = 3 (0.15%)
N Δψ > 10% = 20 (1%)
N Δψ < -10% = 10 (0.51%)
Srsf2P95H/+/Sf3b1+/+ Ψ (%)
Srsf2+/+/Sf3b1K700E/+ Ψ (%)
Srsf2P95H/+/Sf3b1+/+ Ψ (%)
Srsf2+/+/Sf3b1+/+ Ψ (%)
Srsf2+/+/Sf3b1+/+ Ψ (%)
D
Srsf2 P95H/+ Sf3b1 K700E/+
Srsf2 P95H/+
Smg7
Wsb1
A230046K03Rik
Sf3b1 K700E/+
165
51
119
7
43
6
70
E
Smg7
A230046K03Rik
Wsb1
read coverage
Sf3b1 +/+ Srsf2 +/+
Srsf2 P95H/+
Sf3b1 K700E/+
Sf3b1 K700E/+ Srsf2 P95H/+
152,841,593
152,844,036
83,555,615
83,556,013
79,242,156
79,244,463

Figure S4

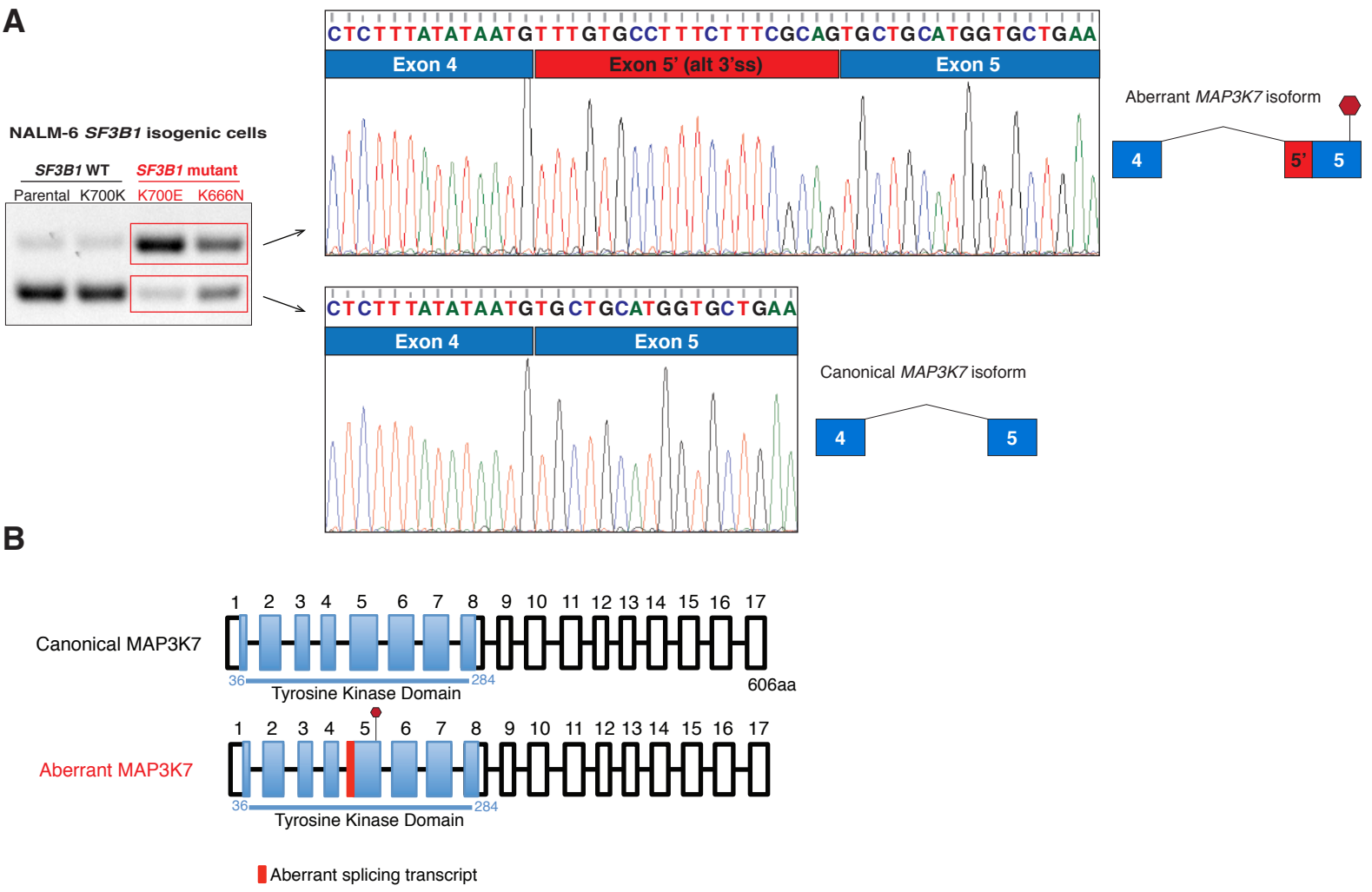
A
NALM-6 SF3B1 isogenic cells
SF3B1 WT
SF3B1 mutant
Parental
K700K
K700E
K666N
CTCTTTATATAATGTTTGTGCCTTTCTTTCGCAGTGCTGCATGGTGCTGAA
Exon 4
Exon 5' (alt 3'ss)
Exon 5
Aberrant MAP3K7 isoform
4
5'
5
CTCTTTATATAATGTGCTGCATGGTGCTGAA
Exon 4
Exon 5
Canonical MAP3K7 isoform
4
5
B
Canonical MAP3K7
1 2 3 4 5 6 7 8 9 10 11 12 13 14 15 16 17
36
284
Tyrosine Kinase Domain
606aa
Aberrant MAP3K7
1 2 3 4 5 6 7 8 9 10 11 12 13 14 15 16 17
36
284
Tyrosine Kinase Domain
Aberrant splicing transcript
C
Parental
+ Reporter construct
sh-Luciferase
C9-11 control
sh-Luciferase
sh-Renilla
sh-MAP3K7.1166
sh-MAP3K7.1378
sh-MAP3K7.1041
sh-MAP3K7.748
MAP3K7
Actin

Figure S5

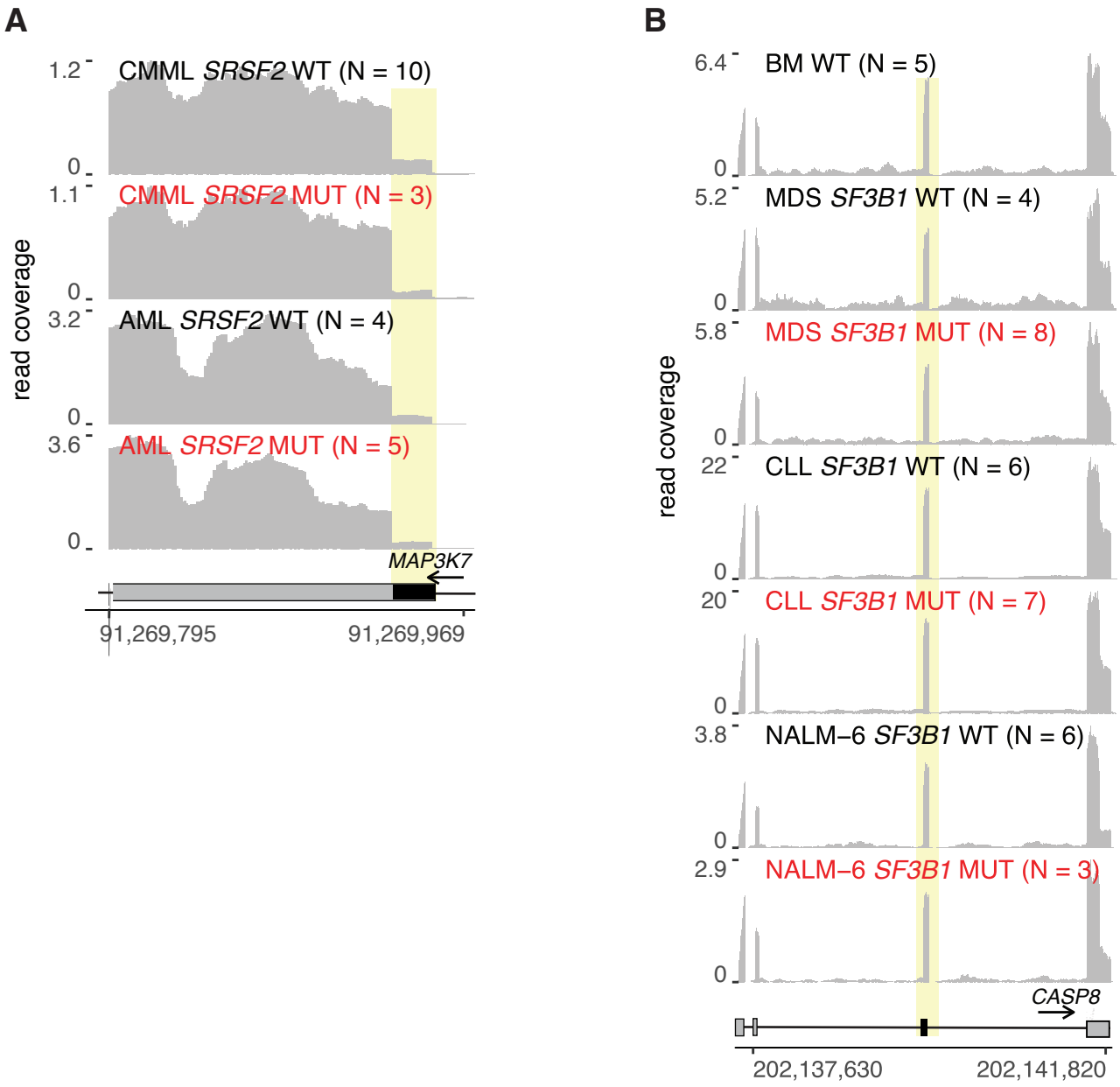
A
1.2
CMML SRSF2 WT (N = 10)
0
1.1
CMML SRSF2 MUT (N = 3)
0
3.2
AML SRSF2 WT (N = 4)
0
3.6
AML SRSF2 MUT (N = 5)
0
read coverage
MAP3K7
91,269,795
91,269,969
B
6.4
BM WT (N = 5)
0
5.2
MDS SF3B1 WT (N = 4)
0
5.8
MDS SF3B1 MUT (N = 8)
0
22
CLL SF3B1 WT (N = 6)
0
20
CLL SF3B1 MUT (N = 7)
0
3.8
NALM–6 SF3B1 WT (N = 6)
0
2.9
NALM–6 SF3B1 MUT (N = 3)
0
read coverage
CASP8
202,137,630
202,141,820

Figure S6

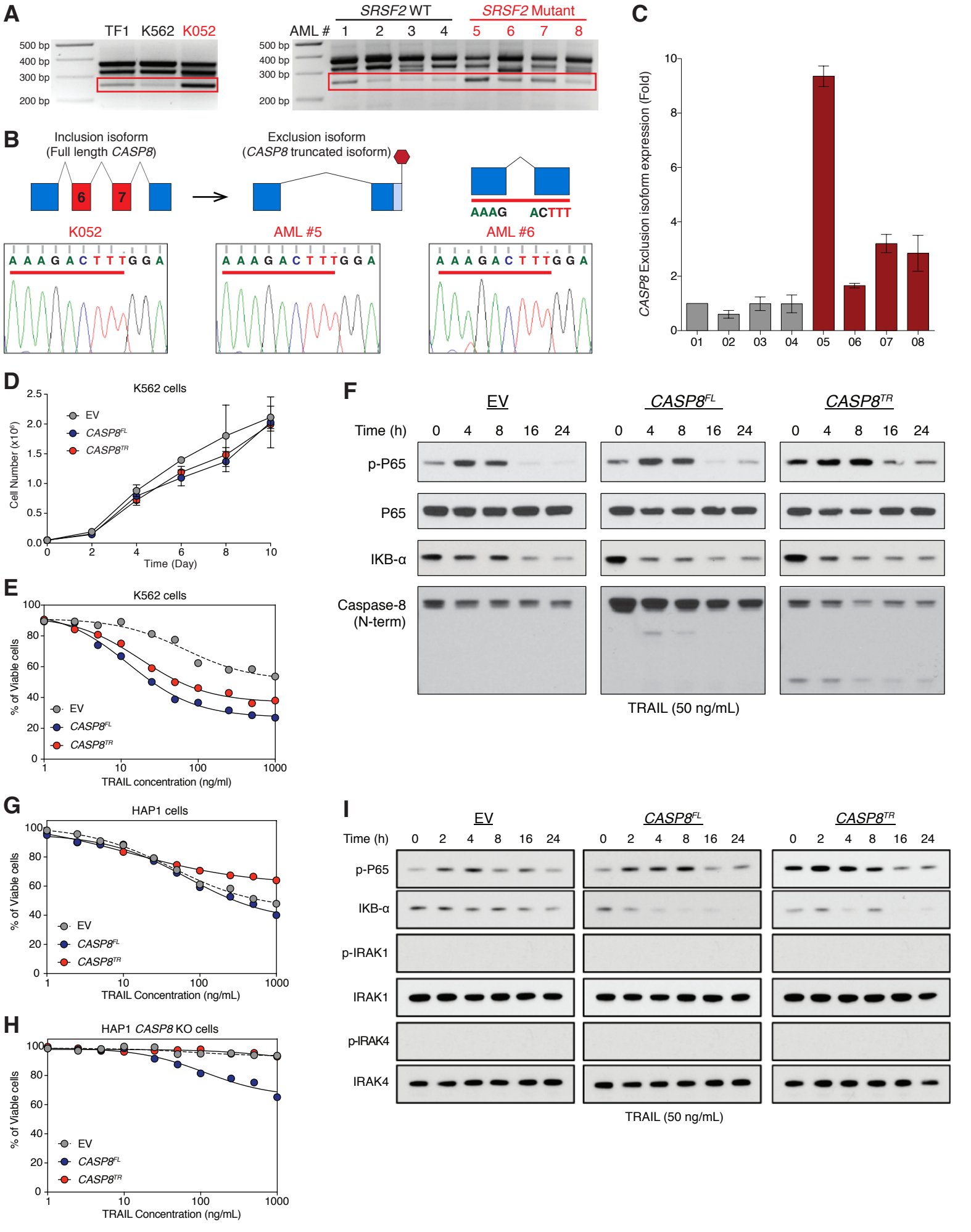
A
TF1 K562 K052
500 bp
400 bp
300 bp
200 bp
SRSF2 WT
SRSF2 Mutant
AML # 1 2 3 4 5 6 7 8
B
Inclusion isoform
(Full length CASP8)
Exclusion isoform
(CASP8 truncated isoform)
6
7
AAAG ACTTT
K052
AML #5
AML #6
A A A G A C T T T G G A
C
CASP8 Exclusion isoform expression (Fold)
01 02 03 04 05 06 07 08
D
K562 cells
EV
CASP8FL
CASP8TR
Cell Number (x10⁶)
Time (Day)
E
K562 cells
% of Viable cells
TRAIL concentration (ng/ml)
F
EV
CASP8FL
CASP8TR
Time (h) 0 4 8 16 24
p-P65
P65
IKB-α
Caspase-8
(N-term)
TRAIL (50 ng/mL)
G
HAP1 cells
% of Viable cells
TRAIL Concentration (ng/mL)
H
HAP1 CASP8 KO cells
% of Viable cells
TRAIL Concentration (ng/mL)
I
EV
CASP8FL
CASP8TR
Time (h) 0 2 4 8 16 24
p-P65
IKB-α
p-IRAK1
IRAK1
p-IRAK4
IRAK4
TRAIL (50 ng/mL)